

Supporting information for

Strategically Designed Azolyl-Carboxylate MOFs for Potential Humid CO₂ Capture

Shyamapada Nandi,¹ Sattwick Halder,¹ Debanjan Chakraborty,¹ and Ramanathan Vaidhyanathan^{1,2,*}

¹ Department of Chemistry, Indian Institute of Science Education and Research, Pune.

² Centre for excellence in energy, Indian Institute of Science Education and Research, Pune.

1. Materials and Methods:

Synthesis

Single Crystal XRD

2. Analytical Characterization:

PXRD Analysis

TGA Analysis

IR Analysis

3. Gas Sorption analysis:

Virial Analysis

IAST Fitting

Diffusion Kinetics Study

4. Stability Study:

PXRD

Steam Condition Experiments

5. Computational details:

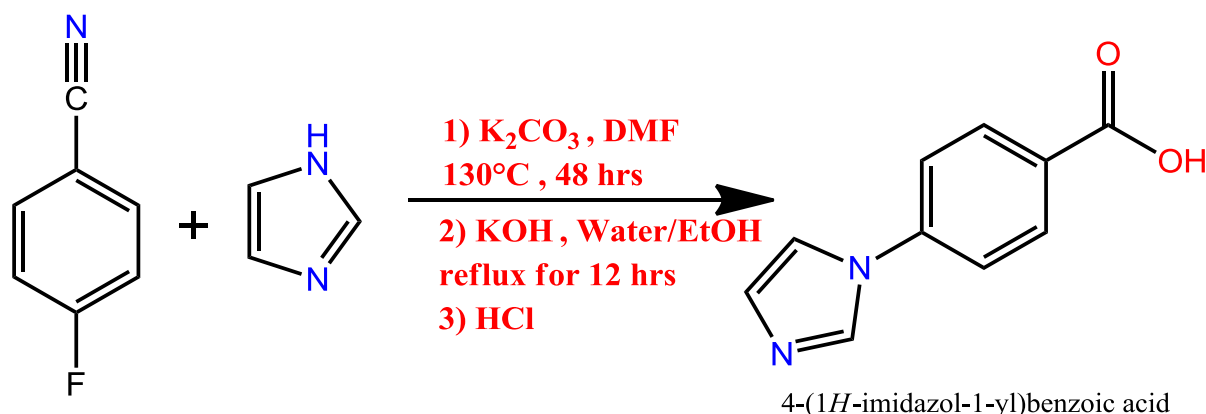
Simulated Annealing and CASTEP routines.

1. Materials and Methods:

All the chemicals were bought from Sigma Aldrich and used without further purification.

4-(1H-Imidazol-1-yl) benzoic acid and 4-(1H-1,2,4-triazol-1-yl)benzoic acid were synthesized according to the reported procedure with slight modification.

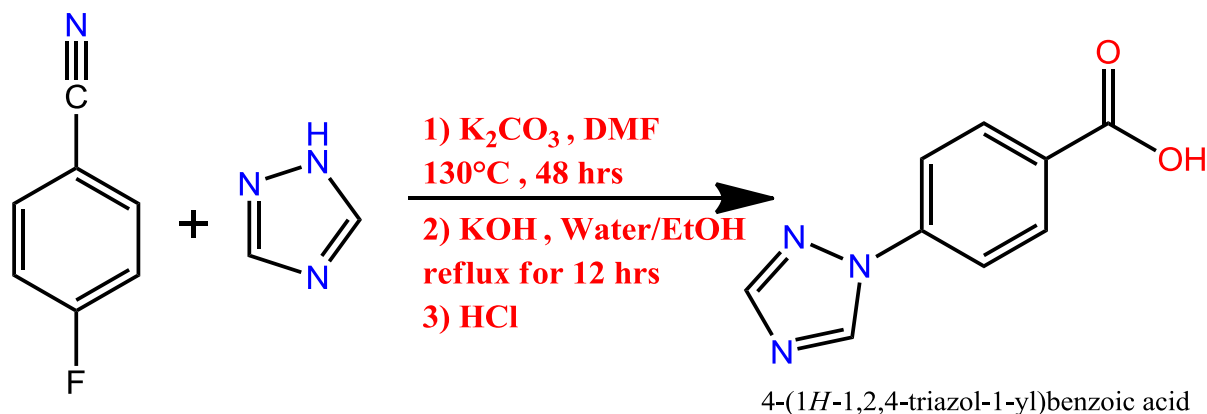
Synthesis of 4-(1H-Imidazol-1-yl) benzoic acid: Imidazole (4.1 g, 0.06 mol), 4-Fluorobenzonitrile (7.26 g, 0.06 mol) and potassium carbonate (16.6 g, 0.12 mol) were taken in 100 ml of DMF. The reaction mixture was heated at 130°C for 24 hours with constant stirring under N₂ atmosphere. The mixture was cooled to room temperature and poured into 200 mL of ice-cold water. The white precipitate was then filtered resulting in a yield of 8.48 g of 4-(1H-Imidazol-1-yl) benzonitrile. In the second step 5 g of 4-(1H-Imidazol-1-yl) benzonitrile was dissolved in 100 ml of Ethanol followed by addition of 100ml of 6M KOH solution. The mixture was then refluxed for 12 hrs. After cooling the mixture to room temperature it was acidified with 3N HCl until the P^H of the solution become 6. The White precipitate was filtered, washed with water and finally dried in hot air oven resulting in 5.2 g of Synthesis of 4-(1H-Imidazol-1-yl) benzoic acid.



Scheme 1: Synthesis procedure of 4-(1H-Imidazol-1-yl) benzoic acid.

Synthesis of 4-(1H-1,2,4-triazol-1-yl)benzoic acid: 1,2,4-Triazole (4.15 g, 0.06 mol), 4-Fluorobenzonitrile (7.26 g, 0.06 mol) and potassium carbonate (16.6 g, 0.12 mol) were taken in 100 ml of DMF. The reaction mixture was heated at 130°C for 24 hours with constant stirring under N₂ atmosphere. The mixture was cooled to room temperature and poured into 200 mL of ice-cold water. The white precipitate was then filtered resulting in a yield of 8.54 g of 4-(1H-1,2,4-triazol-1-yl)benzonitrile. In the second step 5 g of 4-(1H-1,2,4-triazol-1-yl)benzonitrile was dissolved in 100 ml of Ethanol followed by addition of 100ml of 6M KOH solution. The mixture was then refluxed for 12

hrs. After cooling the mixture to room temperature it was acidified with 3N HCl until the P^H of the solution become 6. The White precipitate was filtered, washed with water and finally dried in hot air oven resulting in 5.32 g of Synthesis of 4-(1H-1,2,4-triazol-1-yl) benzoic acid.



Scheme 2: Synthesis procedure of 4-(1H-1,2,4-triazol-1-yl)benzoic acid.

Synthesis of Mg(Tz-Bz) (CH₃COO).solvent; IISERP-MOF4(1): A solvothermal reaction between Magnesium(II) acetate tetra hydrate (0.107 g; 0.5 mmol), 4-(1H-1,2,4-triazol-1-yl) benzoic acid (0.142 g; 0.75 mmol) in a solution containing 4 ml of Dimethylformamide (DMF) and 3 ml of Acetonitrile (ACN) was carried out at 120°C for 48 hours. Colourless needle shaped crystals were isolated by filtration and was washed with plenty of methanol. The air-dried sample yielded ~71% (based on Mg). The PXRD pattern indicated this to be a pure phase of 1. CHN analysis (calculated values within parentheses): C, 48.15% (48.51%); H, 4.89% (5.23%); N, 16.39% (16.16%).

Synthesis of Mn(Tz-Bz) (CH₃COO).solvent; IISERP-MOF5 (2): A solvothermal reaction between Manganese(II) acetate tetra hydrate (0.123 g; 0.5 mmol), 4-(1H-1,2,4-triazol-1-yl) benzoic acid (0.142 g; 0.75 mmol) in a solution containing 4 ml of Dimethylformamide (DMF) and 3 ml of Acetonitrile (ACN) was carried out at 120°C for 48 hours. Colourless needle shaped crystals were isolated by filtration and was washed with plenty of methanol. The air-dried sample yielded ~76% (based on Mn). The PXRD pattern indicated this to be a pure phase of 1. CHN analysis (calculated values within parentheses): C, 44.95% (44.57%); H, 4.42% (4.81%); N, 14.32% (14.85%).

Synthesis of Co(Tz-Bz) (CH₃COO).solvent; IISERP-MOF6 (3): A solvothermal reaction between Cobalt(II) acetate tetra hydrate (0.125 g; 0.5 mmol), 4-(1H-1,2,4-triazol-1-yl) benzoic acid (0.142 g; 0.75 mmol) in a solution containing 4 ml of Dimethylformamide (DMF) and 3 ml of Acetonitrile (ACN)

was carried out at 130°C for 72 hours. Colourless needle shaped crystals were isolated by filtration and was washed with plenty of methanol. The air-dried sample yielded ~71% (based on Co). The PXRD pattern indicated this to be a pure phase of 1. CHN analysis (calculated values within parentheses): C, 43.85% (44.10%); H, 4.62% (4.76%); N, 14.12% (14.70%).

Synthesis of Mg(Im-Bz) (CH₃COO).solvent; IISERP-MOF7 (4): A solvothermal reaction between Magnesium(II) acetate tetra hydrate (0.107 g; 0.5 mmol), 4-(1H-Imidazol-1-yl) benzoic acid (0.141 g; 0.75 mmol) in a solution containing 4 ml of Dimethylformamide (DMF) and 3 ml of Acetonitrile (ACN) was carried out at 120°C for 72 hours. Colourless needle shaped crystals were isolated by filtration and was washed with plenty of methanol. The air-dried sample yielded ~73% (based on Mg). The PXRD pattern indicated this to be a pure phase of 1. CHN analysis (calculated values within parentheses): C, 51.85% (52.28%); H, 5.12% (5.26%); N, 12.68% (12.19%).

Synthesis of Mn(Im-Bz) (CH₃COO).solvent; IISERP-MOF8 (5): A solvothermal reaction between Manganese(II) acetate tetra hydrate (0.123 g; 0.5 mmol), 4-(1H-Imidazol-1-yl) benzoic acid (0.141 g; 0.75 mmol) in a solution containing 4 ml of Dimethylformamide (DMF) and 3 ml of Acetonitrile (ACN) was carried out at 120°C for 48 hours. Colourless needle shaped crystals were isolated by filtration and was washed with plenty of methanol. The air-dried sample yielded ~70% (based on Mn). The PXRD pattern indicated this to be a pure phase of 1. CHN analysis (calculated values within parentheses): C, 48.45% (48.01%); H, 5.22% (4.83%); N, 11.62% (11.20%).

Synthesis of Co(Im-Bz) (CH₃COO).solvent; IISERP-MOF9 (6): A solvothermal reaction between Cobalt(II) acetate tetra hydrate (0.125 g; 0.5 mmol), 4-(1H-Imidazol-1-yl) benzoic acid (0.141 g; 0.75 mmol) in a solution containing 4 ml of Dimethylformamide (DMF) and 3 ml of Acetonitrile (ACN) was carried out at 120°C for 48 hours. Colourless needle shaped crystals were isolated by filtration and was washed with plenty of methanol. The air-dried sample yielded ~77% (based on Co). The PXRD pattern indicated this to be a pure phase of 1. CHN analysis (calculated values within parentheses): C, 47.87% (47.50%); H, 4.12% (4.78%); N, 11.58% (11.08%).

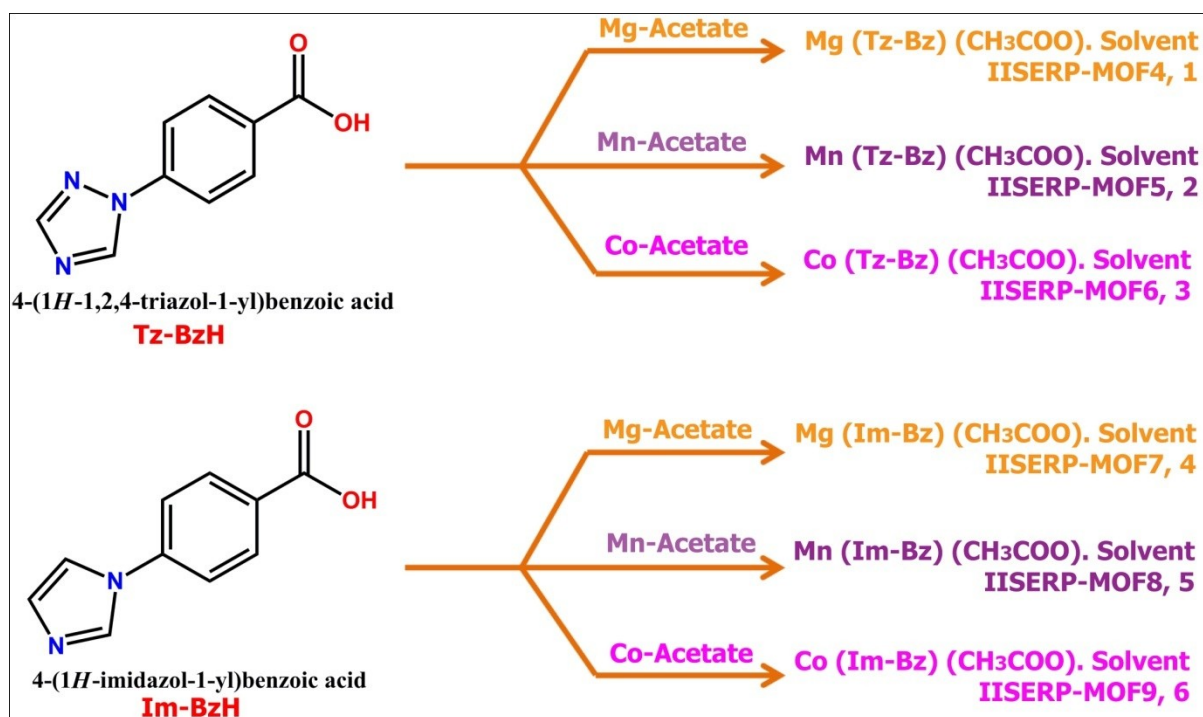


Figure S1. Schematic representation of the six MOFs that have been developed using metals (Mg, Mn and Co) of different Lewis acidity.

2. Analytical characterization:

Single crystal structure determination:

Single-crystals data were collected on a Bruker SMART APEX four-circle diffractometer equipped with a CMOS photon 100 detector (Bruker Systems Inc.) and with a Cu K α radiation (1.5418 Å). The incident X-ray beam was focused and monochromated using Micro focus (1 μ S). Crystal of all the three compounds were mounted on nylon Cryo loops with Paratone-N oil. Data was collected at 153(2) K. Data was integrated using Bruker SAINT Software and was corrected for absorption using SADABS. Structure was solved by Intrinsic Phasing module of the direct methods and refined using the SHELXTL 97 software suite. All non-hydrogen atoms were located from iterative examination of difference F-maps following which the structure was refined using least-squares method. Hydrogen atoms were placed geometrically and placed in a riding model.

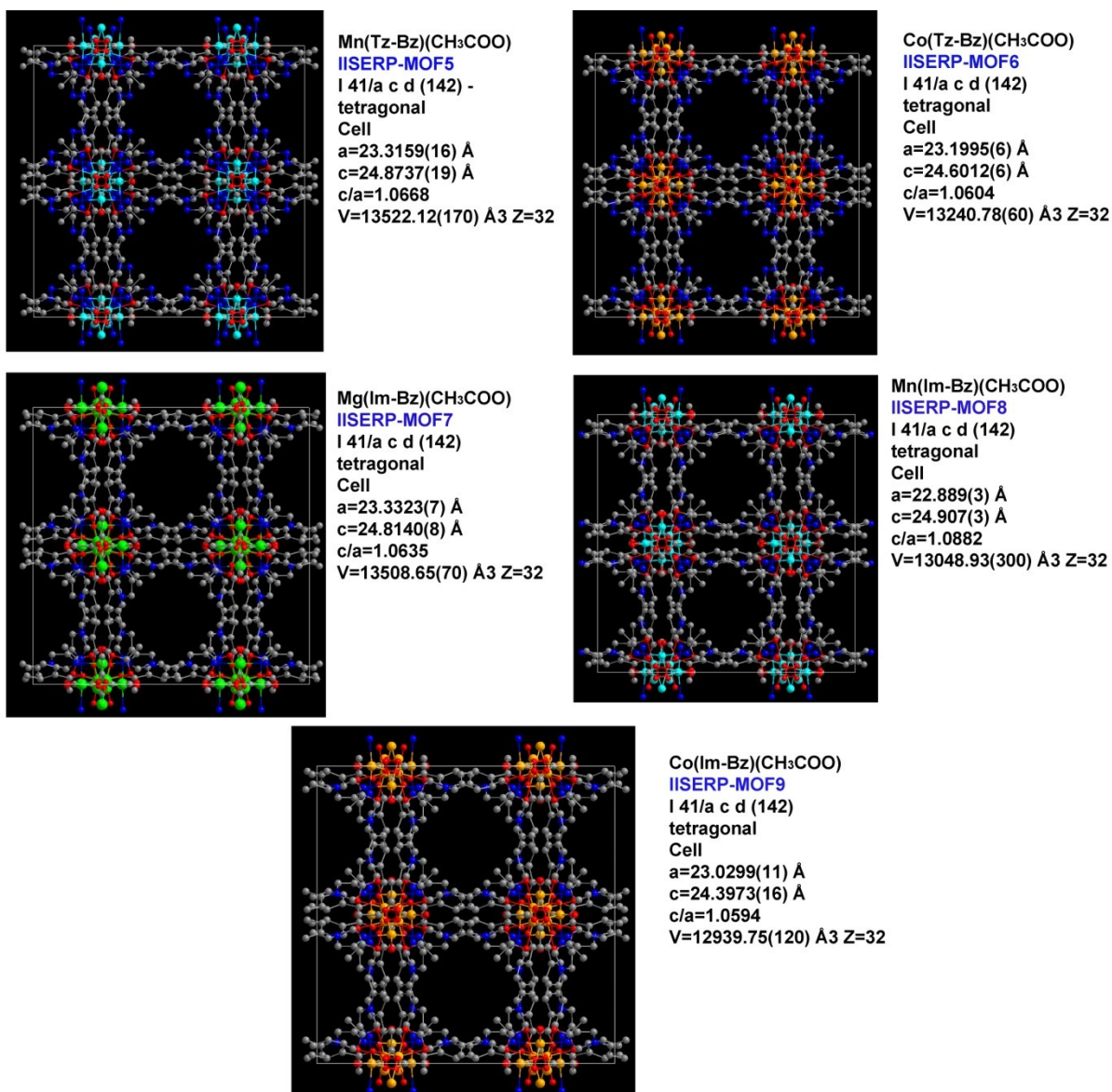


Figure S2. C-axis view of the IISERP-MOFs showing their isostructural frameworks. There are only subtle differences in their lattice parameters.

Powder X-ray diffraction:

Powder XRDs were carried out using a Rigaku Miniflex-600 instrument and processed using PDXL software.

Thermo gravimetric Analysis:

Thermogravimetry was carried out on NETSZCH TGA-DSC system. The routine TGAs were done under N₂ gas flow (20ml/min) (purge + protective) and samples were heated from 25°C to 550°C at 2K/min.

IR spectroscopy:

IR spectra were obtained using a Nicolet ID5 attenuated total reflectance IR spectrometer operating at ambient temperature. The KBr pellets were used for IR data collection.

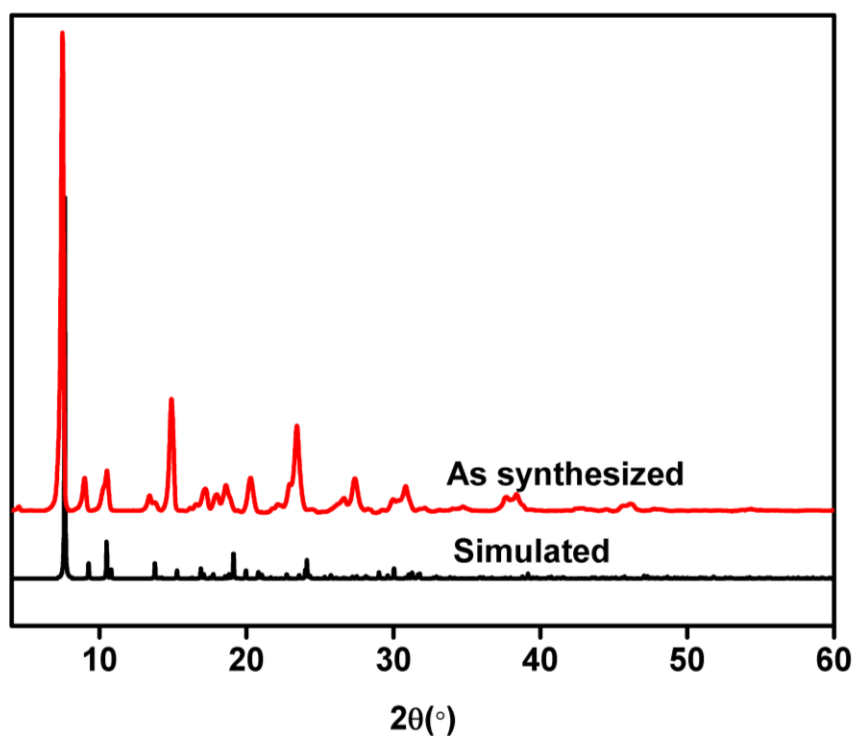


Figure S3. A comparative PXRD plot showing the bulk purity of IISERP-MOF4.

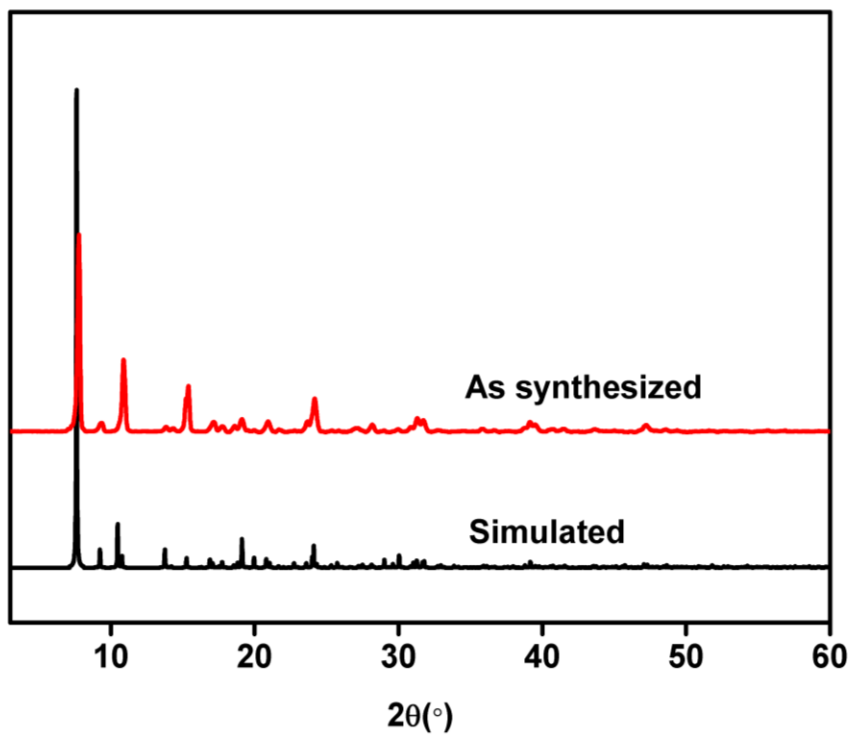


Figure S4. A comparative PXRD plot showing the bulk purity of IISERP-MOF5.

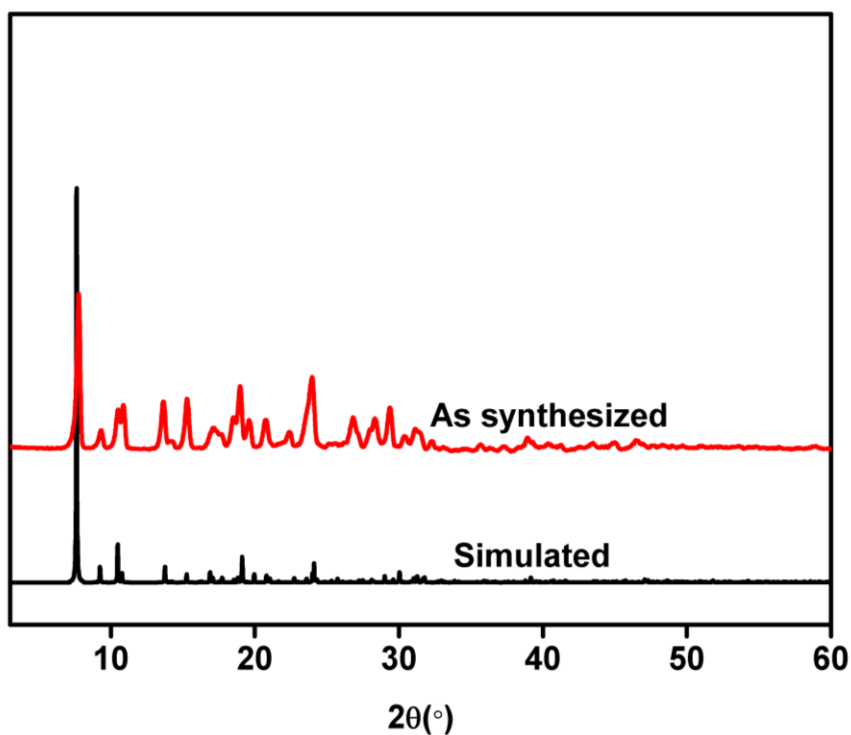


Figure S5. A comparative PXRD plot showing the bulk purity of IISERP-MOF6.

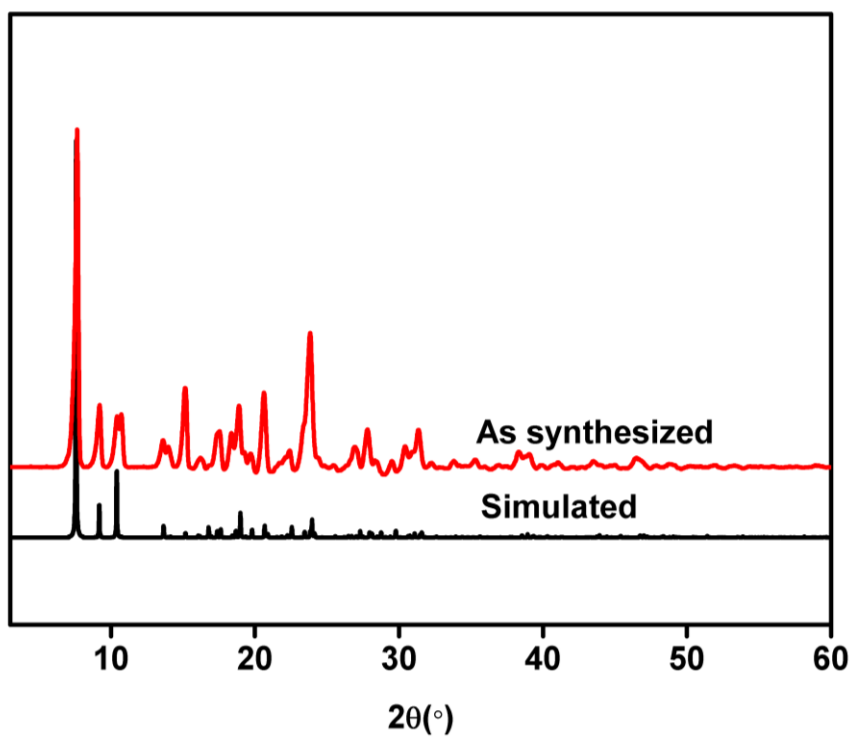


Figure S6. A comparative PXRD plot showing the bulk purity of IISERP-MOF7.

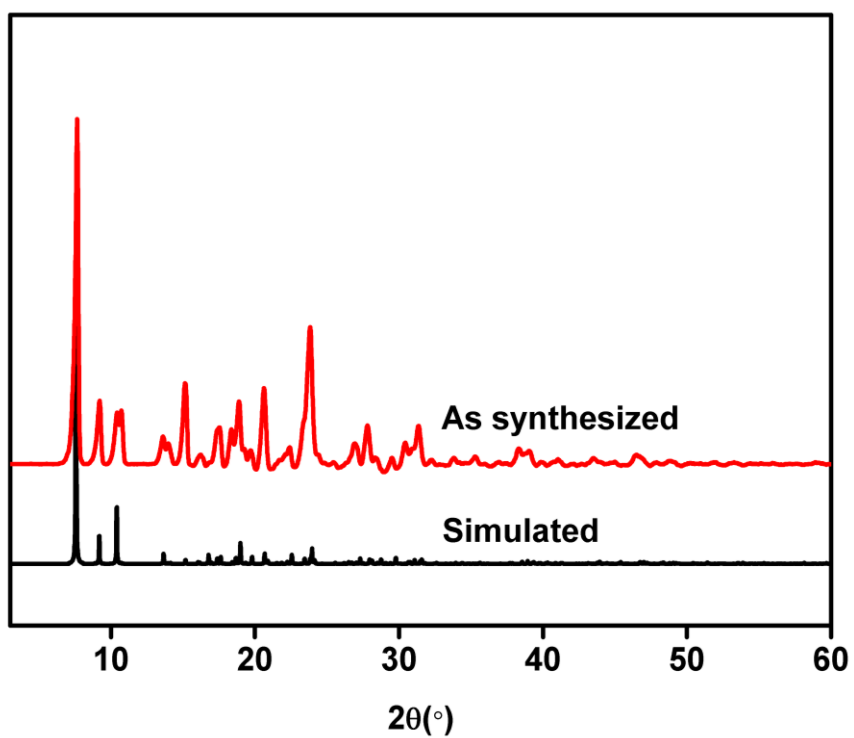


Figure S7. A comparative PXRD plot showing the bulk purity of IISERP-MOF8.

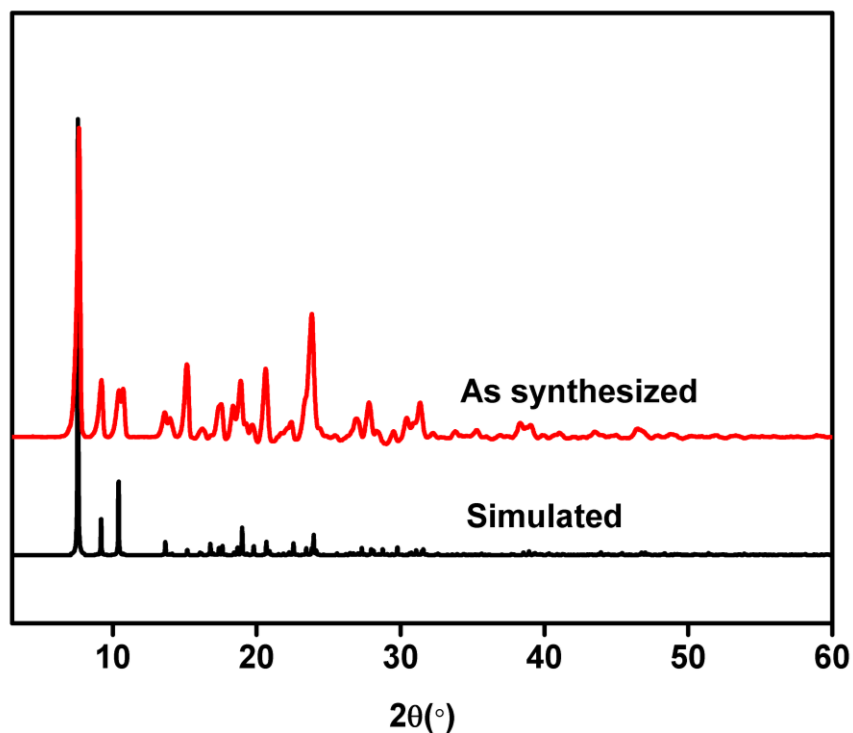


Figure S8. A comparative PXRD plot showing the bulk purity of **IISERP-MOF9**.

Note: In all cases, there are some differences between the simulated and the experimental PXRDs, particularly in their relative intensities. These differences are arising due to preferred orientation, which is expected considering that these MOFs grow as thin-needle shaped crystals and even thorough grinding of the sample could not correct this mis-match in relative intensities. Of course, some contribution could be coming from the solvent variations.

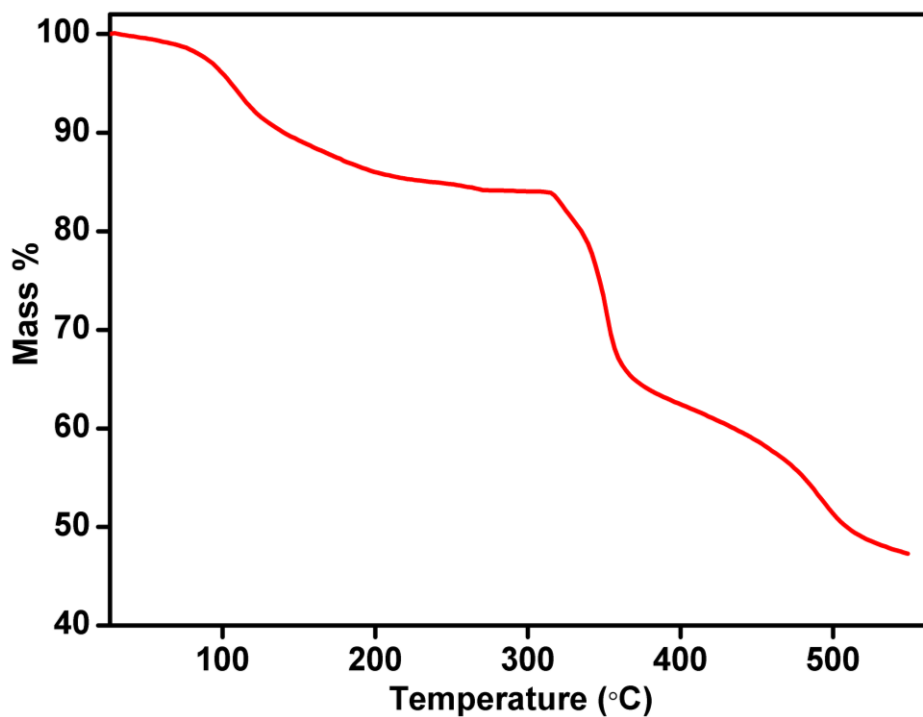


Figure S9. TGA plot for the as synthesized sample of **IISERP-MOF4**. Solvent loss in temperature range 30 to 250°C is 16.90% (calculated=18.24).

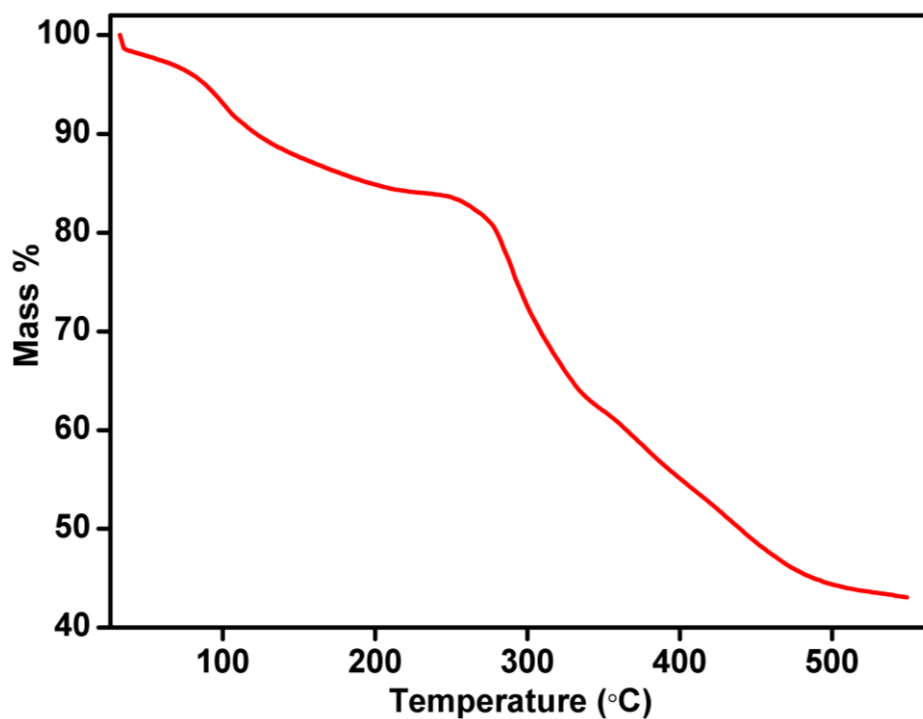


Figure S10. TGA plot for the as synthesized sample of **IISERP-MOF5**. Solvent loss in temperature range 30 to 220°C is 16.22% (calculated=17.67%).

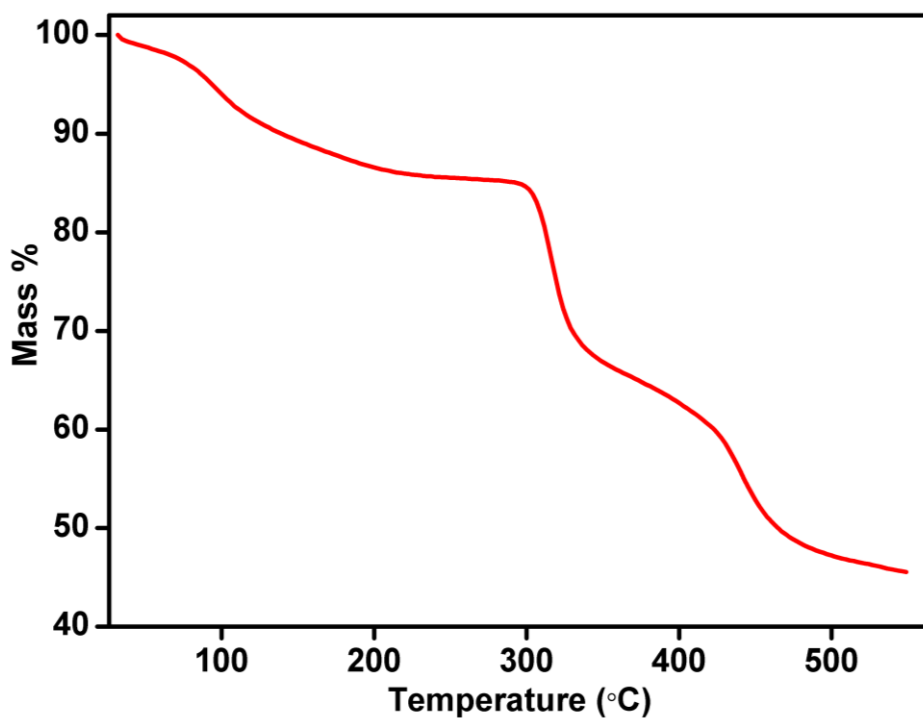


Figure S11. TGA plot for the as synthesized sample of **IISERP-MOF6**. Solvent loss in temperature range 30 to 175° is 15.72% (calculated=16.89%).

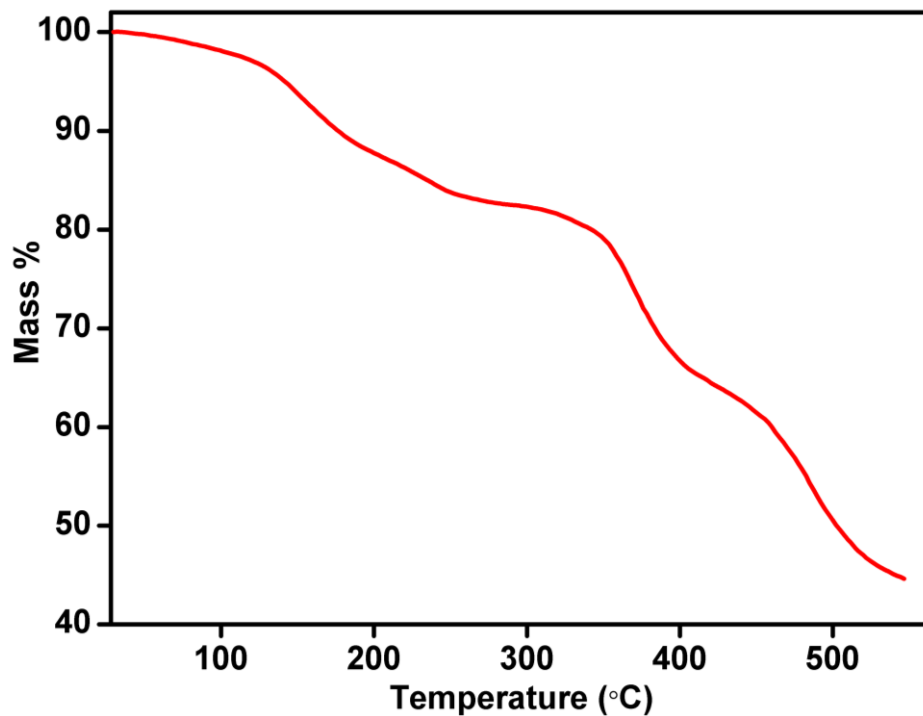


Figure S12. TGA plot carried out using the as synthesized sample of **IISERP-MOF7**. Solvent loss in temperature range 30 to 250°C is 19.22% (calculated=20.39%)

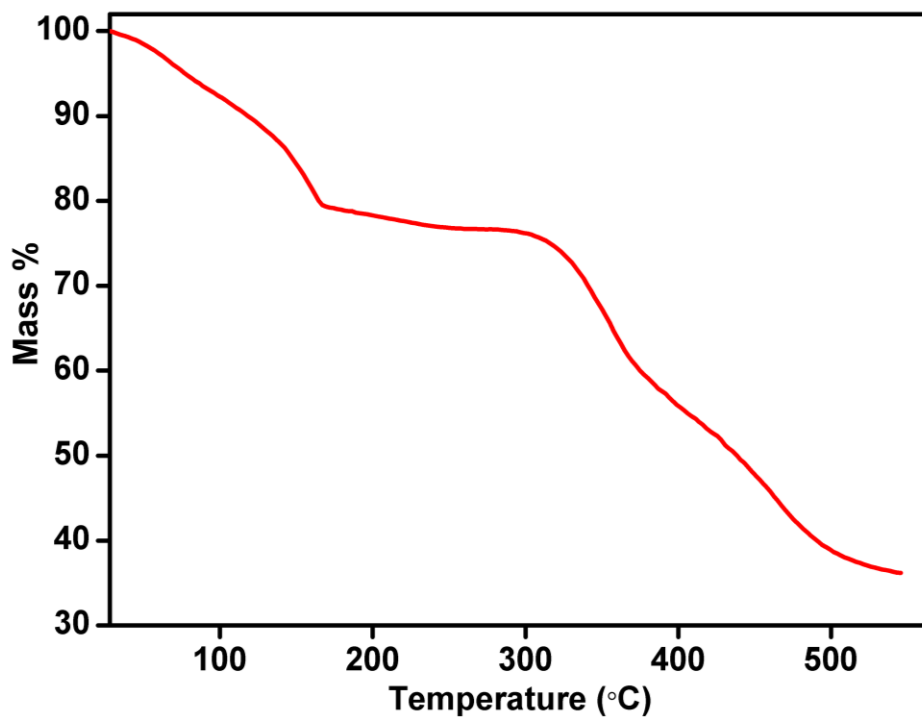


Figure S13. TGA plot for the as synthesized sample of IISERP-MOF8. Solvent loss in temperature range 30 to 200°C is 21.22% (calculated=22.09%).

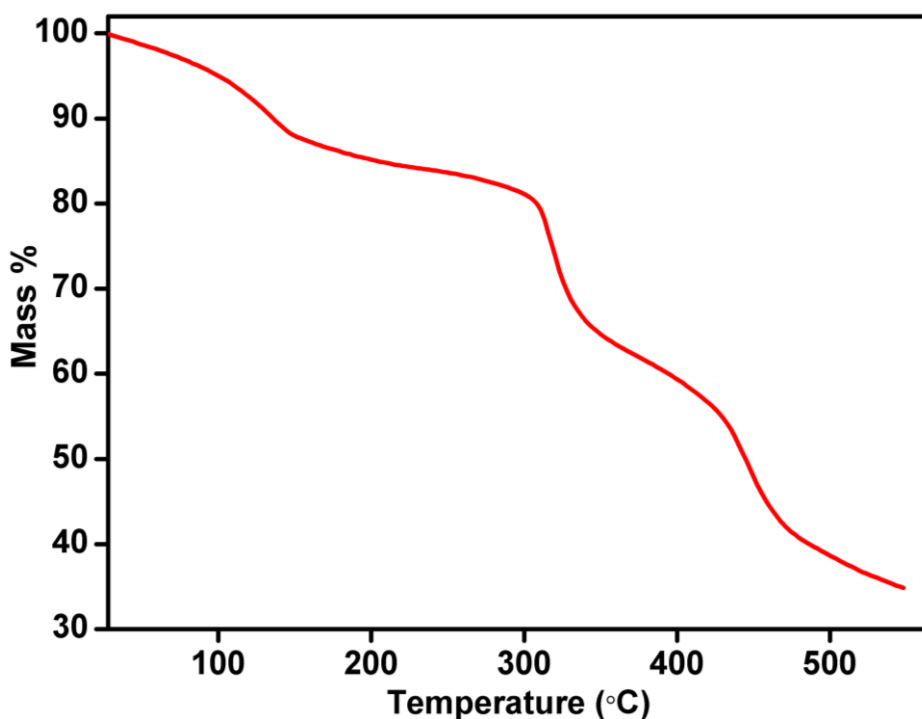


Figure S14. TGA plot for the as synthesized sample of IISERP-MOF9. Solvent loss in temperature range 30 to 220°C is 15.72% (calculated=16.89%).

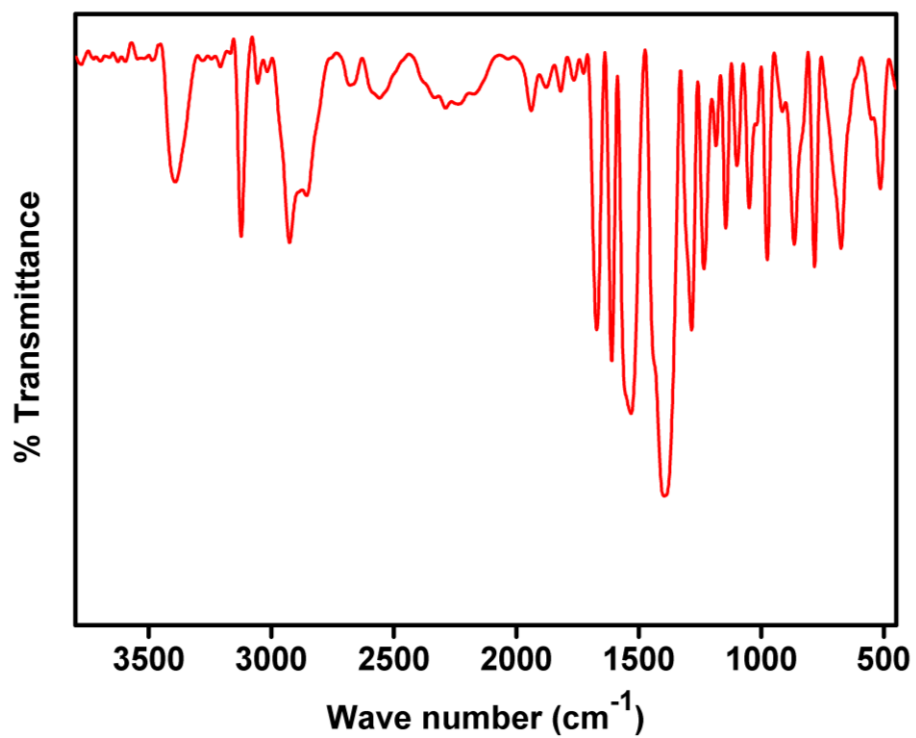


Figure S15. IR spectra of IISERP-MOF4 showing the characteristic stretching frequencies.

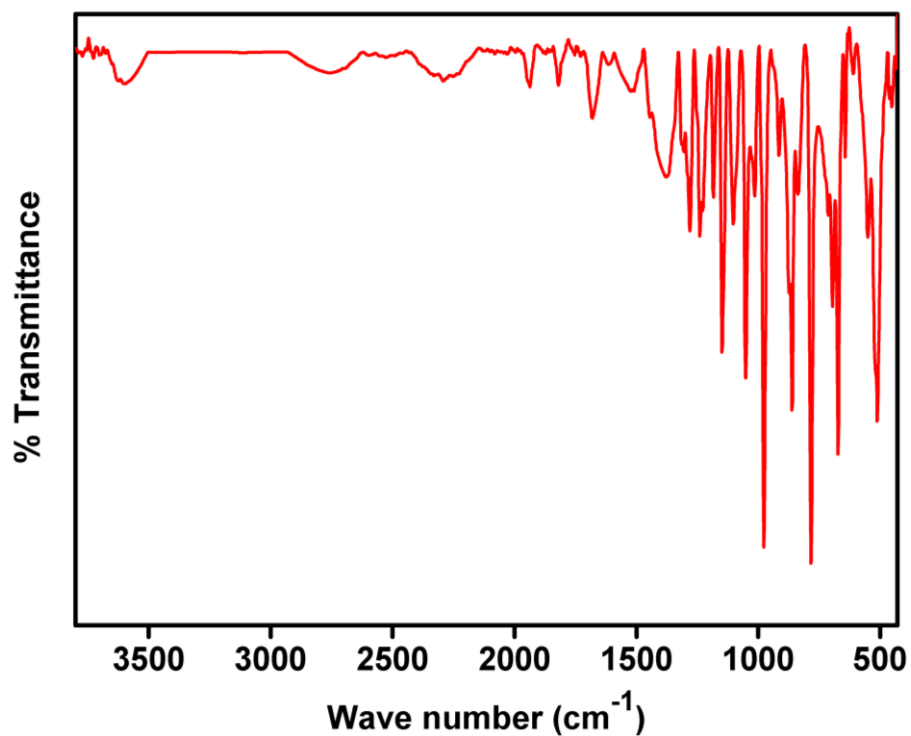


Figure S16. IR spectra of IISERP-MOF5 showing the characteristic stretching frequencies.

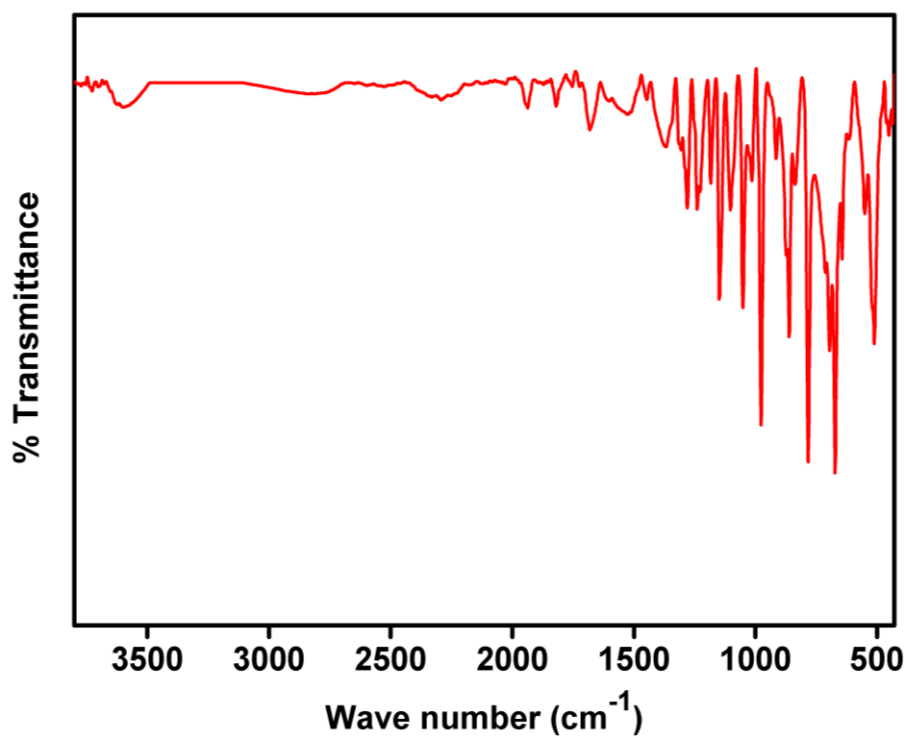


Figure S17. IR spectra of IISERP-MOF6 showing different characteristics stretching frequencies.

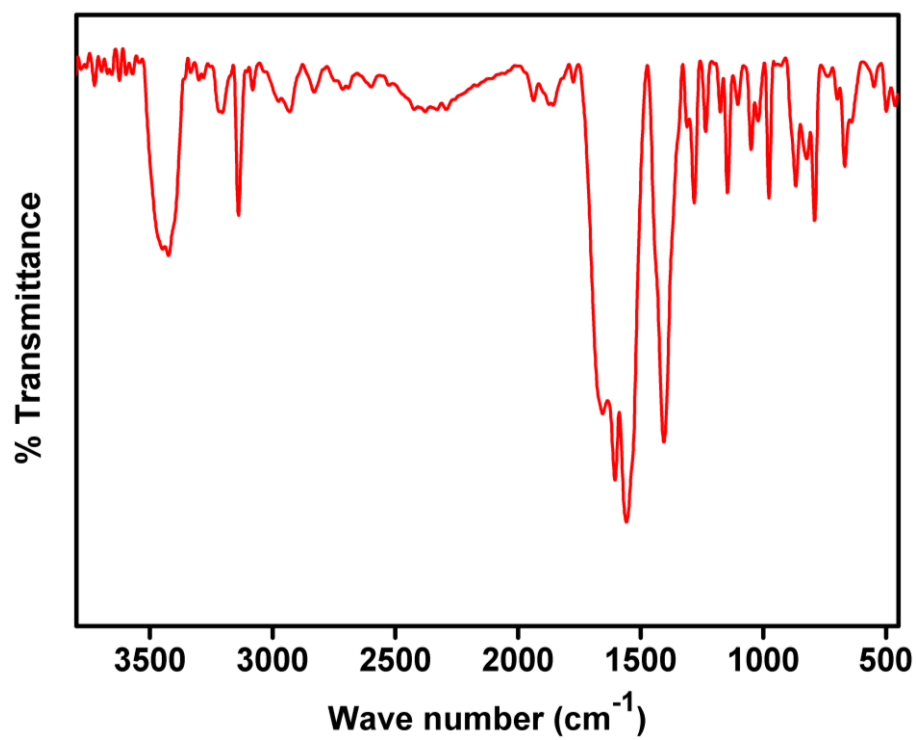


Figure S18. IR spectra of IISERP-MOF7 showing characteristic stretching frequencies.

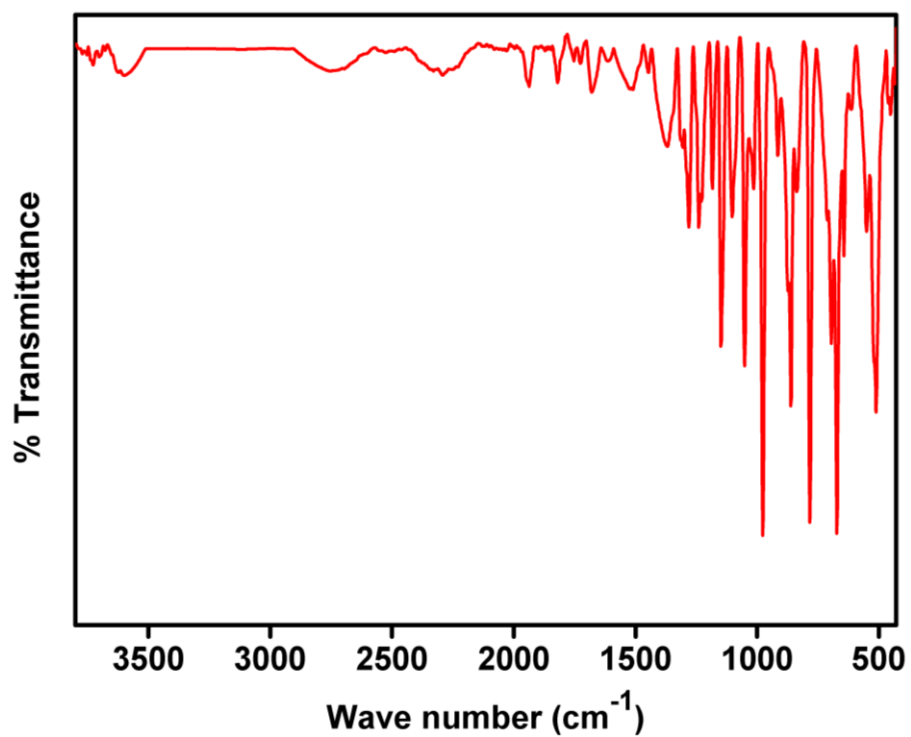


Figure S19. IR spectra of IISERP-MOF8 showing characteristics stretching frequencies.

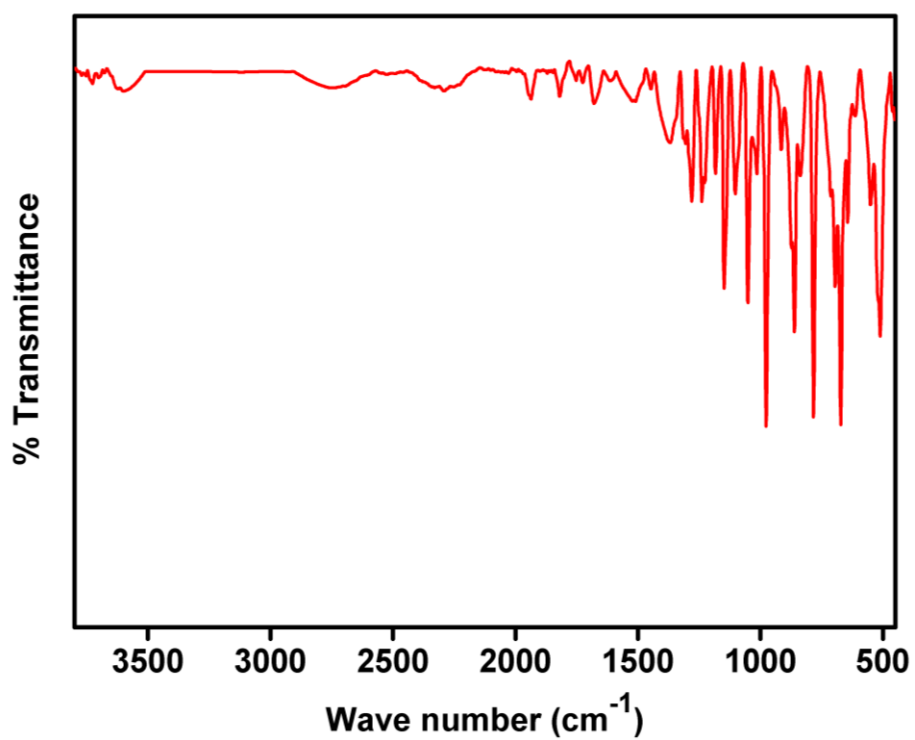


Figure S20. IR spectra of IISERP-MOF9 showing different characteristic stretching frequencies.

3. Adsorption Analyses:

All gas sorption isotherms were measured on a Micromeritics ASAP 2020HD instrument using ultra-high purity gases (≥ 4.8 grade). Samples were first soaked in DCM and MeOH mixture for 4 days with replenishing the solvent in every 12 hrs. Then the solvent exchanged and dried sample (about 100mg) was transferred to a glass tube for analysis, with one step activation: evacuation at 120°C on the degas port for 24hrs (10^{-6} mbar), at which point the outgas rate was ≤ 2 μ bar/min.

Langmuir Fits:

In most cases the isotherms were fit to the Single-Site Langmuir (SSL) equation. Also modified Langmuir equations were utilized to account for significant errors in the Langmuir model. It is widely known that even small fitting errors will have a devastating impact on selectivity calculations.

The isotherms were fit by solving the Langmuir equation using the Microsoft Excel following a similar protocol to Keller *et al.*^{s2} Utilizing this routine circumvents some of the problems associated with favouring either high or low pressure regions when linearizing the Langmuir equation^{s3} and offers a balanced approach.

Single-Site Langmuir (SSL):

$$q_i = q_m \frac{K_i P}{1 + K_i P}$$

Dual-Site Langmuir (DSL):

$$q_i = q_{m,1} \frac{K_1 P}{1 + K_1 P} + q_{m,2} \frac{K_2 P}{1 + K_2 P}$$

Dual-Site Langmuir (DSL):

$$q_i = q_{m,1} \frac{K_1 P}{1 + K_1 P} + q_{m,2} \frac{K_2 P}{1 + K_2 P}$$

Ideal Adsorbed Solution Theory (IAST):

IAST calculations were undertaken as described by Nandi *et al.*^{S4} The selectivity equation is provided below.

Selectivity:

$$S_{1,2} = \frac{q_1/q_2}{P_1/P_2}$$

(S2) Kemmer, G.; Keller, S. *Nat. Protoc.* **2010**, *5*, 267–81.

(S3) Richter, E.; Schuetz, W.; Myers, A. L. *Chem. Eng. Sci.* **1989**, *44*, 1609–1616.

(S4) Nandi *et al. Sci. Adv.* **2015**, *1* DOI:e1500421

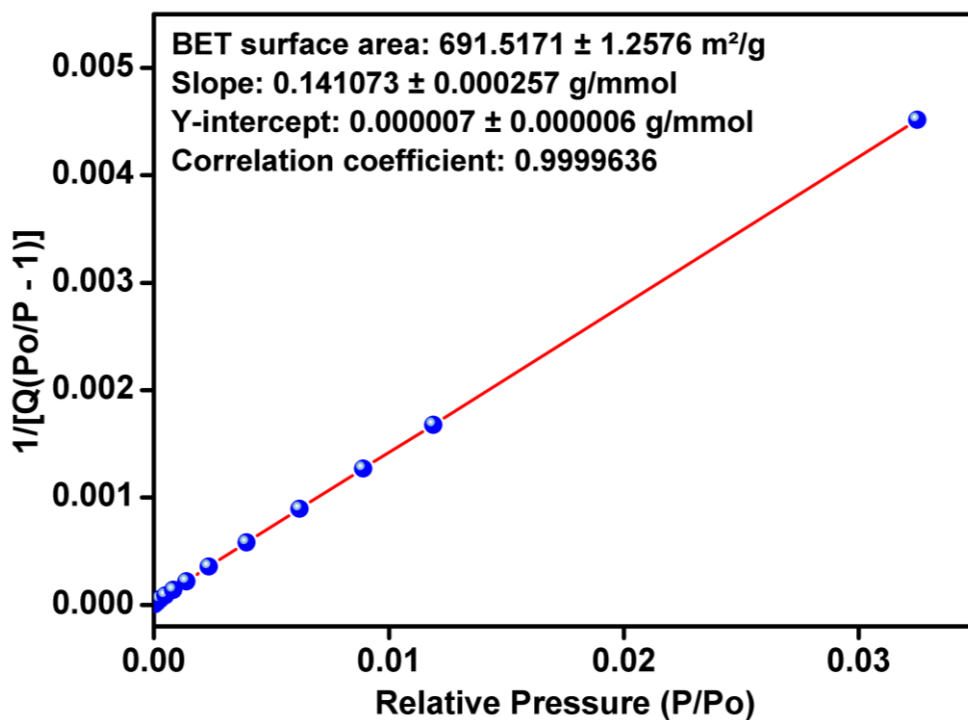


Figure S21. BET fit for IISERP-MOF4 from the 77K N₂ data.

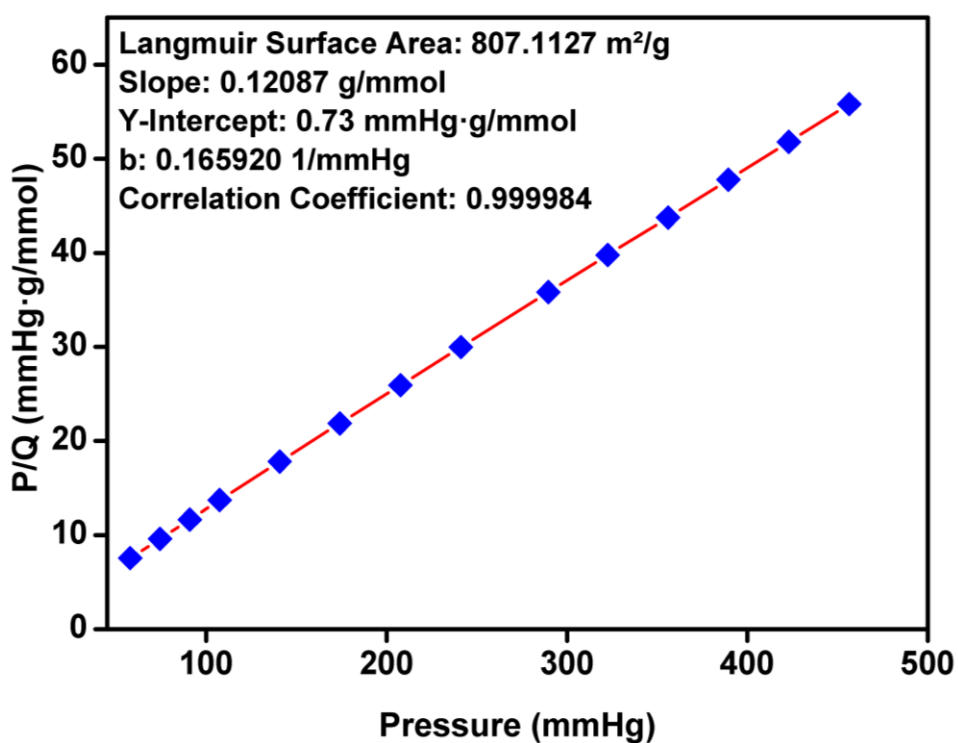


Figure S22. Langmuir fit for IISERP-MOF4 from the 77K N₂ data.

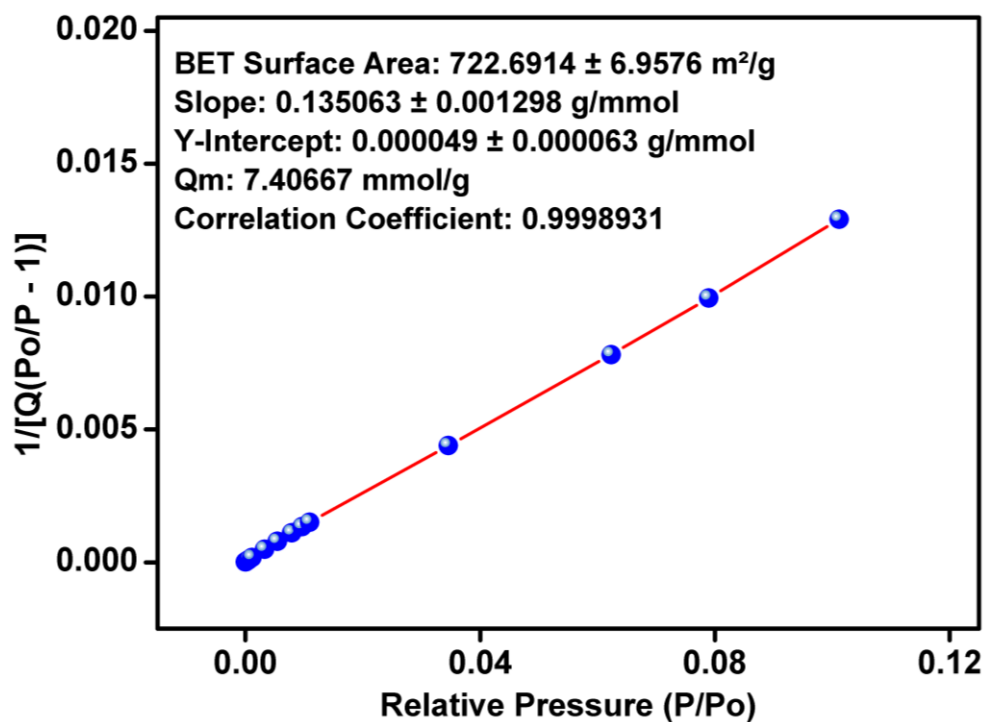


Figure S23. BET fit for IISERP-MOF5 from the 77K N₂ data.

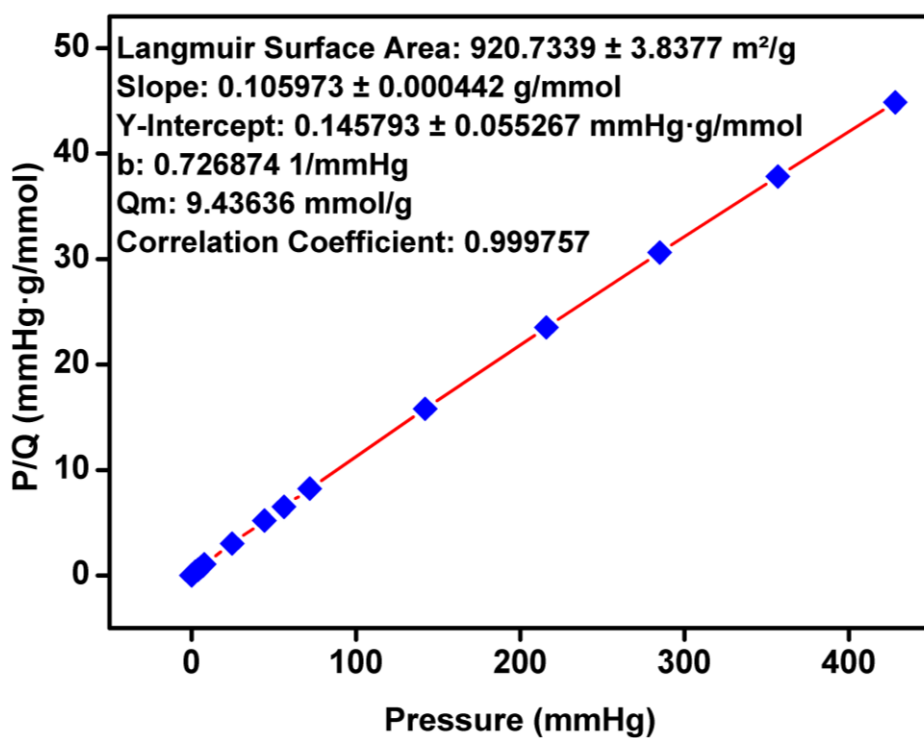


Figure S24. Langmuir fit for IISERP-MOF5 from the 77K N₂ data.

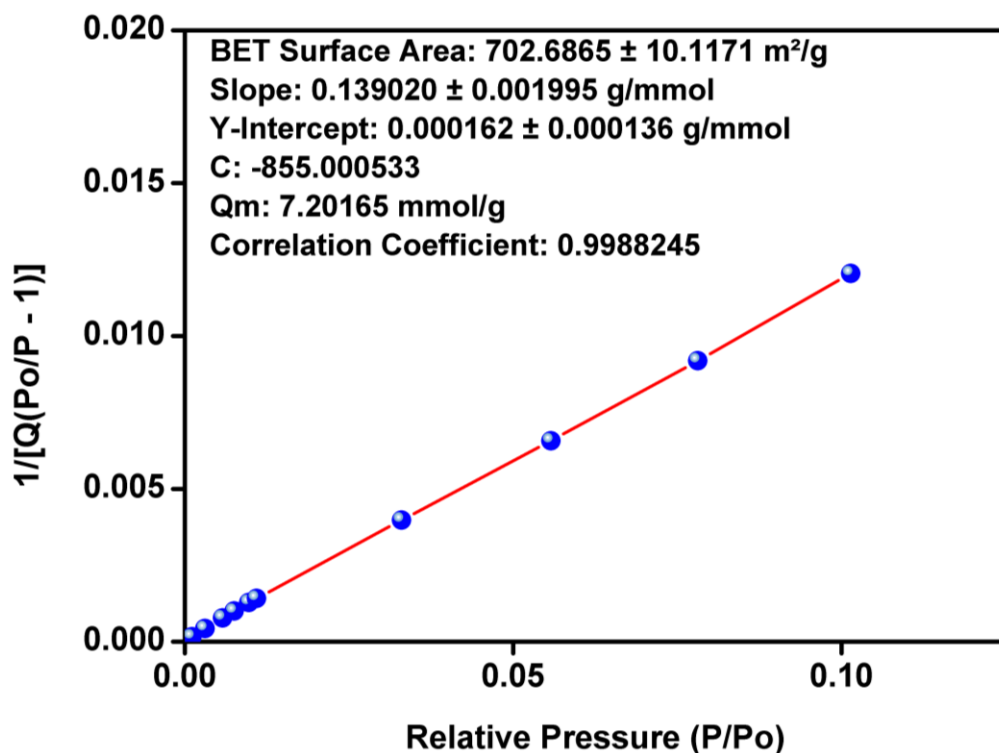


Figure S25. BET fit for IISERP-MOF6 from the 77K N₂ data.

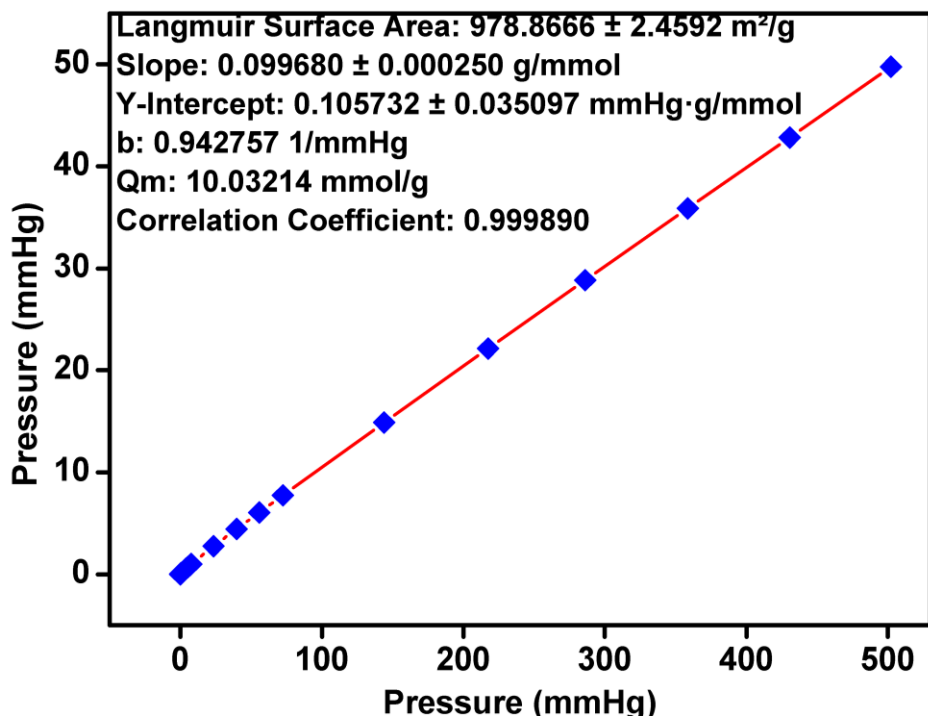


Figure S26. Langmuir fit for IISERP-MOF6 from the 77K N₂ data.

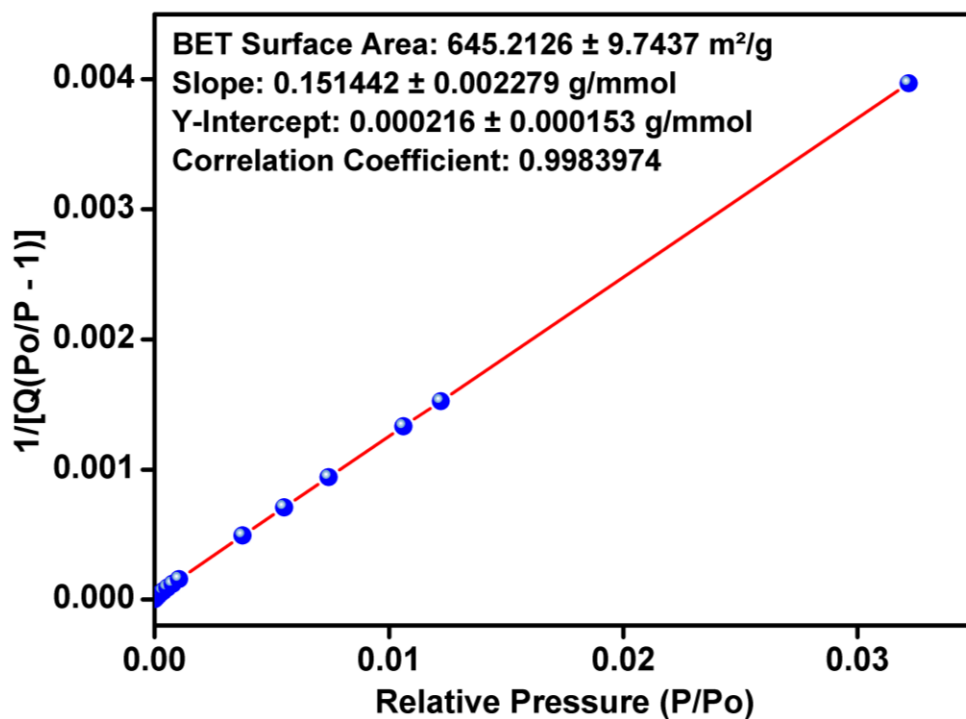


Figure S27. BET fit for IISERP-MOF7 from the 77K N₂ data.

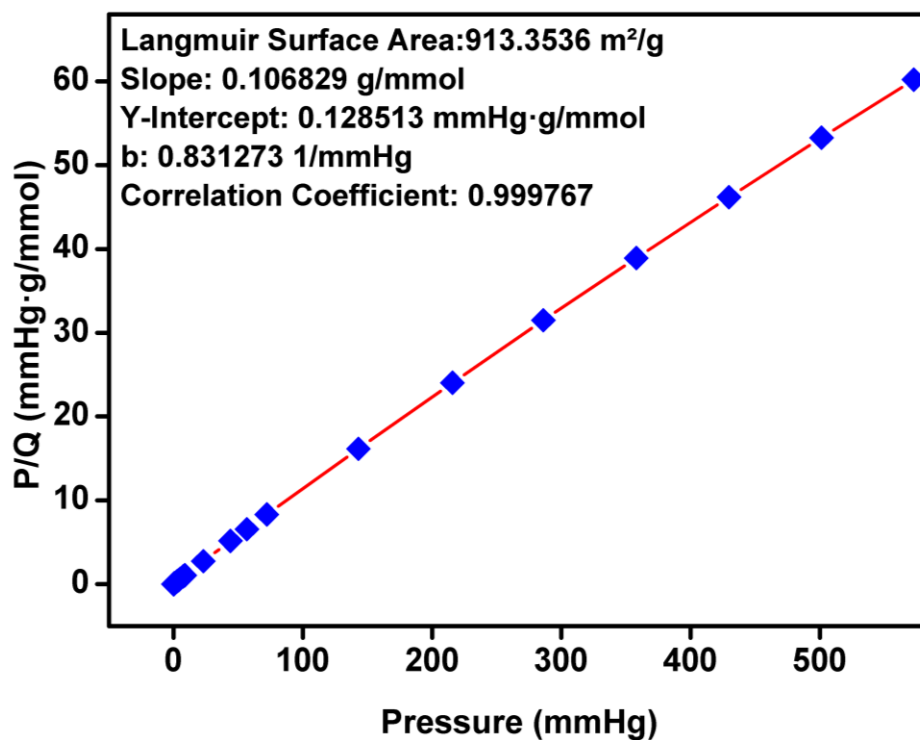


Figure S28. Langmuir fit for IISERP-MOF7 from the 77K N₂ data.

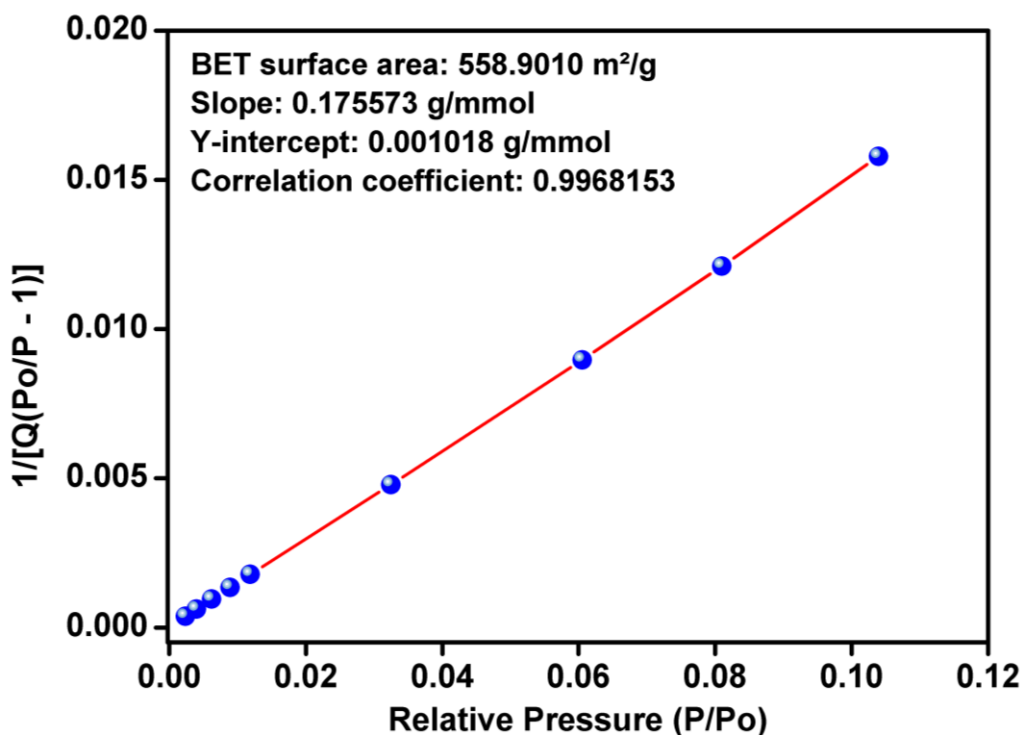


Figure S29. BET fit for IISERP-MOF8 from the 77K N₂ data.

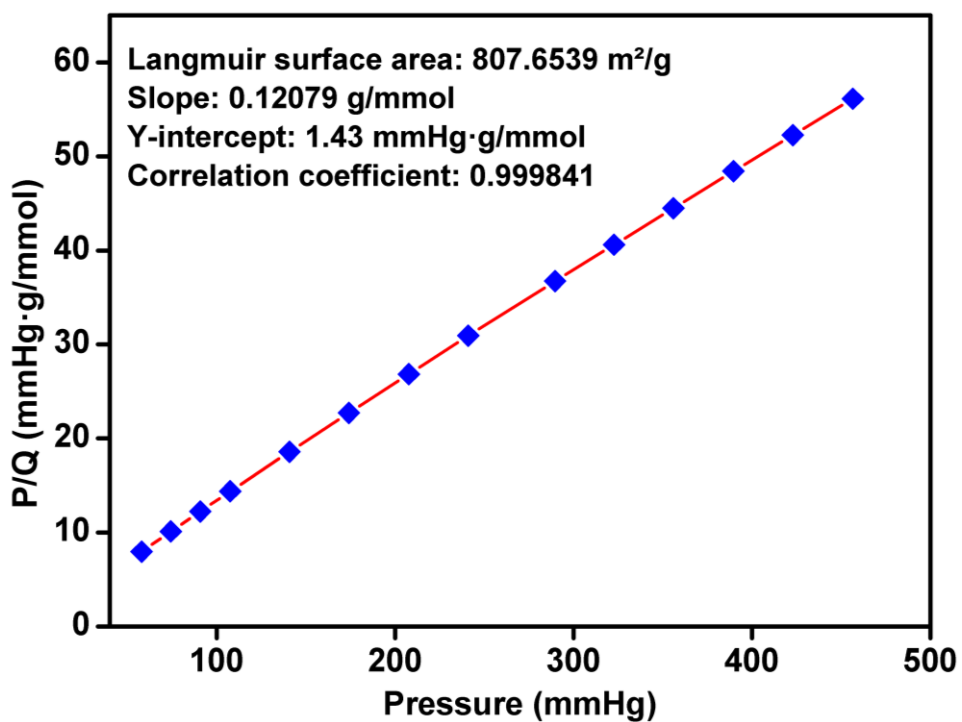


Figure S30. Langmuir fit for IISERP-MOF8 from the 77K N₂ data.

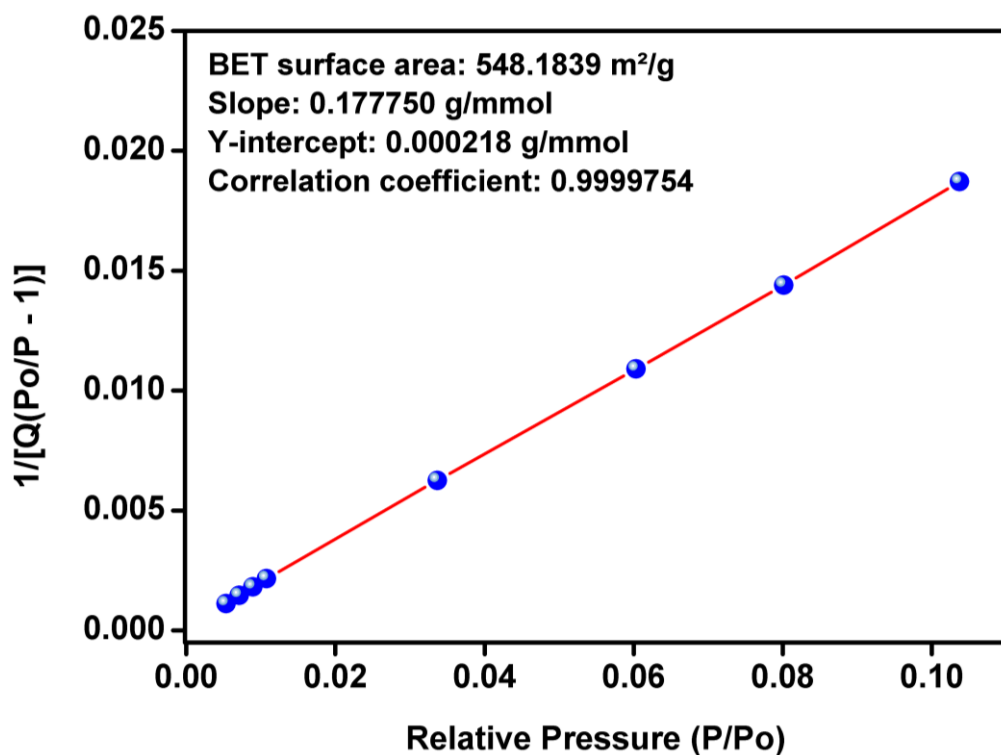


Figure S31. BET fit for IISERP-MOF9 from the 77K N₂ data.

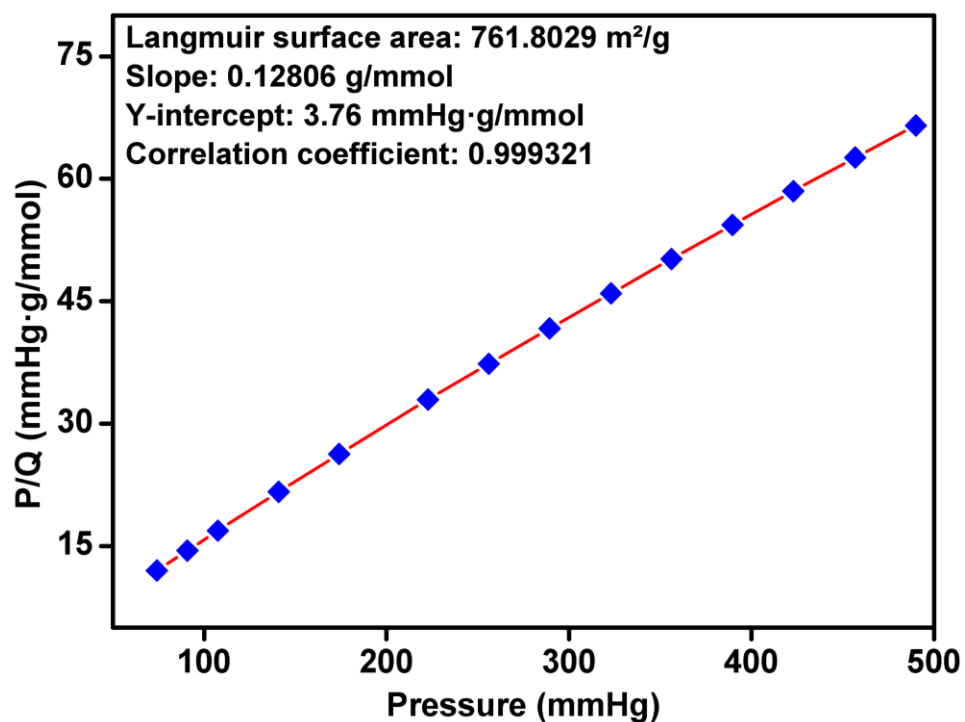


Figure S32. Langmuir fit for IISERP-MOF9 from the 77K N₂ data.

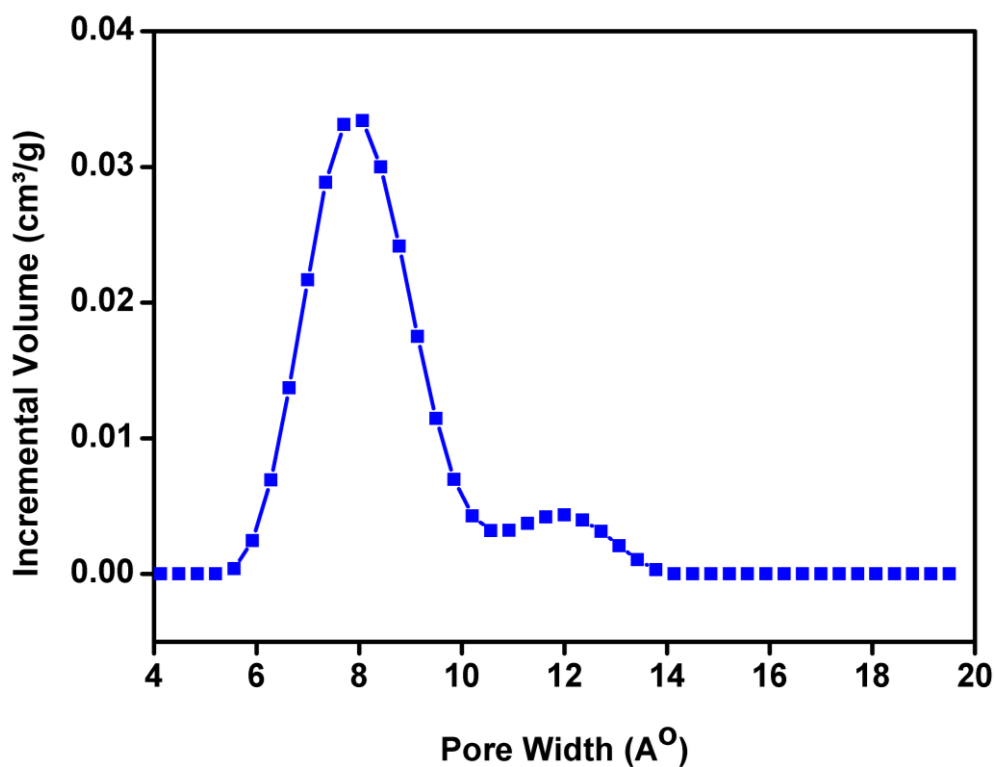


Figure S33. Pore size distribution in IISERP-MOF4 obtained by fitting NLDFT model to the 77K N₂ adsorption branch. Note the average pore diameter of 8.0 Å was obtained from the fit. This agrees well with the pore dimension observed in the single crystal structure.

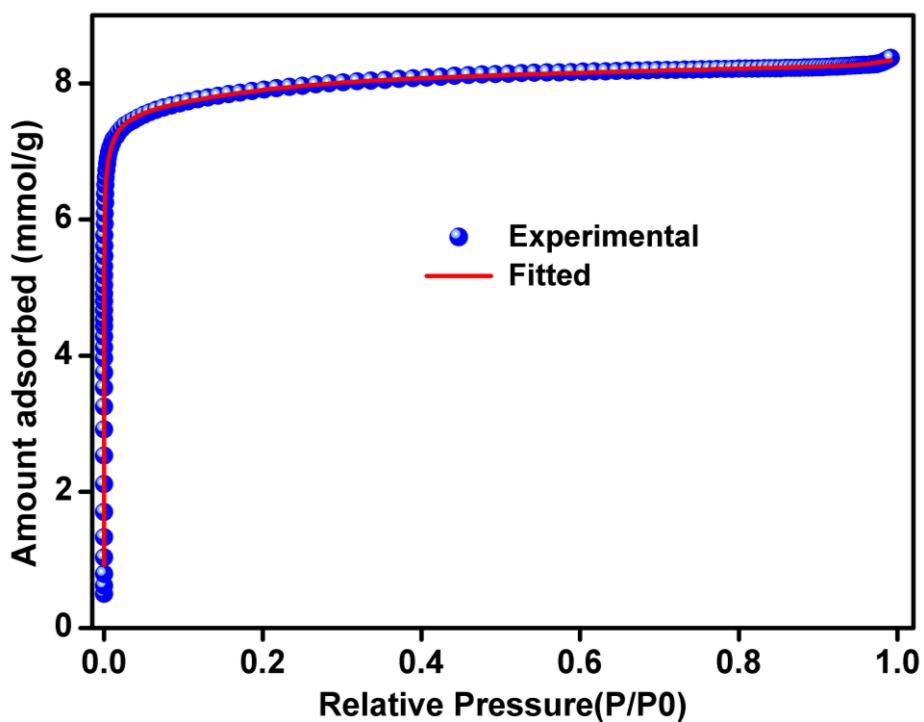


Figure S34. Shows the fitting comparison for IISERP-MOF4 obtained for the NLDFT fit done using the adsorption branch of the 77K N₂ adsorption data.

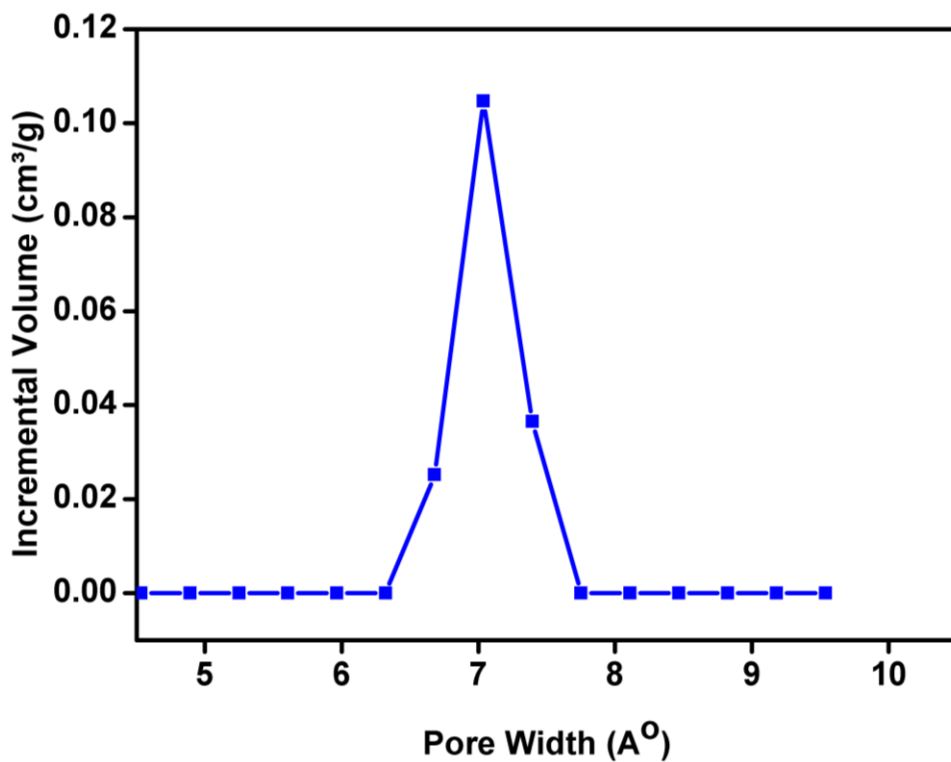


Figure S35. Pore size distribution in IISERP-MOF5 obtained by fitting the NLDFT model to the 77K N₂ adsorption branch. Note the an average pore diameter of 7.0 Å was estimated from the fit.

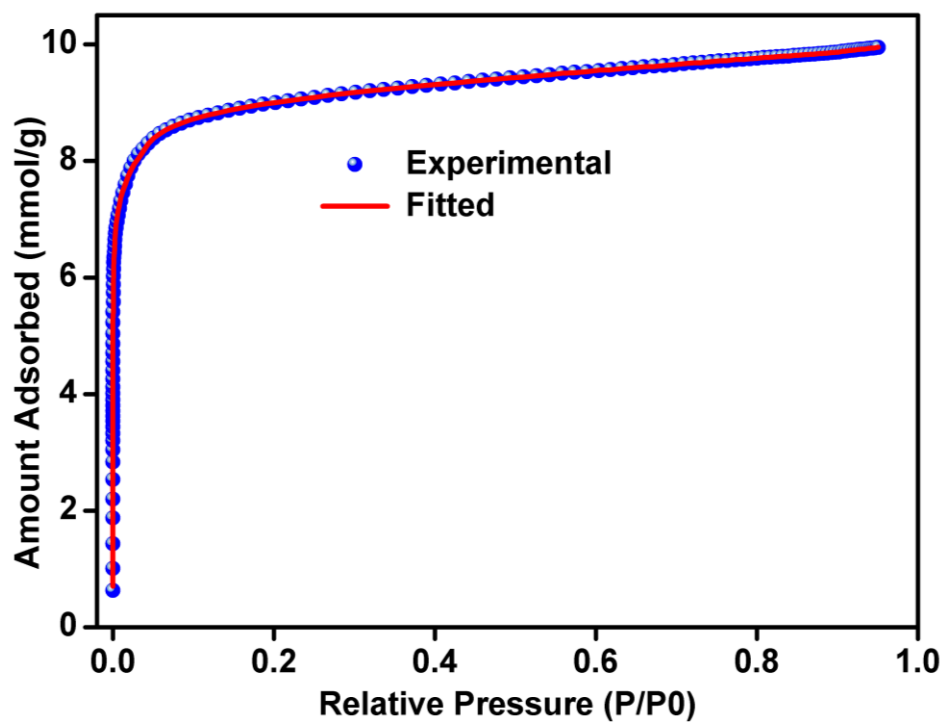


Figure S36. Shows the fitting comparison for IISERP-MOF5 obtained for the NLDFT fit done using the adsorption branch of the 77K N₂ adsorption data.

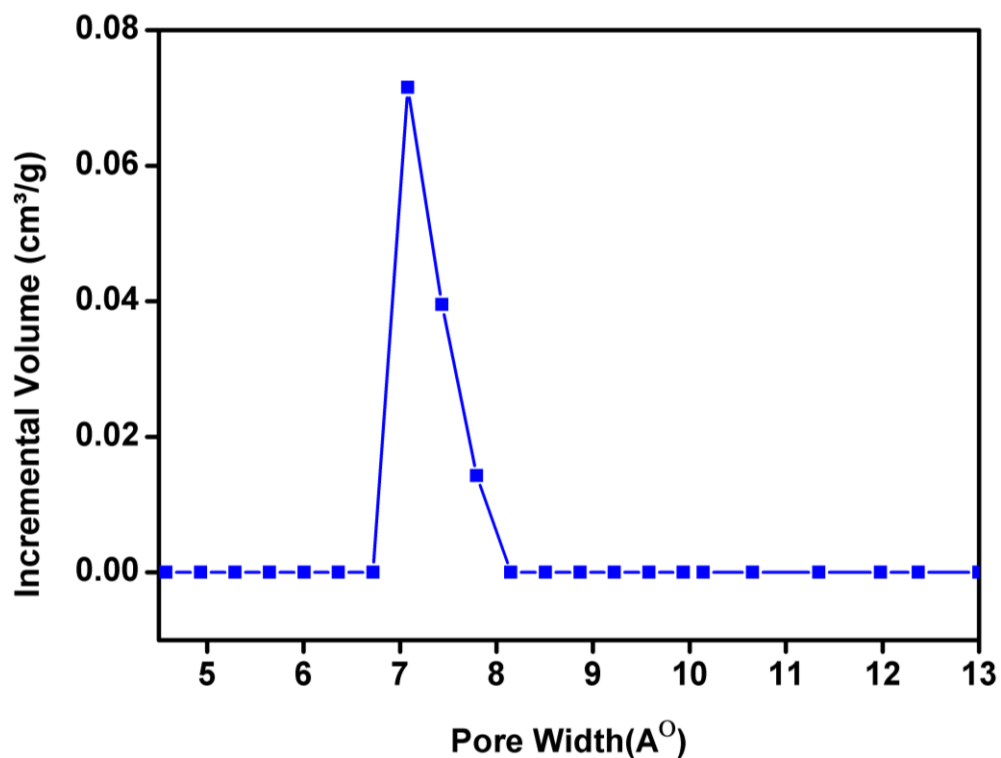


Figure S37. Pore size distribution in **IISERP-MOF6** obtained by fitting the NLDFT model to the 77K N₂ adsorption branch. Note the average pore diameter of 7.1 Å was obtained from the fit. This agrees well with the pore dimension observed in the single crystal structure.

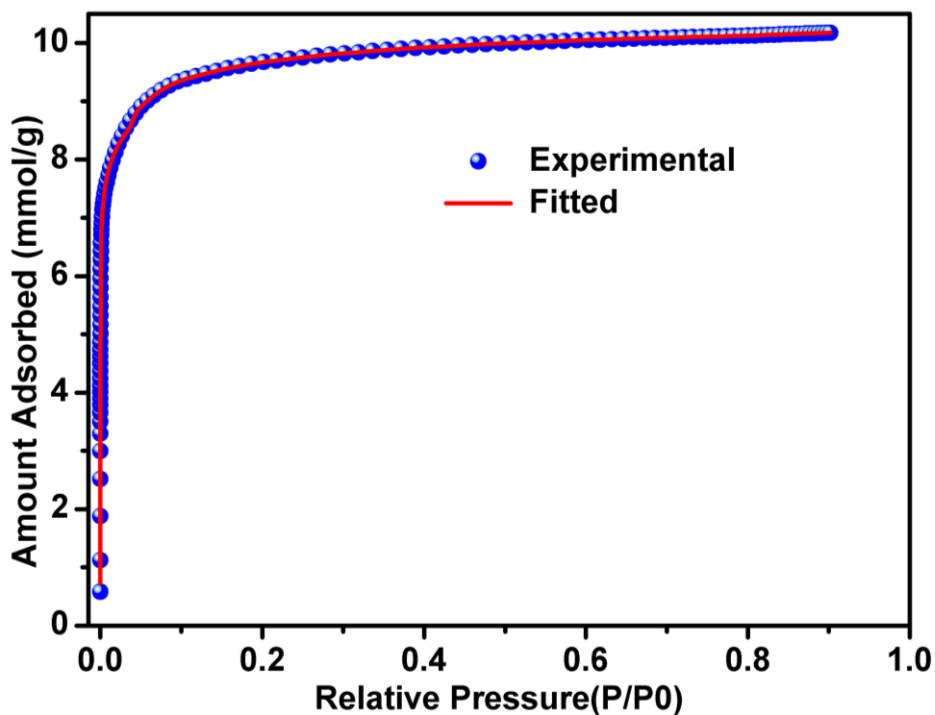


Figure S38. Shows the fitting comparison for **IISERP-MOF6** obtained for the NLDFT fit carried out using the adsorption branch of the 77K N₂ adsorption data.

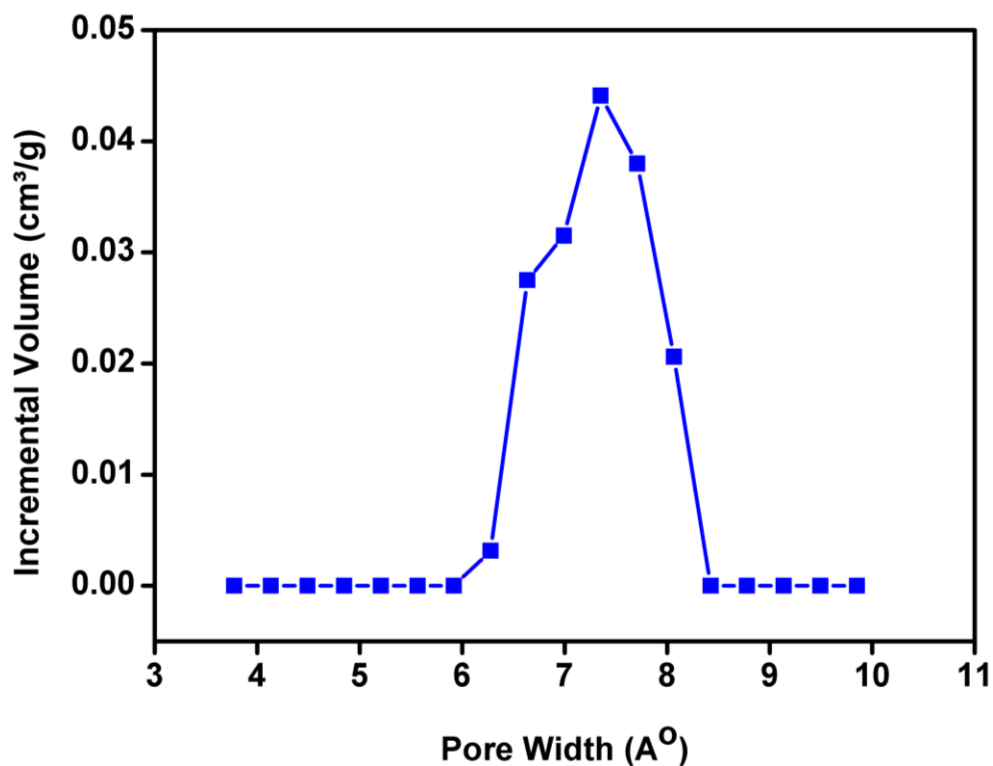


Figure S39. Pore size distribution in IISERP-MOF7 obtained by fitting the NLDFT model to the 77K N₂ adsorption branch. Note the average pore diameter of 7.3 Å was obtained from the fit.

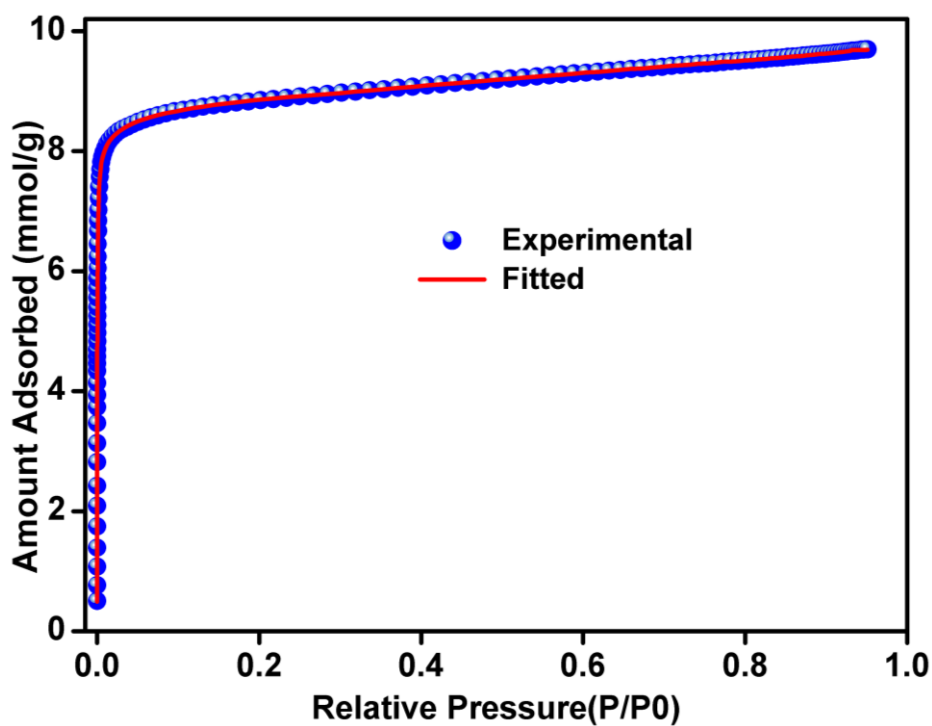


Figure S40. Shows the fitting comparison for IISERP-MOF7 obtained for the NLDFT fit from the adsorption branch of the 77K N₂ adsorption data.

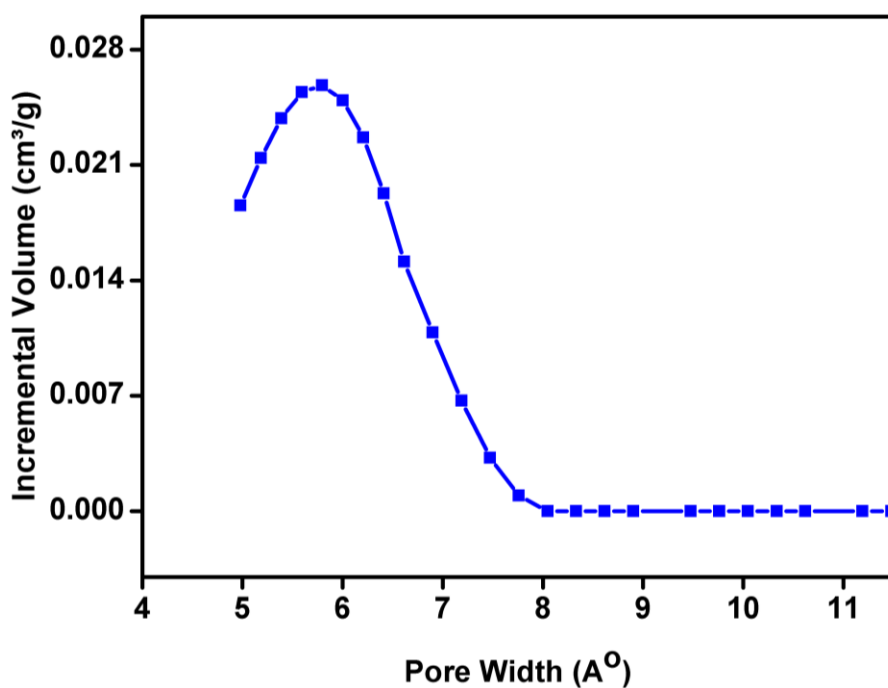


Figure S41. Pore size distribution in **IISERP-MOF8** obtained by fitting the NLDFT model to the 77K N₂ adsorption branch. Note the average pore diameter of 6.0 Å . This agrees well with the pore dimension observed in the single crystal structure.

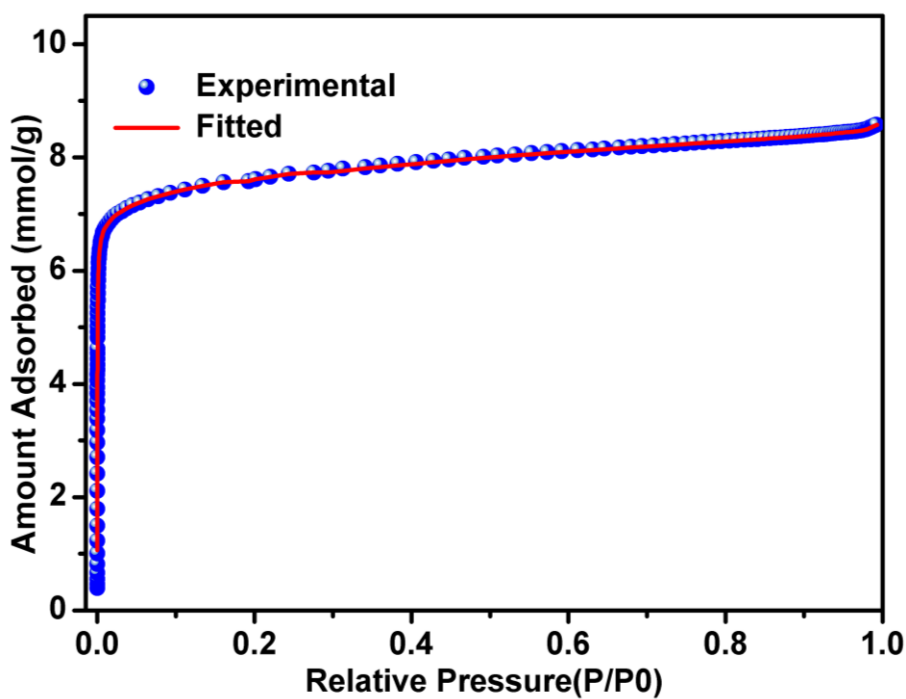


Figure S42. Shows the fitting comparison for **IISERP-MOF8** obtained for the NLDFT fit done using the adsorption branch of the 77K N₂ adsorption data.

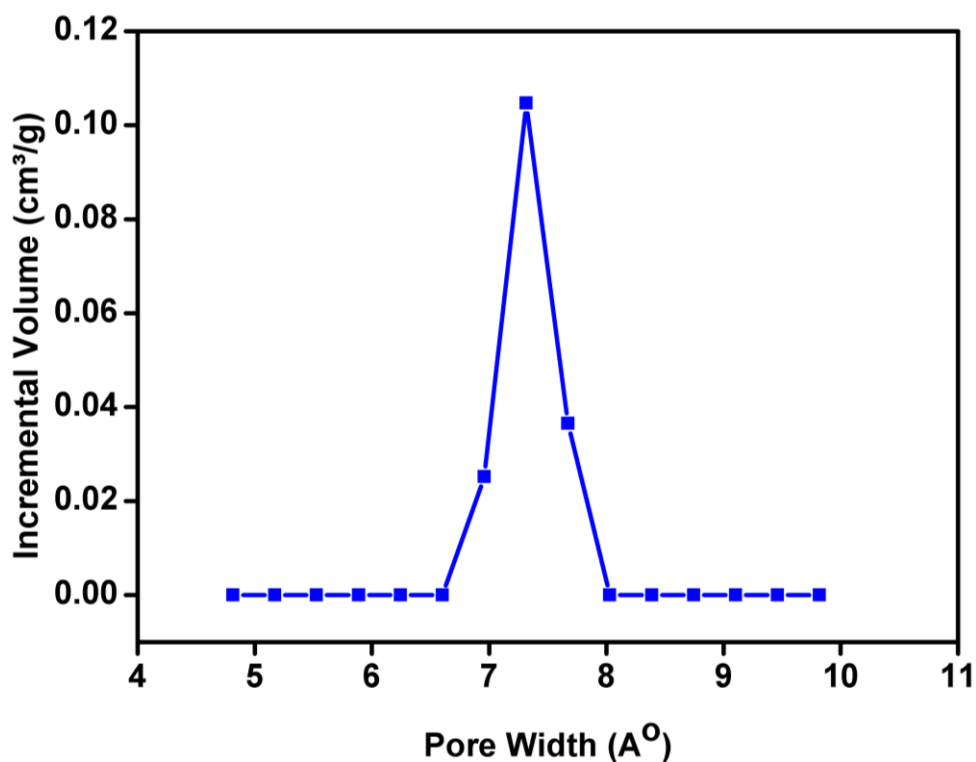


Figure S43. Pore size distribution in **IISERP-MOF9** obtained by fitting the NLDFT model to the 77K N₂ adsorption branch. Note the average pore diameter of 7.2 Å was obtained from the fit.

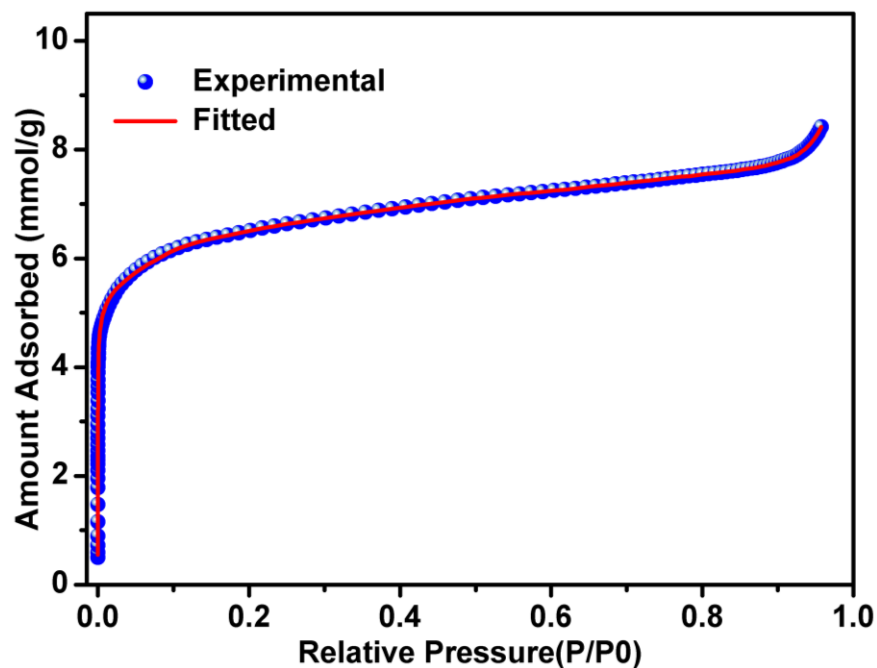


Figure S44. Shows the fitting comparison for **IISERP-MOF9** obtained for the NLDFT fit done using the adsorption branch of the 77K N₂ adsorption data.

Virial analysis:

The CO₂ adsorption data were measured from 0- 1bar at 303, 283, 273, 263, 248 and 195K. For virial fitting the 303, 283, 273 and 263K isotherms were taken and fitted by the virial equation (1).

$$\ln(P) = \ln(Va) + (A0 + A1*Va + A2*Va^2 \dots + A6*Va^6)/T + (B0 + B1*Va) \dots \dots \dots (1)$$

Where P is pressure, Va is amount adsorbed, T is temperature, and A0, A1, A2 ... , A4 and B0, B1 are temperature independent empirical parameters

Table S1: Summary of the fitted Virial parameters for IISERP-MOF4

A0	-2722.621886
A1	190.7436991
A2	-6.407377843
A3	-14.83487308
A4	3.691722007
B0	14.46887252
B1	-0.413493728
B2	-0.018961943

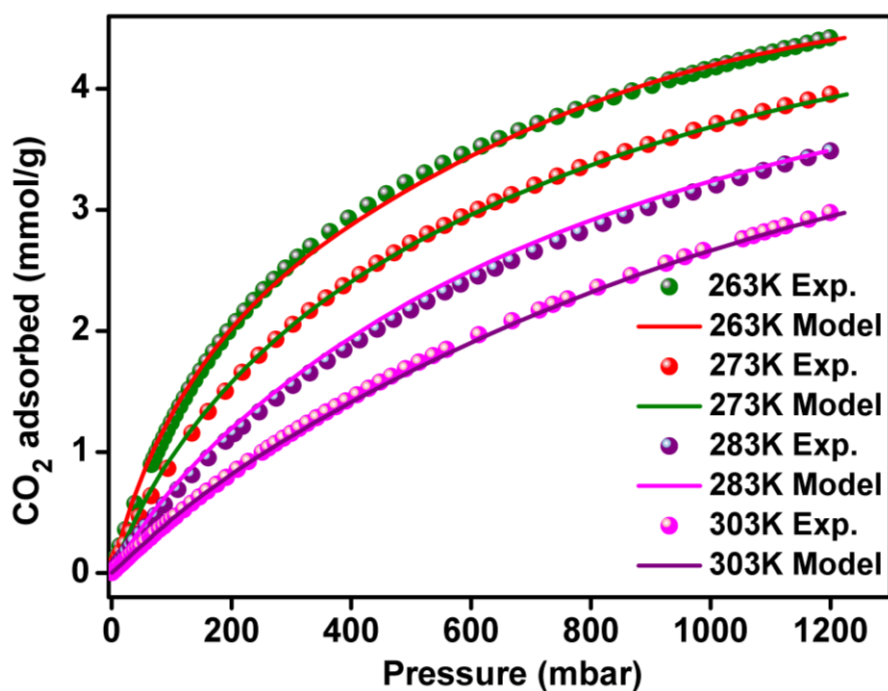


Figure S45. Comparison of experimental isotherms of IISERP-MOF4 to the ones obtained from virial modelling carried out using CO₂ isotherms collected at 303, 283, 273 and 263K.

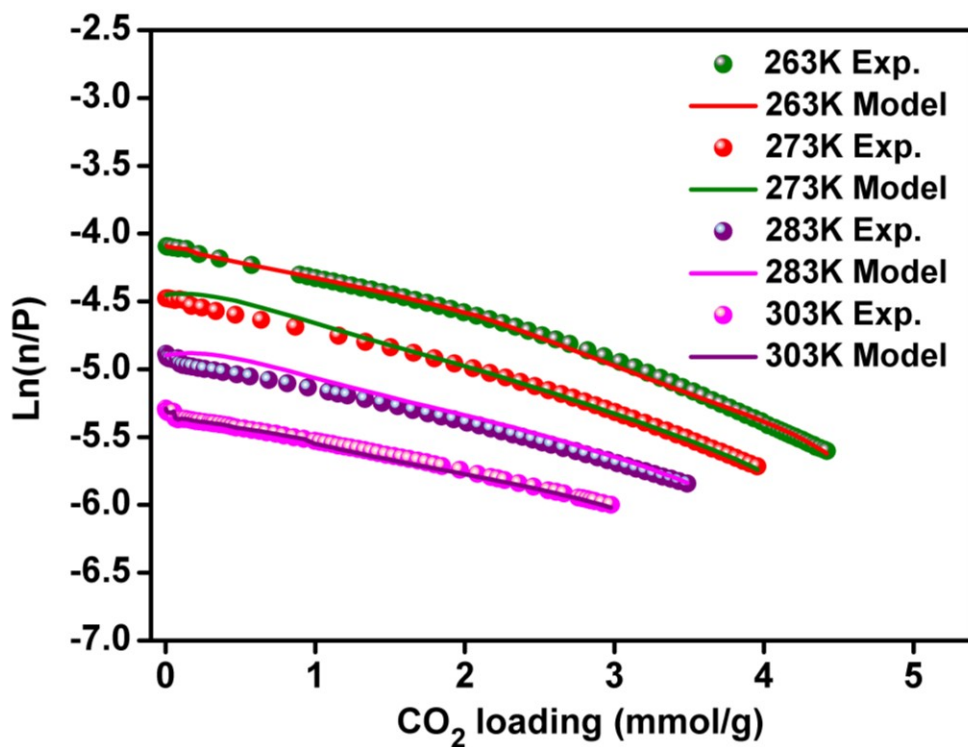


Figure S46. Virial plots of IISERP-MOF4 fitted using CO_2 isotherms collected at 303, 283, 273, 263K.

Table S2: Summary of the fitted Virial parameters for IISERP-MOF5

A0	-3722.897697
A1	344.3082188
A2	-14.27309033
A3	39.10437077
A4	-23.27685376
A5	5.297546747
B0	18.05161446
B1	-1.12532556
B2	0.032517904

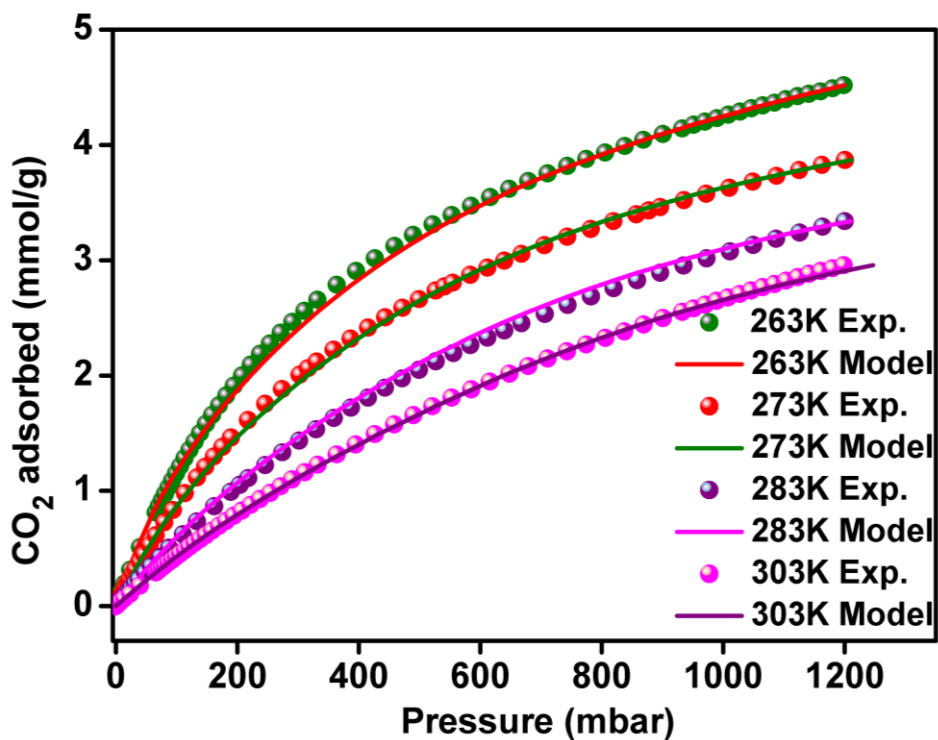


Figure S47. Comparison of experimental isotherms of IISERP-MOF5 to the ones obtained from virial modelling carried out using CO₂ isotherms collected at 303, 283, 273 and 263K.

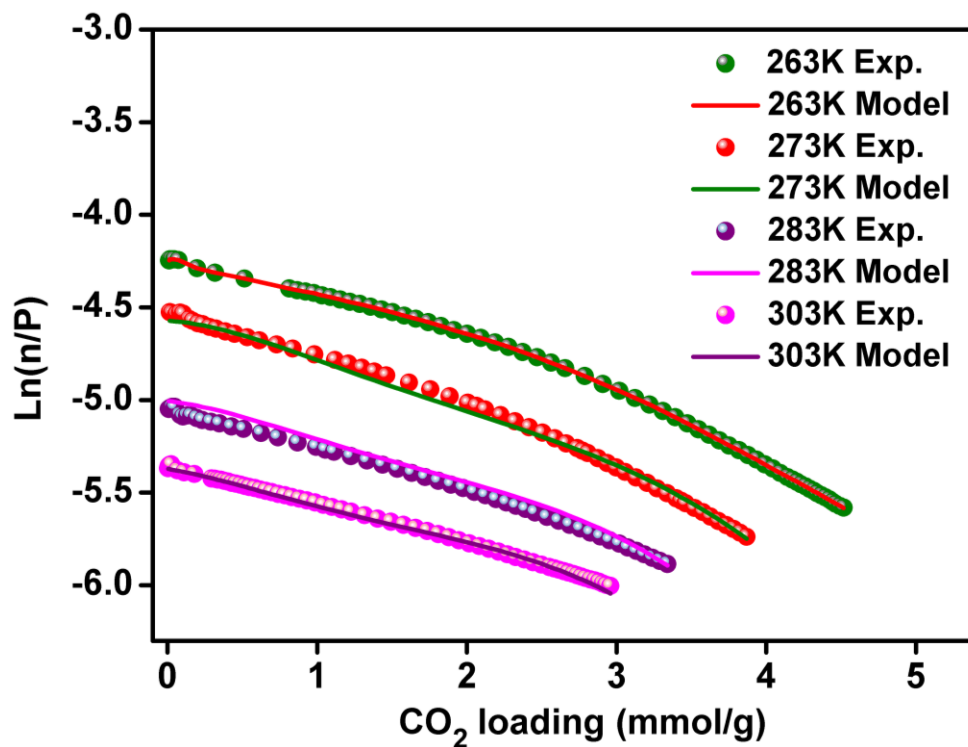


Figure S48. Virial plots of IISERP-MOF5 carried out using CO₂ isotherms collected at 303, 283, 273 and 263K.

Table S3: Summary of the fitted Virial parameters for IISERP-MOF6.

A0	-2600.715089
A1	-293.4125092
A2	443.6772838
A3	-125.8865206
A4	9.169630617
B0	14.09790329
B1	1.125173531
B2	-1.345110573
B3	0.312526809

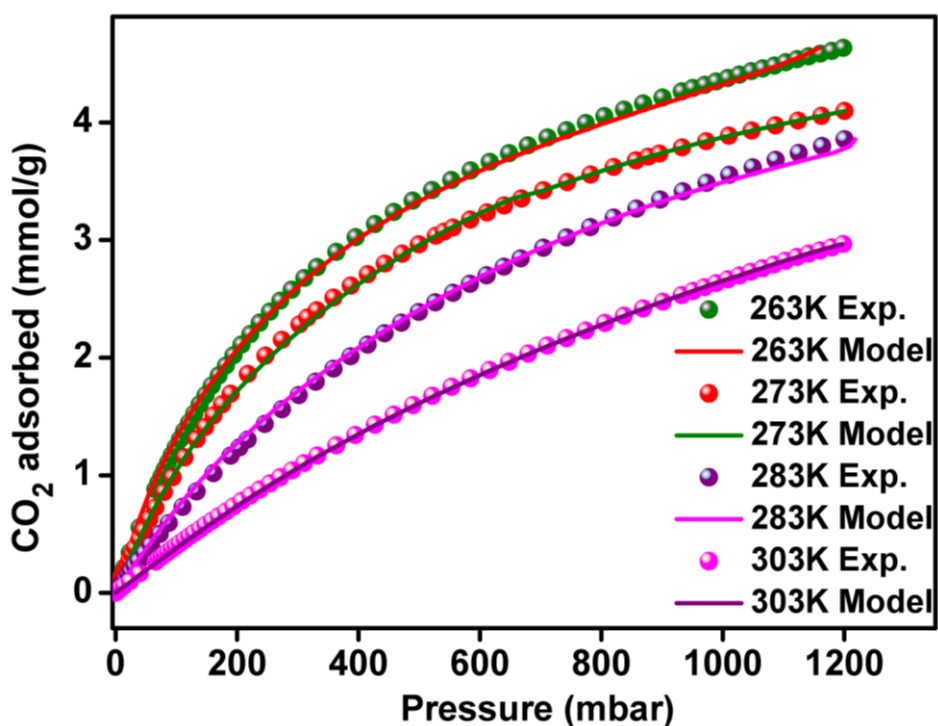


Figure S49. Comparison of experimental isotherms of IISERP-MOF6 to the ones obtained from virial modelling carried out using CO₂ isotherms collected at 303, 283, 273 and 263K.

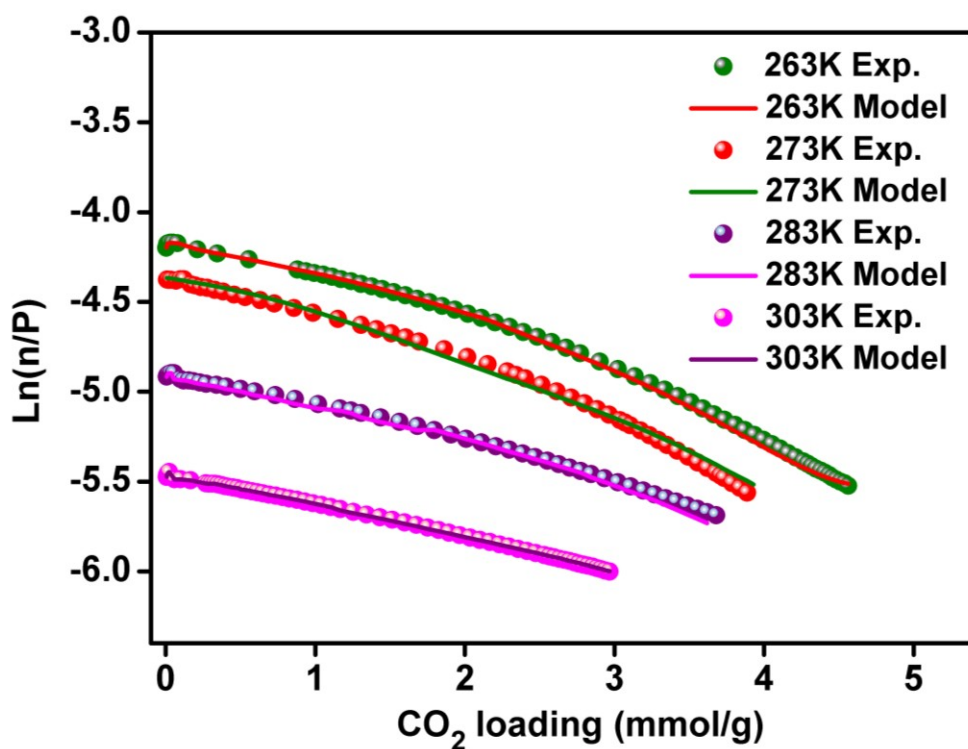


Figure S50. Virial plots of **IISERP-MOF6** carried out using CO_2 isotherms collected at 303, 283, 273 and 263K.

Table S4: Summary of the fitted Virial parameters for **IISERP-MOF7**

A0	-2591.665002
A1	-31.96990944
A2	160.0040647
A3	-68.68509774
A4	14.36764174
A5	-1.406571934
B0	14.62093607
B1	-0.220428586
B2	-0.095600681

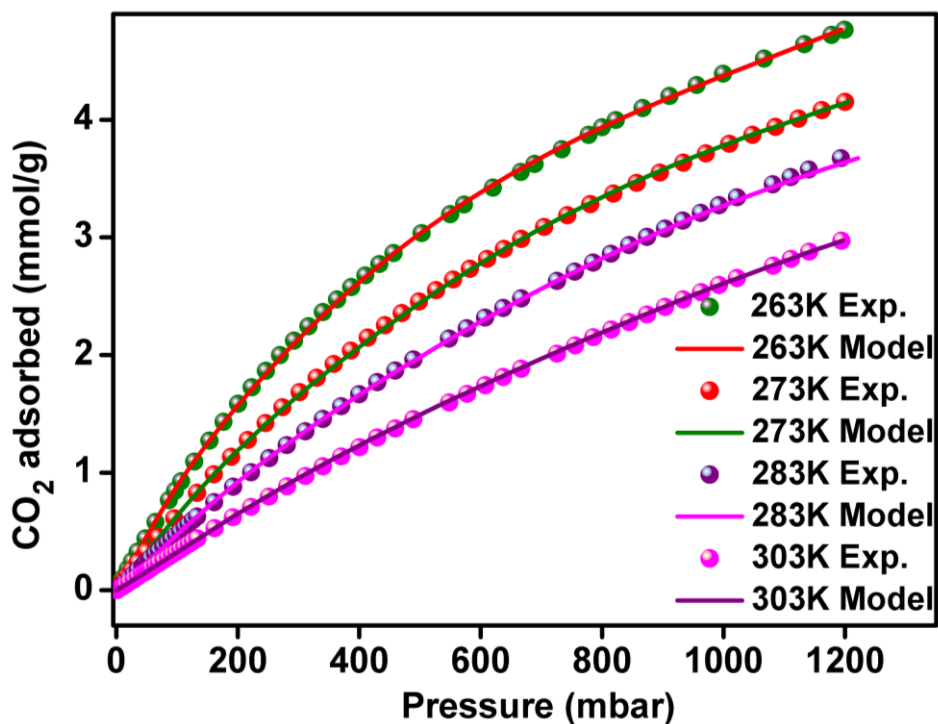


Figure S51. Comparison of experimental isotherms of IISERP-MOF7 to the ones obtained from virial modelling carried out using CO₂ isotherms collected at 303, 283, 273 and 263K.

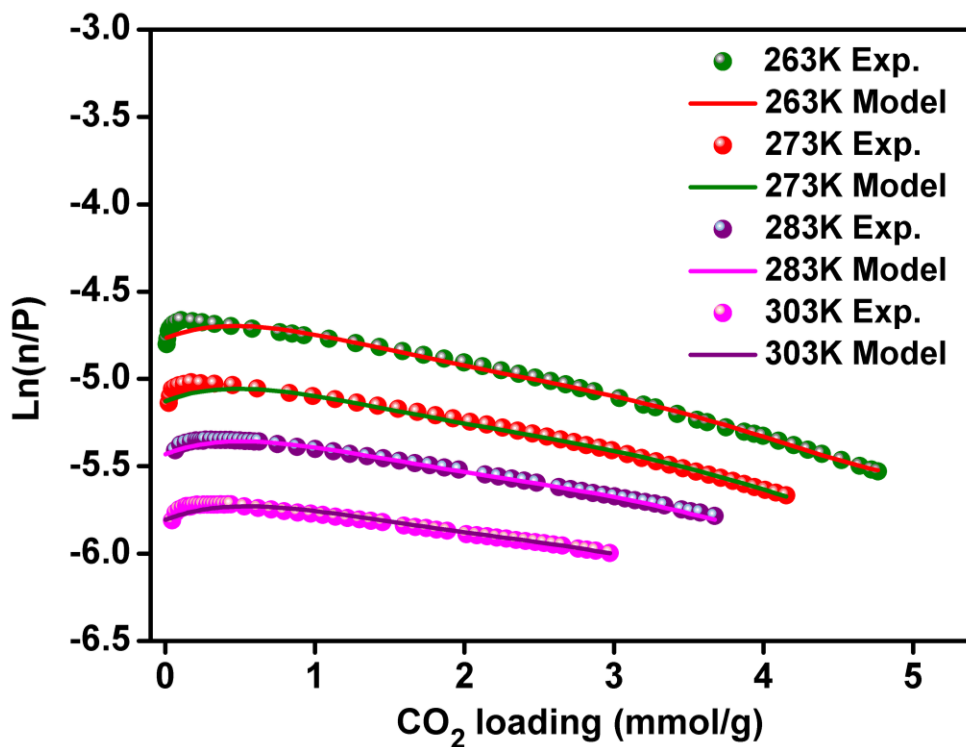


Figure S52. Virial plots of IISERP-MOF7 carried out using CO₂ isotherms collected at 303, 283, 273 and 263K.

Table S5: Summary of the fitted Virial parameters for **IISERP-MOF8**

A0	-3484.048896
A1	325.3775294
A2	-25.41147895
A3	24.36751631
A4	-8.476011206
B0	17.0712821
B1	-0.713741803
B2	-0.200622832

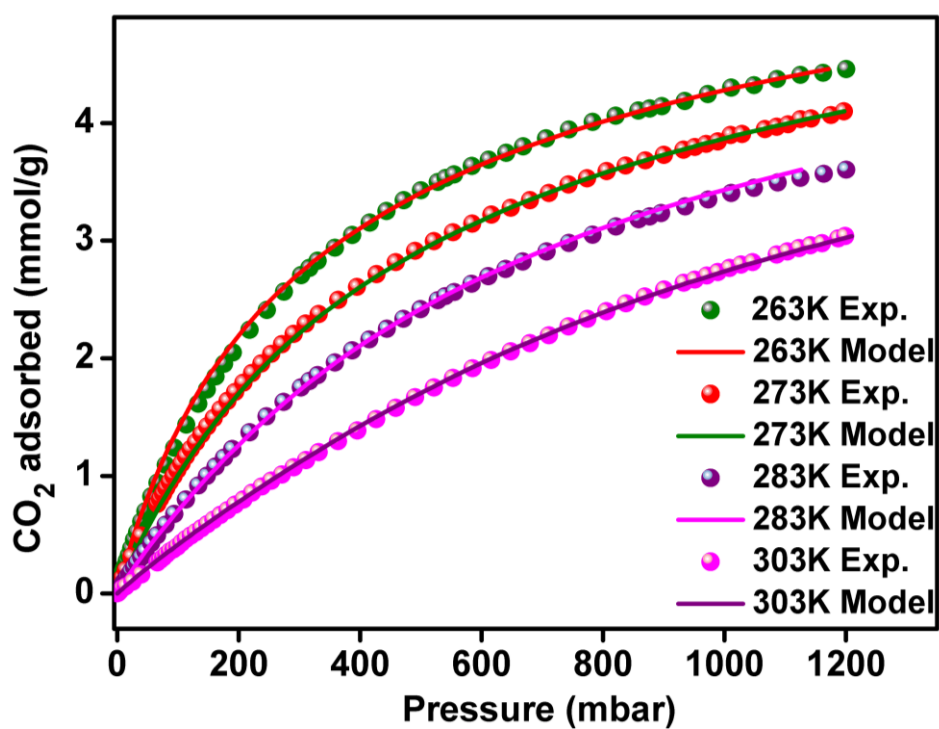


Figure S53. Comparison of experimental isotherms of **IISERP-MOF8** to the ones obtained from virial modelling carried out using CO₂ isotherms collected at 303, 283, 273 and 263K.

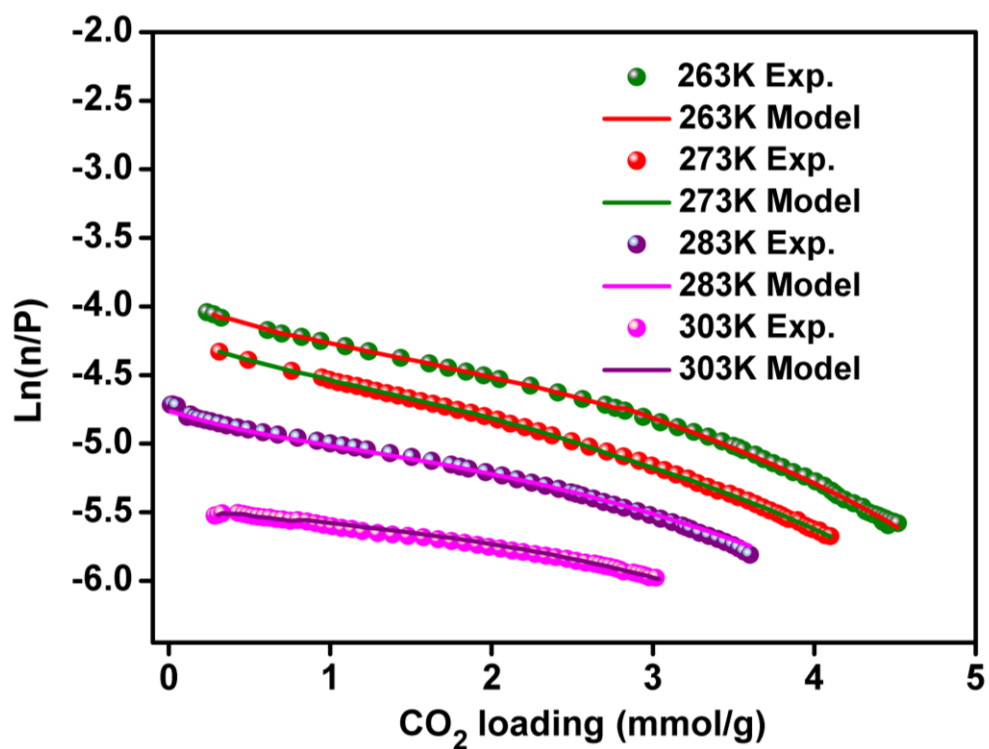


Figure S54. Virial plots of **IISERP-MOF8** carried out using CO_2 isotherms collected at 303, 283, 273 and 263K.

Table S6: Summary of the fitted Virial parameters for **IISERP-MOF9**

A0	-3715.045707
A1	739.7098862
A2	-115.6895656
A3	-4.55114152
A4	-0.70258173
A5	0.414276324
B0	17.71470962
B1	-2.148985695
B2	0.201819793
B3	0.113948412

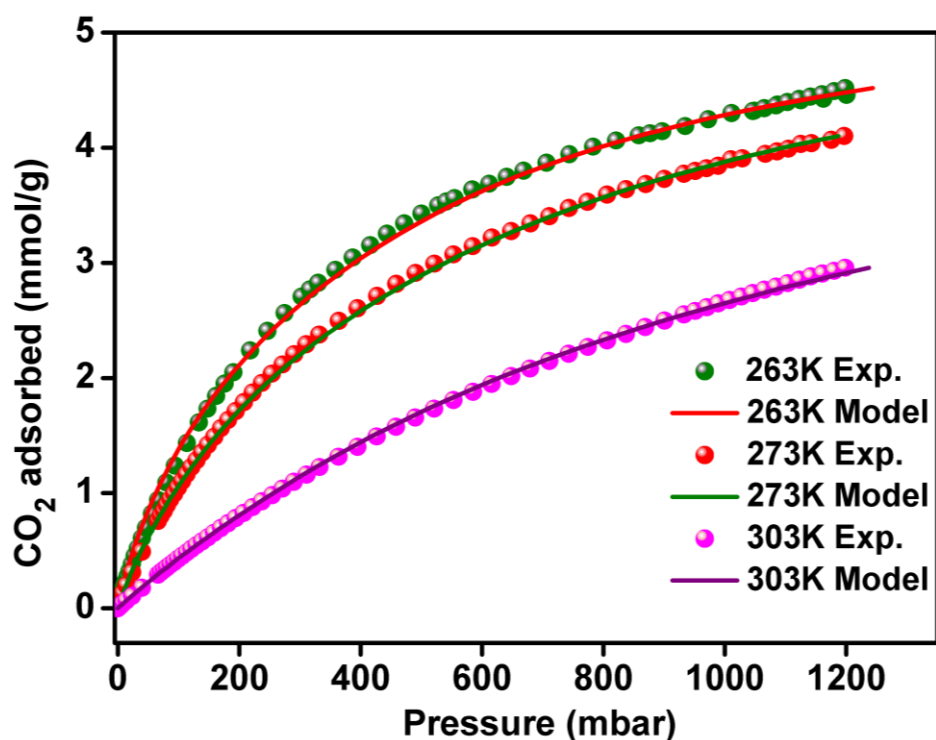


Figure S55. Comparison of experimental isotherms of **IISERP-MOF9** to the ones obtained from virial modelling carried out using CO_2 isotherms collected at 303, 273 and 263K. Note: The isotherm at 283K for this particular sample we are not able to fit despite of our enormous effort, That is why we have calculated the HOA by fitting 263K, 273K and 303K CO_2 isotherms.

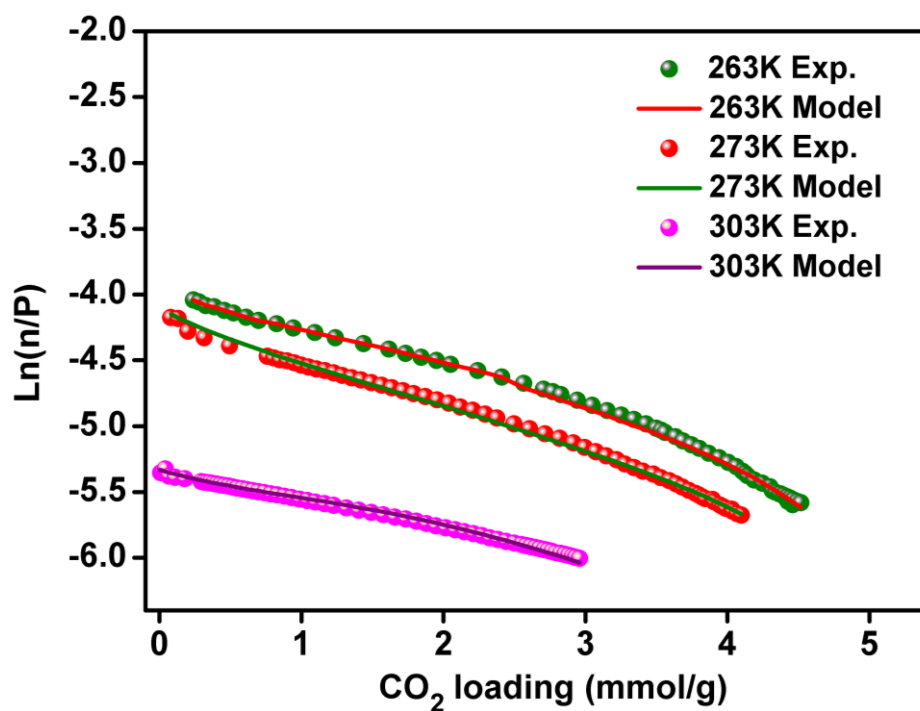


Figure S56. Virial plots of **IISERP-MOF9** carried out using CO_2 isotherms collected at 303, 273 and 263K.

IAST fitting parameters for IISERP-MOF4 (CO₂/N₂):

273K

Gas A =CO₂

Gas B = N₂

Gas Mixture			
YA =	0.15		
YB =	0.85		
Gas A Constants		Gas B Constants	
qA1 =	5.665099622	qA1 =	0.2166862
qA2 =	0	qA2 =	0
kA1 =	0.001869241	kA1 =	7.9759E-05
kA2 =	0	kA2 =	0
na1 =	0.784739867	na1 =	1.00001056
na2 =	0	na2 =	0
HA1 =	0.010589435	HB1 =	1.7283E-05
HA2 =	0	HB2 =	0

303K

Gas Mixture			
YA =	0.15		
YB =	0.85		
Gas A Constants		Gas B Constants	
qA1 =	6.221401951	qA1 =	0.03773723
qA2 =	0	qA2 =	0
kA1 =	0.000757322	kA1 =	0.00036331
kA2 =	0	kA2 =	0
na1 =	1	na1 =	1.00006497
na2 =	0	na2 =	0
HA1 =	0.004291691	HB1 =	4.1083E-05
HA2 =	0	HB2 =	0

IAST fitting parameters for IISERP-MOF5 (CO₂/N₂):

273K

Gas A =CO₂

Gas C = N₂

Gas Mixture			
YA =	0.15		
YB =	0.85		
Gas A Constants		Gas B Constants	
qA1 =	5.560161073	qA1 =	0.27081977
qA2 =	0	qA2 =	0
kA1 =	0.002288432	kA1 =	5.7029E-05
kA2 =	0	kA2 =	0
na1 =	0.784739867	na1 =	1.00006497
na2 =	0	na2 =	0
HA1 =	0.01272405	HB1 =	1.5445E-05
HA2 =	0	HB2 =	0

303K

Gas Mixture			
YA =	0.15		
YB =	0.85		
Gas A Constants		Gas B Constants	
qA1 =	7.257154715	qA1 =	0.27095985
qA2 =	0	qA2 =	0
kA1 =	0.00057532	kA1 =	3.2567E-05
kA2 =	0	kA2 =	0
na1 =	1	na1 =	1.00006497
na2 =	0	na2 =	0
HA1 =	0.004175186	HB1 =	8.8245E-06
HA2 =	0	HB2 =	0

IAST fitting parameters for IISERP-MOF6 (CO₂/N₂):

273K

Gas A =CO₂

Gas B = N₂

Gas Mixture			
YA =	0.15		
YB =	0.85		
Gas A Constants		Gas B Constants	
qA1 =	5.544223285	qA1 =	0.11940436
qA2 =	0	qA2 =	0
kA1 =	0.001864913	kA1 =	0.0001468
kA2 =	0	kA2 =	0
na1 =	0.784739867	na1 =	1.00010651
na2 =	0	na2 =	0
HA1 =	0.010339494	HB1 =	1.7528E-05
HA2 =	0	HB2 =	0

303K

Gas Mixture			
YA =	0.15		
YB =	0.85		
Gas A Constants		Gas B Constants	
qA1 =	6.214401352	qA1 =	0.08105691
qA2 =	0	qA2 =	0
kA1 =	0.0007111	kA1 =	0.00014944
kA2 =	0	kA2 =	0
na1 =	1	na1 =	1.00010651
na2 =	0	na2 =	0
HA1 =	0.004419058	HB1 =	1.2113E-05
HA2 =	0	HB2 =	0

IAST fitting parameters for IISERP-MOF7 (CO₂/N₂):

273K

Gas A =CO₂

Gas C = N₂

Gas Mixture			
YA =	0.15		
YB =	0.85		
Gas A Constants		Gas B Constants	
qA1 =	8.180423116	qA1 =	0.49853529
qA2 =	0	qA2 =	0
kA1 =	0.000857778	kA1 =	2.1234E-05
kA2 =	0	kA2 =	0
na1 =	0.784739867	na1 =	1.00006282
na2 =	0	na2 =	0
HA1 =	0.007016987	HB1 =	1.0586E-05
HA2 =	0	HB2 =	0

303K

Gas Mixture			
YA =	0.15		
YB =	0.85		
Gas A Constants		Gas B Constants	
qA1 =	11.09415015	qA1 =	0.42479508
qA2 =	0	qA2 =	0
kA1 =	0.000306675	kA1 =	2.0337E-05
kA2 =	0	kA2 =	0
na1 =	1	na1 =	1.00006497
na2 =	0	na2 =	0
HA1 =	0.003402301	HB1 =	8.6393E-06
HA2 =	0	HB2 =	0

IAST fitting parameters for IISERP-MOF8 (CO₂/N₂):

273K

Gas A =CO₂

Gas B = N₂

Gas Mixture			
YA =	0.15		
YB =	0.85		
Gas A Constants		Gas B Constants	
qA1 =	6.327508946	qA1 =	0.03503791
qA2 =	0	qA2 =	0
kA1 =	0.001532605	kA1 =	0.00054571
kA2 =	0	kA2 =	0
na1 =	0.784739867	na1 =	1.00006666
na2 =	0	na2 =	0
HA1 =	0.009697573	HB1 =	5.0798E-05
HA2 =	0	HB2 =	0

303K

Gas Mixture			
YA =	0.15		
YB =	0.85		
Gas A Constants		Gas B Constants	
qA1 =	8.775305669	qA1 =	0.02040005
qA2 =	0	qA2 =	0
kA1 =	0.000447148	kA1 =	0.00054726
kA2 =	0	kA2 =	0
na1 =	1	na1 =	1.00006666
na2 =	0	na2 =	0
HA1 =	0.003923862	HB1 =	5.0798E-05
HA2 =	0	HB2 =	0

IAST fitting parameters for IISERP-MOF9 (CO₂/N₂):

273K

Gas A =CO₂

Gas C = N₂

Gas Mixture			
YA =	0.15		
YB =	0.85		
Gas A Constants		Gas B Constants	
qA1 =	6.327508946	qA1 =	0.06789378
qA2 =	0	qA2 =	0
kA1 =	0.001532605	kA1 =	0.000332
kA2 =	0	kA2 =	0
na1 =	0.784739867	na1 =	0.99993817
na2 =	0	na2 =	0
HA1 =	0.009697573	HB1 =	5.0798E-05
HA2 =	0	HB2 =	0

303K

Gas Mixture			
YA =	0.15		
YB =	0.85		
Gas A Constants		Gas B Constants	
qA1 =	7.292259709	qA1 =	0.04519193
qA2 =	0	qA2 =	0
kA1 =	0.000601355	kA1 =	0.00033297
kA2 =	0	kA2 =	0
na1 =	1	na1 =	0.99993817
na2 =	0	na2 =	0
HA1 =	0.004385237	HB1 =	5.0798E-05
HA2 =	0	HB2 =	0

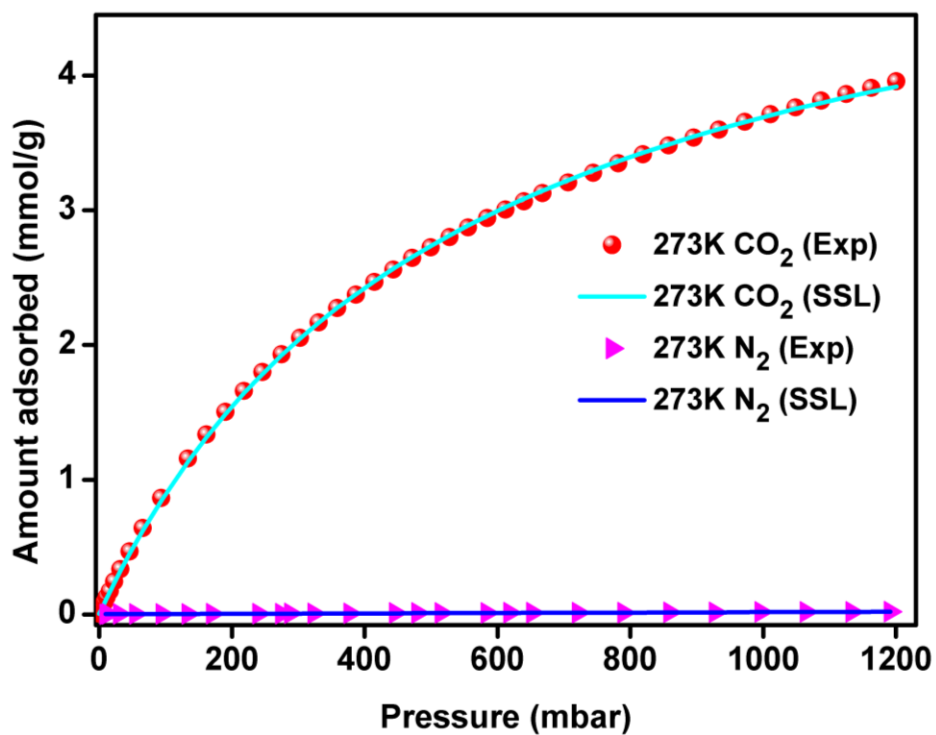


Figure S57. IAST fitting of CO₂ and N₂ isotherms for IISERP-MOF4 collected at 273K.

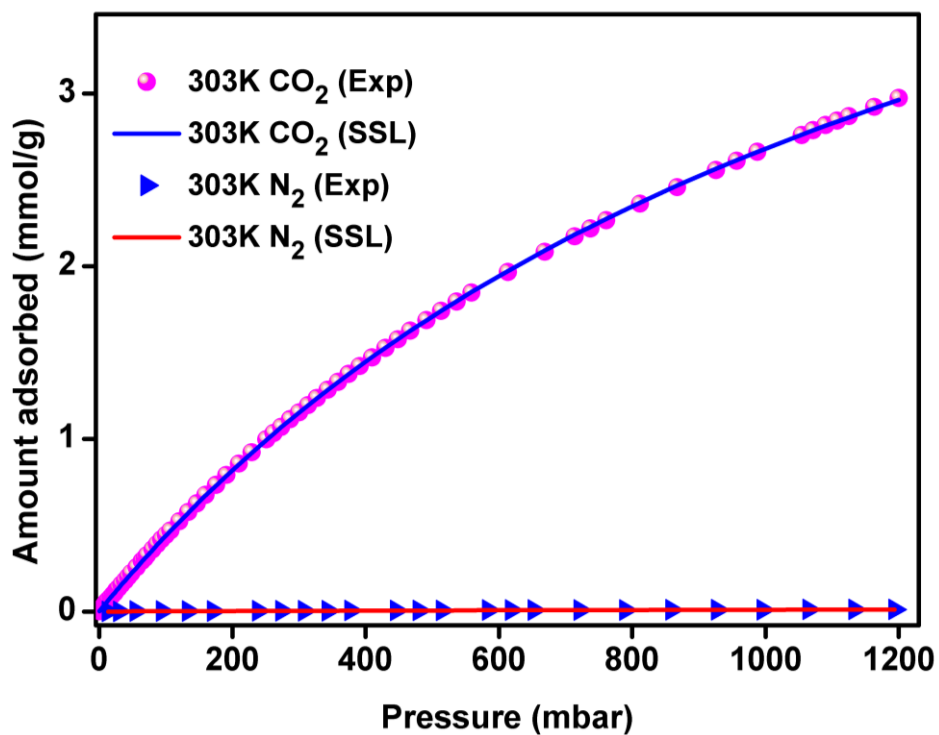


Figure S58. IAST fitting of CO₂ and N₂ isotherms for IISERP-MOF4 collected at 303K.

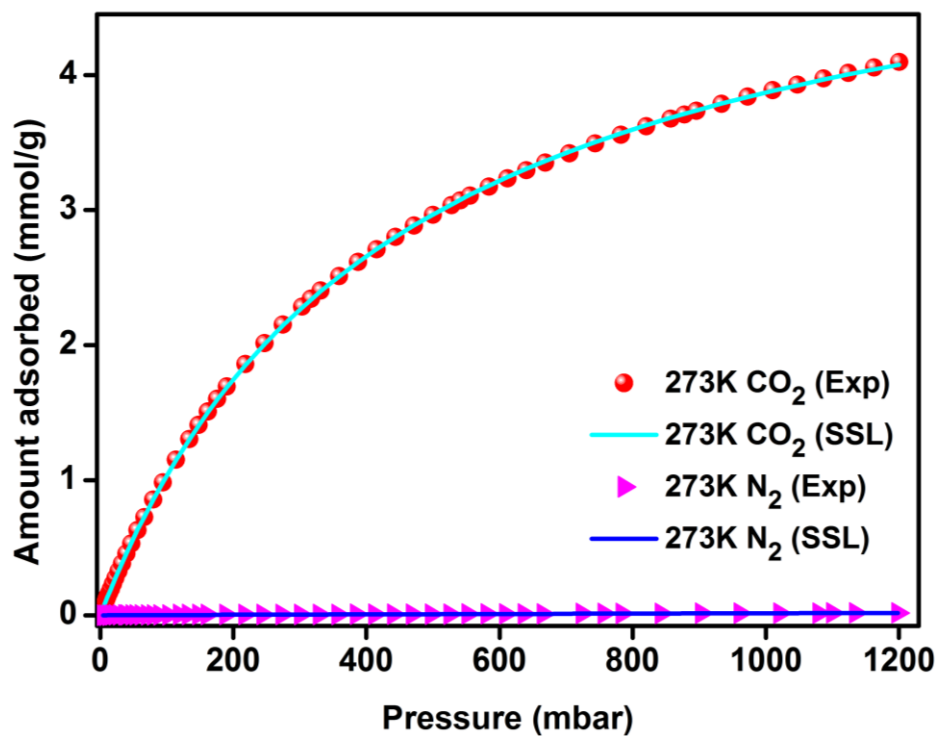


Figure S59. IAST fitting of CO₂ and N₂ isotherms for IISERP-MOF5 collected at 273K.

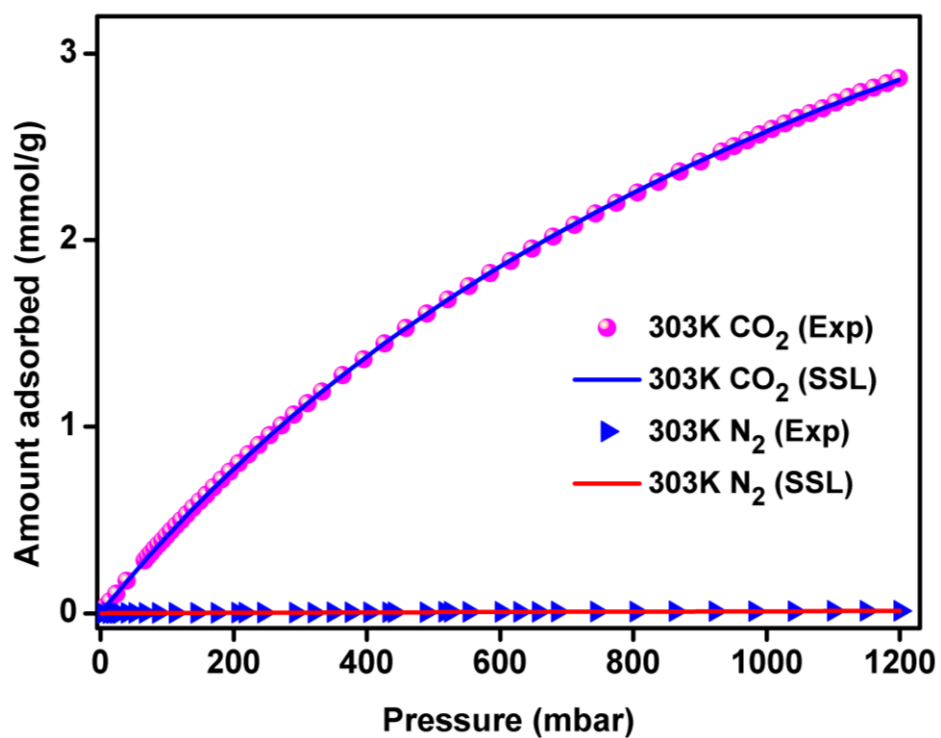


Figure S60. IAST fitting of CO₂ and N₂ isotherms for IISERP-MOF5 collected at 303K.

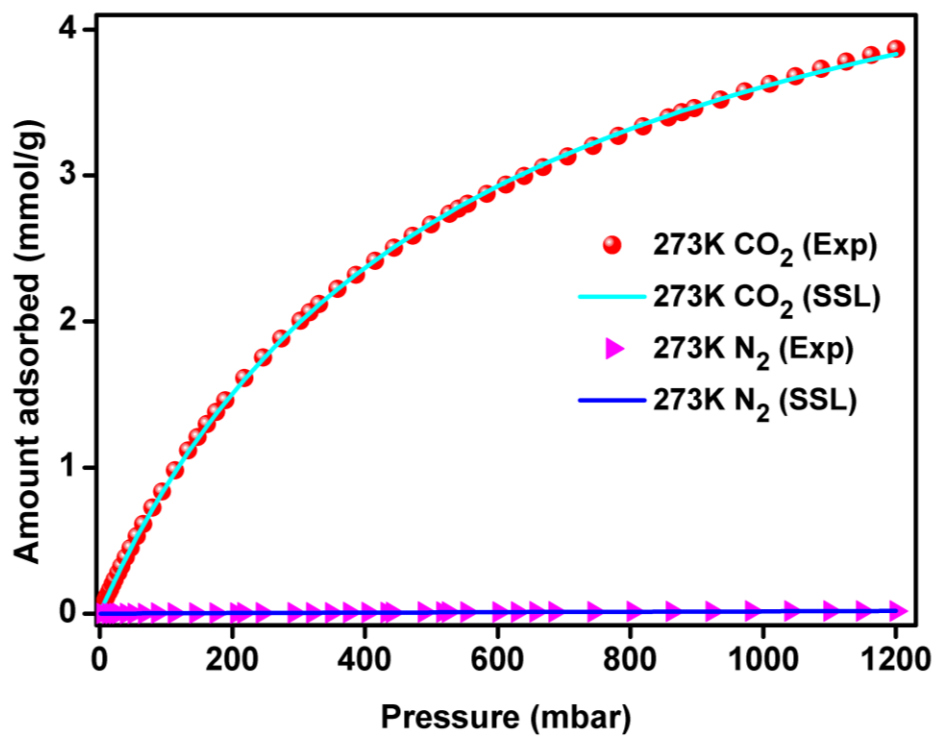


Figure S61. IAST fitting of CO₂ and N₂ isotherms for IISERP-MOF6 collected at 273K.

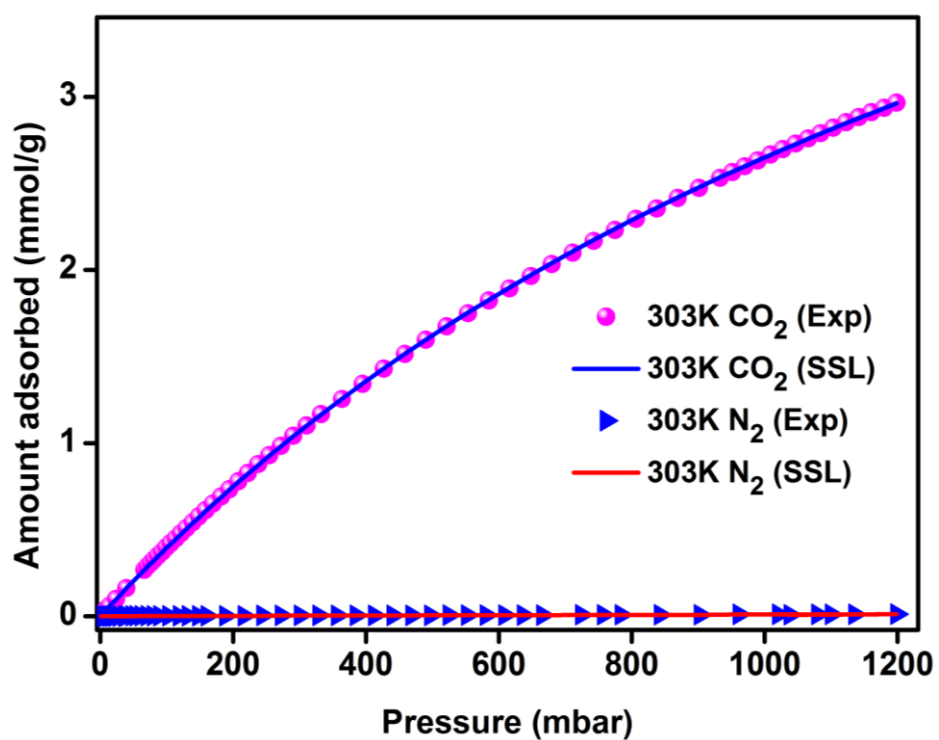


Figure S62. IAST fitting of CO₂ and N₂ isotherms for IISERP-MOF6 collected at 303K.

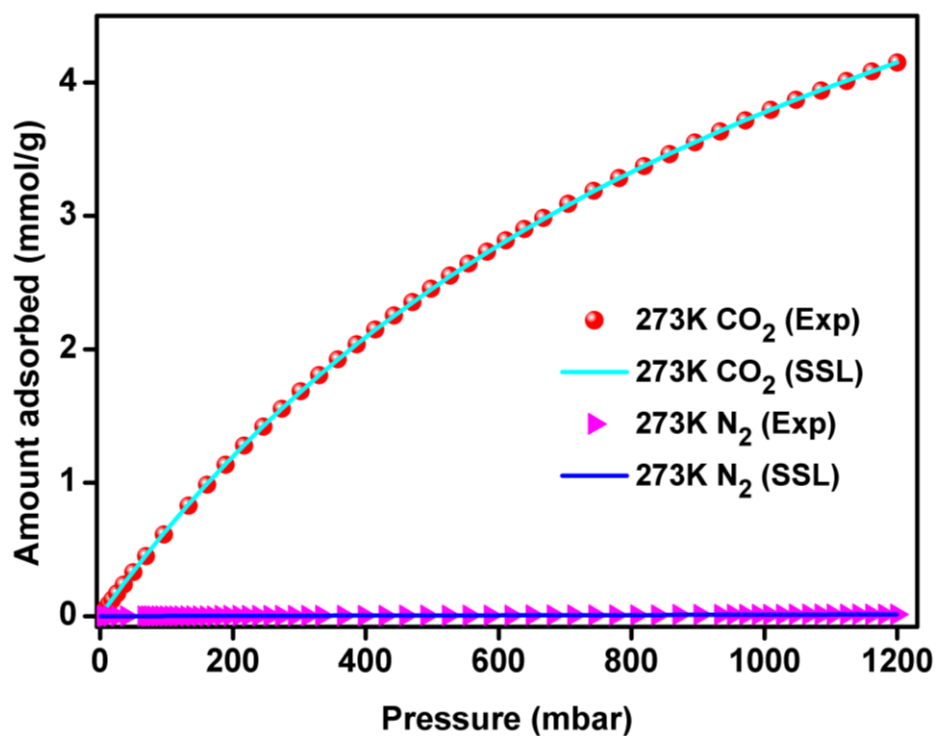


Figure S63. IAST fitting of CO₂ and N₂ isotherms for IISERP-MOF7 collected at 273K.

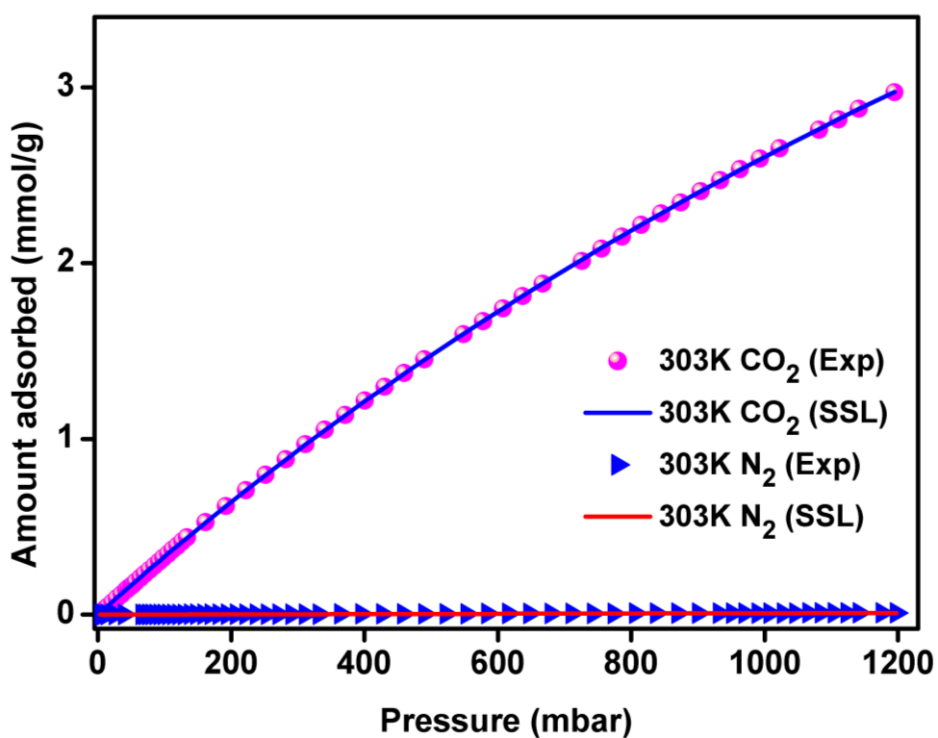


Figure S64. IAST fitting of CO₂ and N₂ isotherms for IISERP-MOF7 collected at 303K.

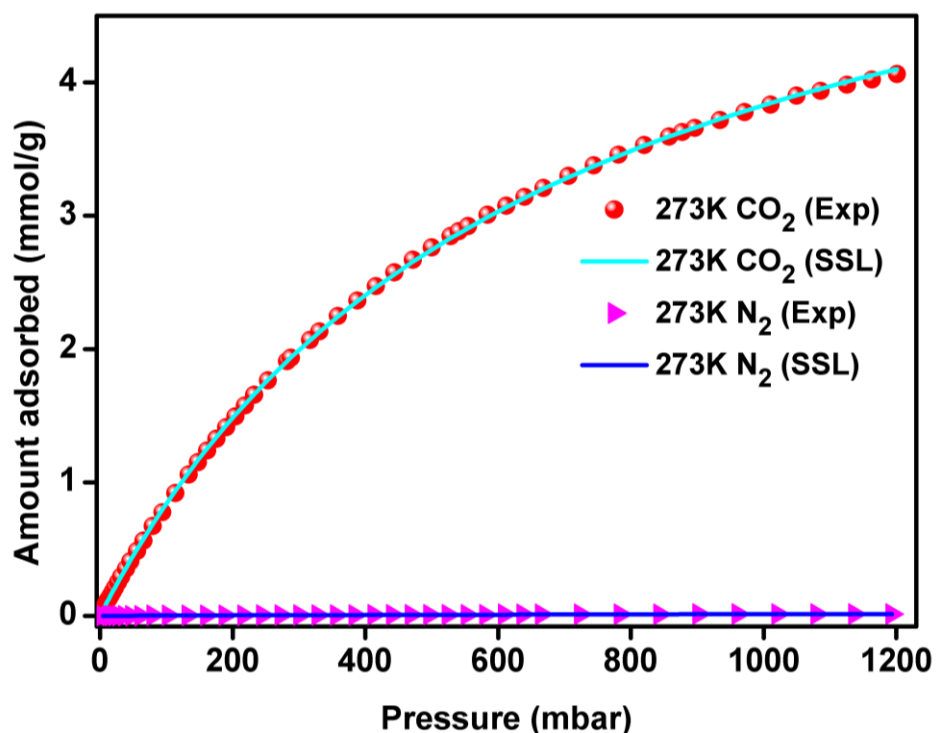


Figure S65. IAST fitting of CO₂ and N₂ isotherms for IISERP-MOF8 collected at 273K.

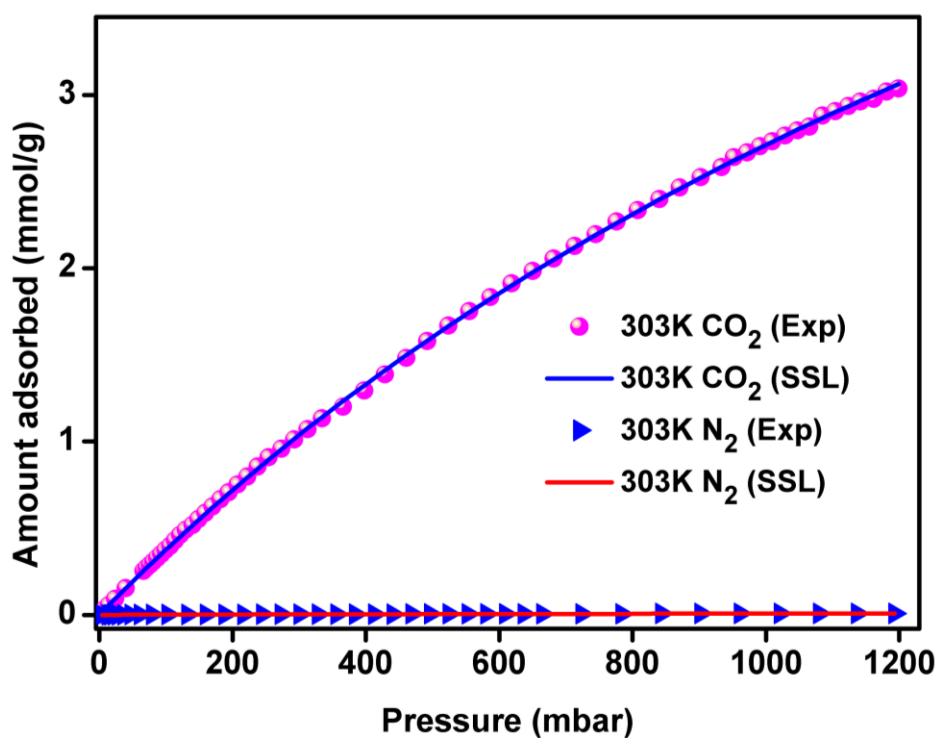


Figure S66. IAST fitting of CO₂ and N₂ isotherms for IISERP-MOF8 collected at 303K.

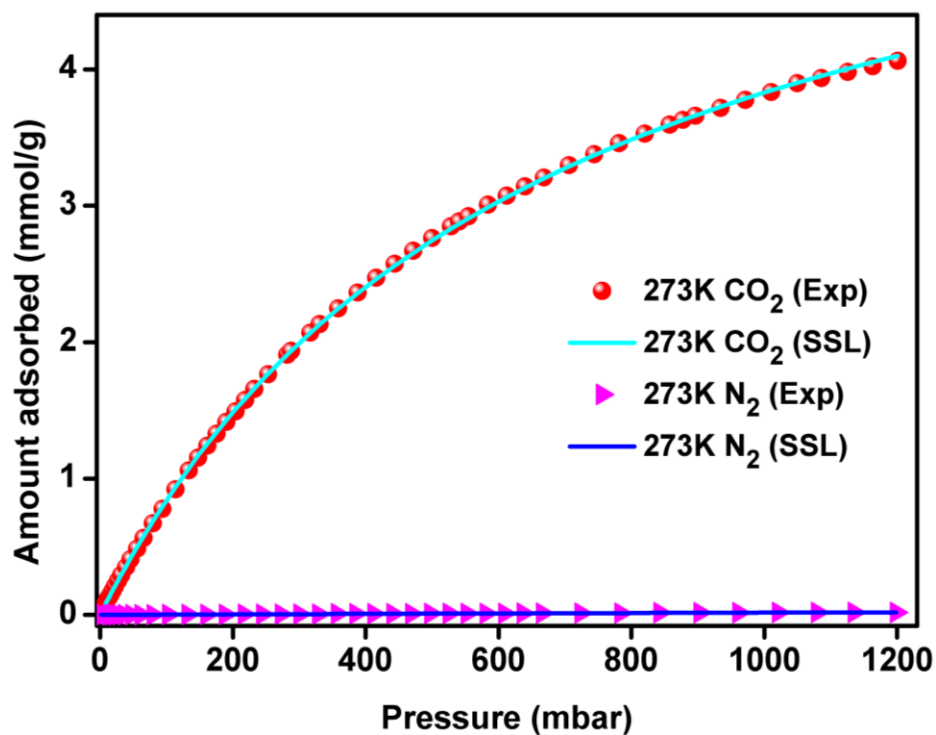


Figure S67. IAST fitting of CO₂ and N₂ isotherms for IISERP-MOF9 collected at 273K.

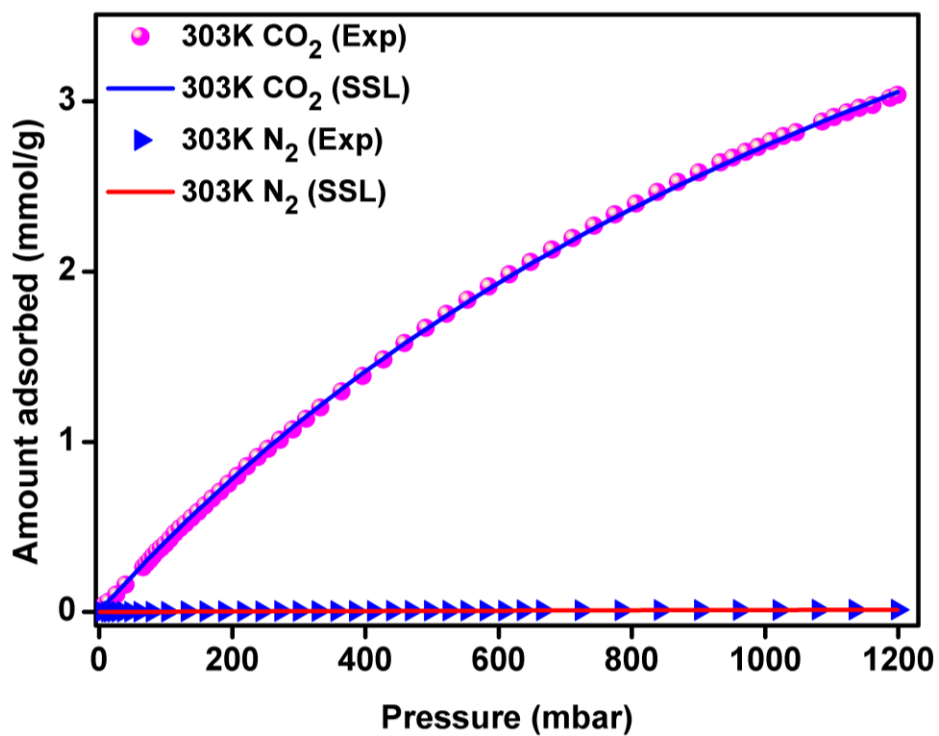


Figure S68. IAST fitting of CO₂ and N₂ isotherms for IISERP-MOF9 collected at 303K.

Working Capacity: Working capacity is defined as the amount of CO₂ recovered per gram of any material using a specific pressure swing. Here, working capacity of all the materials has been calculated for 1.2 bar to 0.1 bar pressure swing. The isotherms, involved in this calculation are all pure component isotherms at 303K. Figure S69 shows the working capacity of all the material.

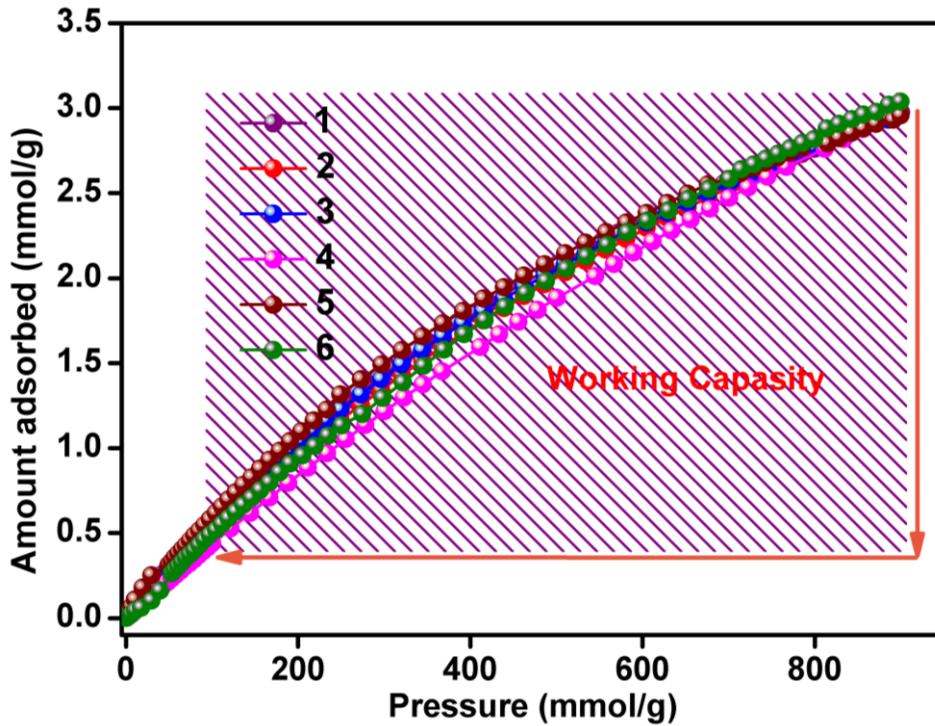


Figure S69: The working capacity of all the materials for a 1.2 to 0.1 bar pressure swing.

Self-diffusion coefficient CO₂ in the material:

Diffusion coefficient determination from Rate of Adsorption (ROA) measurements: For this, an extremely high resolution adsorption isotherm was collected using the rate of adsorption routine available with the Micromeritics instrument (ASAP2020HD), in the pressure range of 0-1bar. The diffusion coefficient was calculated as a function of CO₂ loading using 10 different loading points and each of the ROA data was fitted to a spherical pore model[†]. The fittings were done using the solver method of the Microsoft Excel following our earlier procedure.³⁹

$$F = 1 - \frac{6}{\pi^2} \sum_{n=1}^{\infty} \frac{1}{n^2} \text{Exp}(-n^2 \pi^2 \tau)$$

F = fractional uptake; τ = non-dimensional time given by $\tau = Dt/R^2$, where R= particle size; t= time (secs); D = apparent diffusivity.

The spherical pore model gives the best fit compared to slit or slab models.

The single-component diffusion coefficient was estimated to be $1.025 \times 10^{-8} \text{ m}^2 \text{ s}^{-1}$ taking the average of these 10 points.

‡ Kourosh Malek and Marc-Olivier Coppensa), *J. Chem. Phys.*, Vol. 119, 2801 (2003); Adsorption analysis and equilibria and kinetics, D. D. Do, Imperial College Press, Ed. 2008.

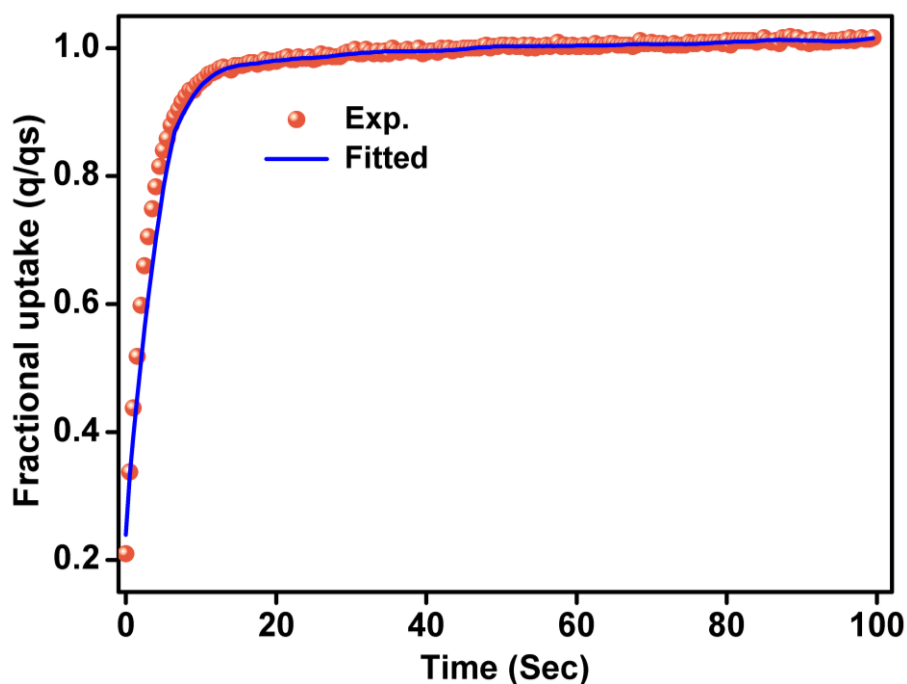


Figure S70. Representative plot of the adsorbate fractional filling vs time showing the fit between the spherical model (line) and the collected data (spheres) obtained from the single component CO₂ isotherm of **IISERP-MOF4** (loading = 7 cc/g). Note 10 such fittings were considered to obtain the average diffusion coefficient.

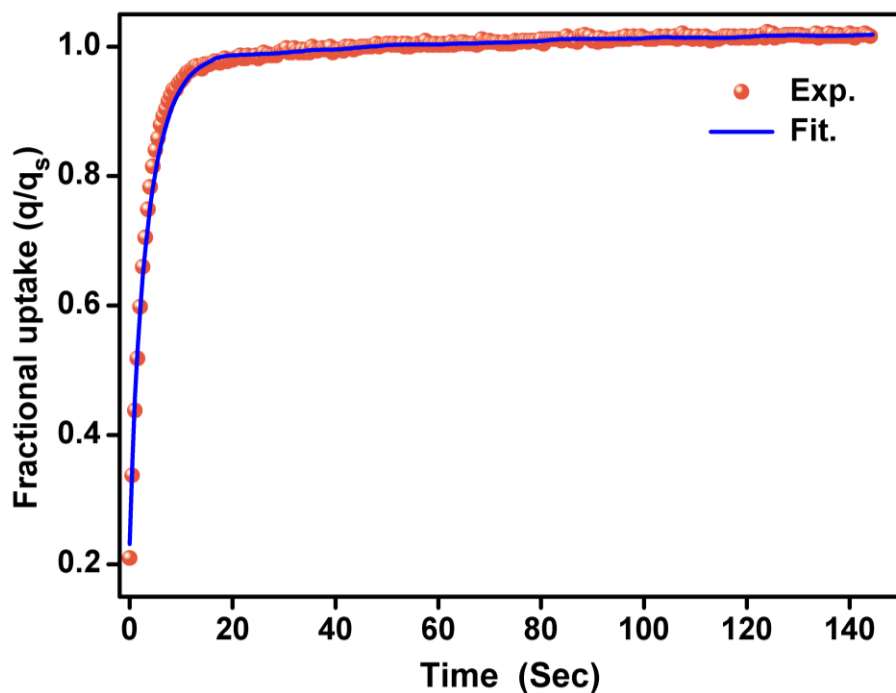


Figure S71. Representative plot of the adsorbate fractional filling vs time showing the fit between the spherical model (line) and the collected data (spheres) obtained from the single component CO₂ isotherm of **IISERP-MOF4** (loading = 26 cc/g). Note 10 such fittings were considered to obtain the average diffusion coefficient.

4. Stability Studies:

Hydrolytic stability of the MOFs have been demonstrated using steam treatment experiments (maintained at 60°C (75%RH) for 7 days) and the stability towards the repeated activation (heat + vacuum) and deactivation cycles (exposure to air + gases) during the gas sorption measurements. There were no major changes in crystallinity as observed from the PXRD of the steam-treated materials. Further to pin down, we have carried out the 195K CO₂ isotherms on all the steam treated phases. The saturation capacity in all the cases almost remains same.

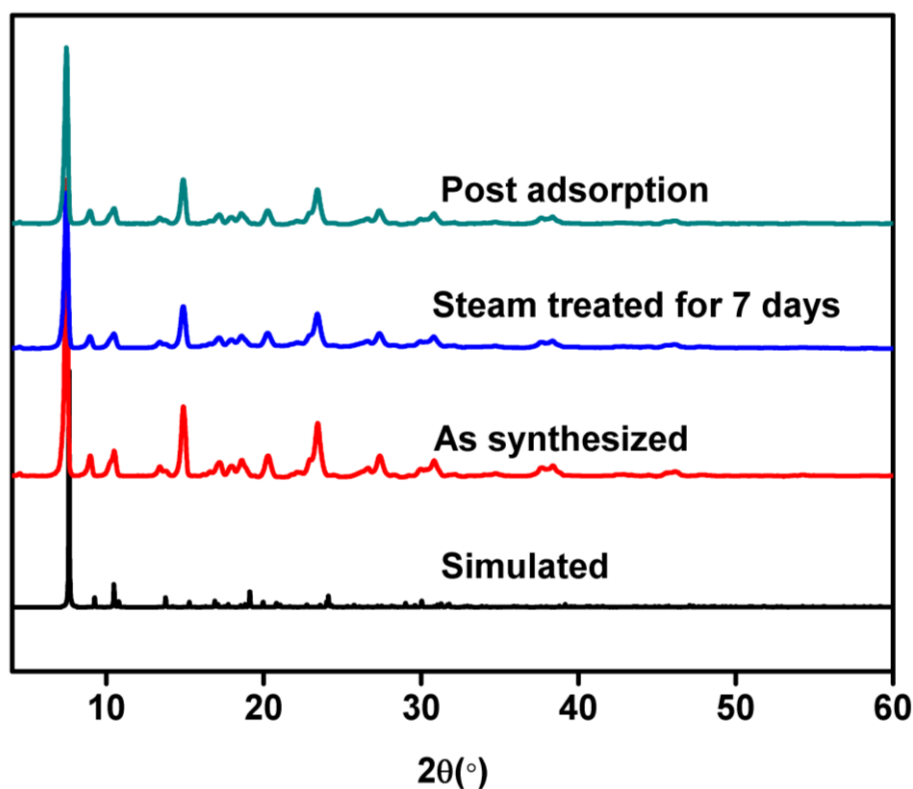


Figure S72. Pxd comparison of the as-synthesized, activated and steam treated sample of **IISERP-MOF4** showing the stability of the sample.

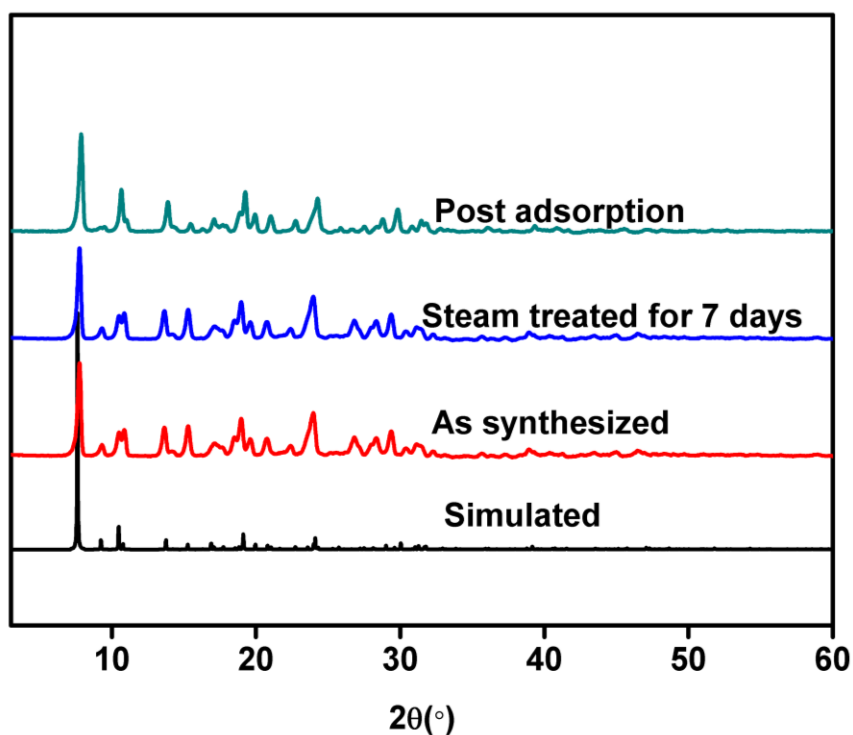


Figure S73. Pxd comparison of the as-synthesized, activated and steam treated sample of **IISERP-MOF5** showing the stability of the sample.

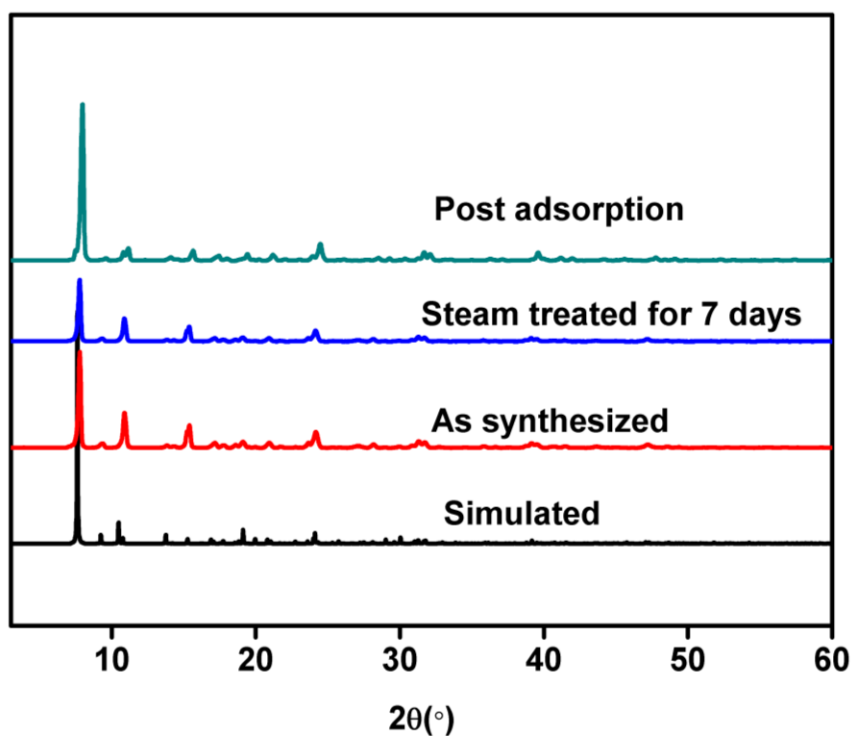


Figure S74. Pxd comparison of the as-synthesized, activated and steam treated sample of **IISERP-MOF6** showing the stability of the sample.

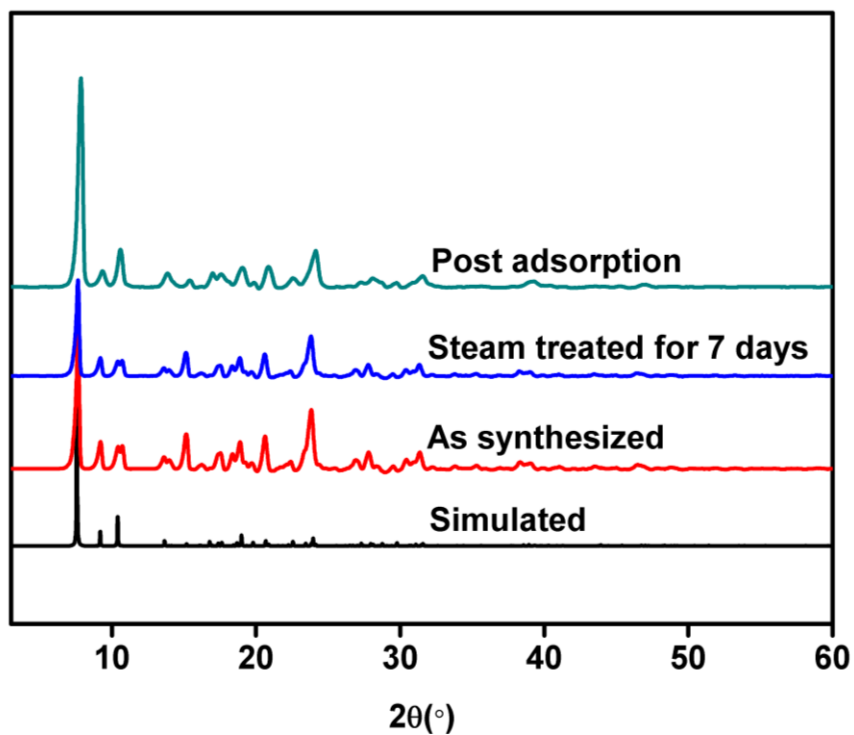


Figure S75. Pxd comparison of the as-synthesized, activated and steam treated sample of **IISERP-MOF7** showing the stability of the sample.

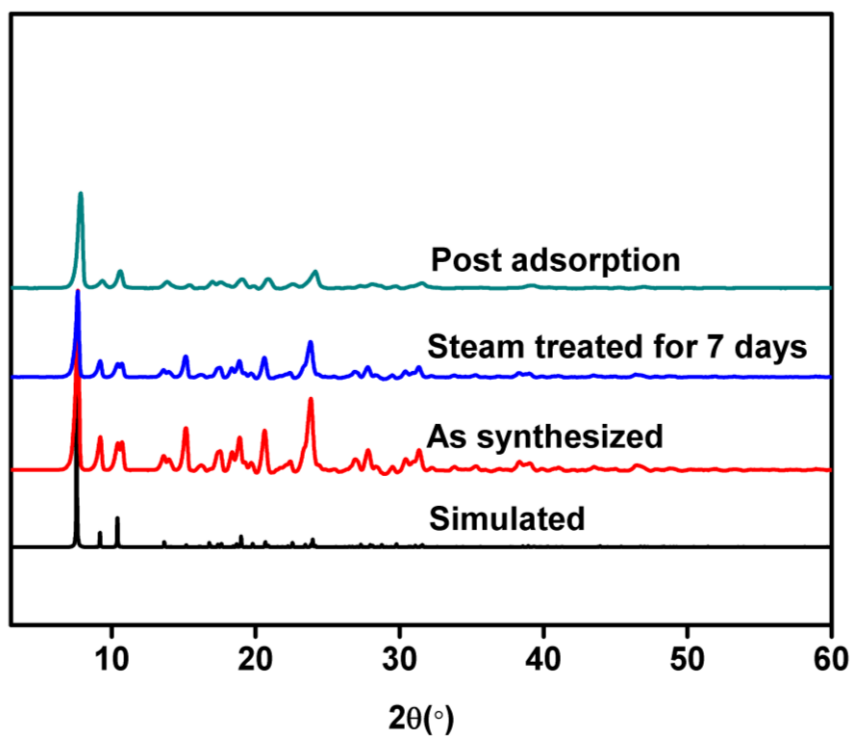


Figure S76. Pxd comparison of the as-synthesized, activated and steam treated sample of **IISERP-MOF8** showing the stability of the sample.

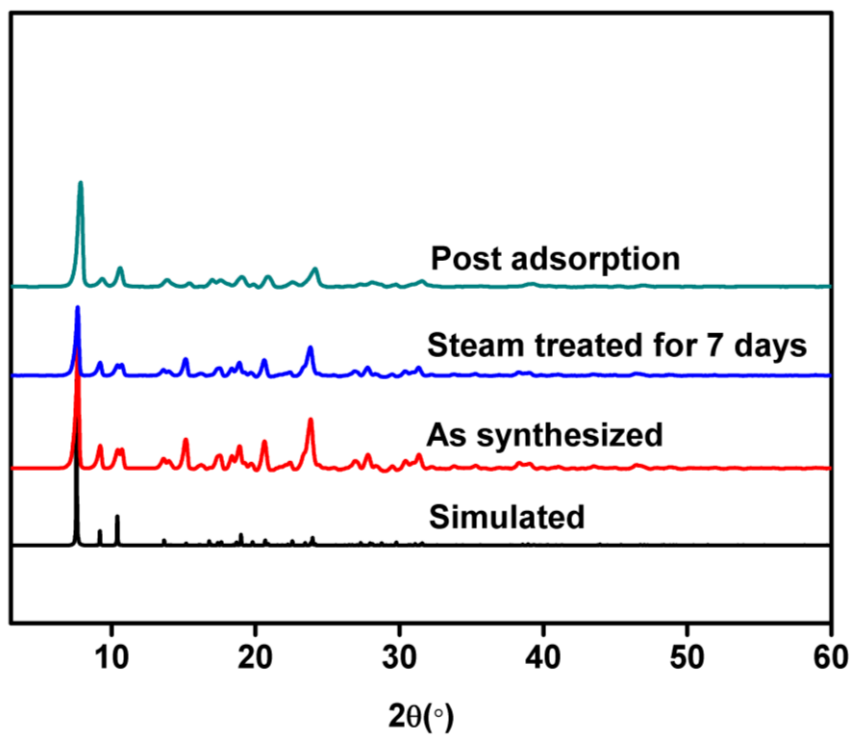


Figure S77. Pxd comparison of the as-synthesized, activated and steam treated sample of IISERP-MOF9 showing the stability of the sample.

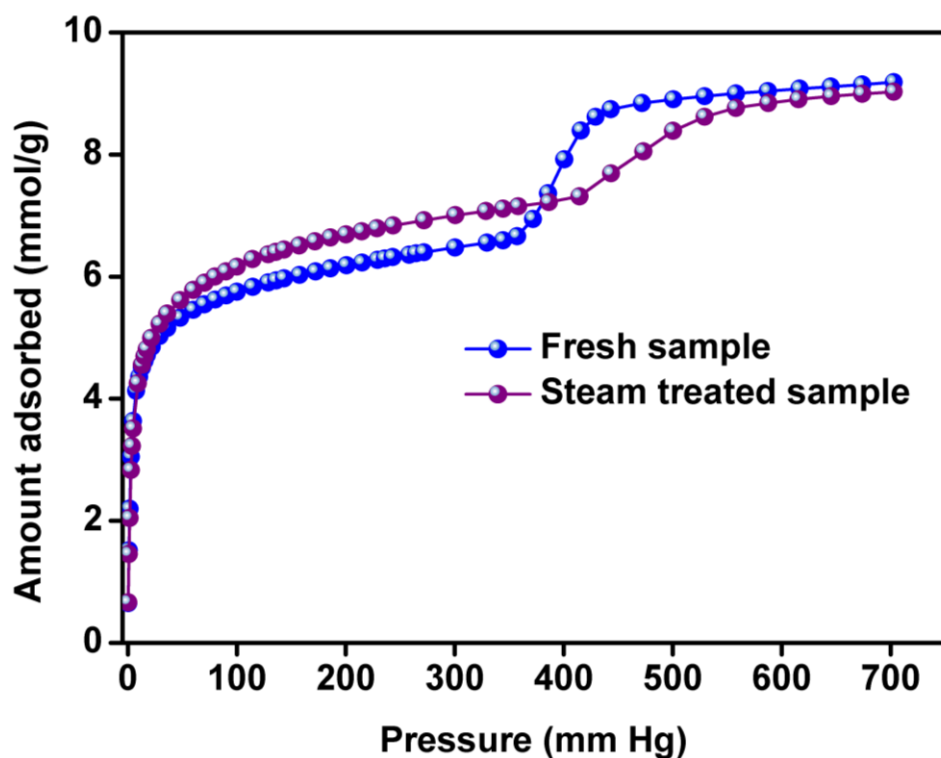


Figure S78. A comparison of 195K CO_2 isotherms obtained from fresh sample vs steam treated sample of IISERP-MOF4.

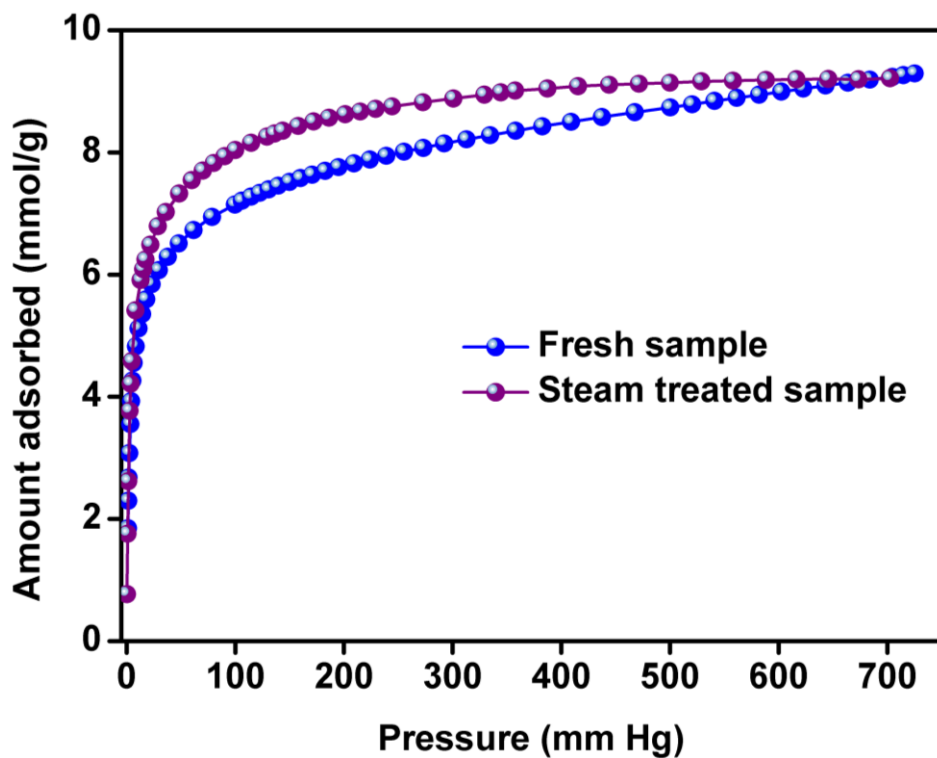


Figure S79. A comparison of 195K CO₂ isotherms obtained from fresh sample vs steam treated sample of IISERP-MOF5.

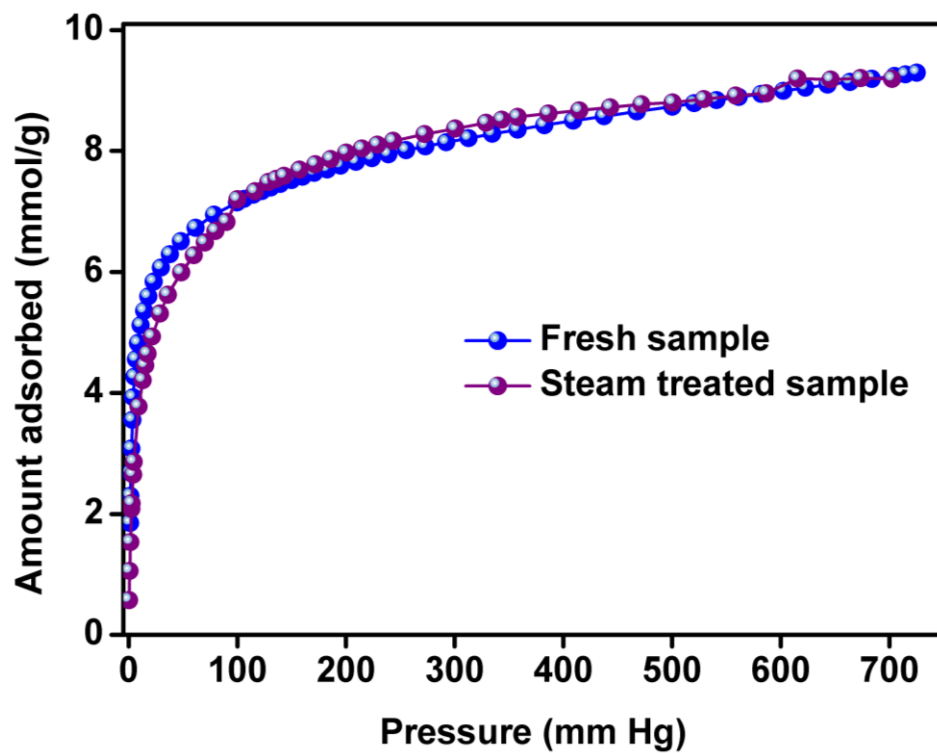


Figure S80. A comparison of 195K CO₂ isotherms obtained from fresh sample vs steam treated sample of IISERP-MOF6.

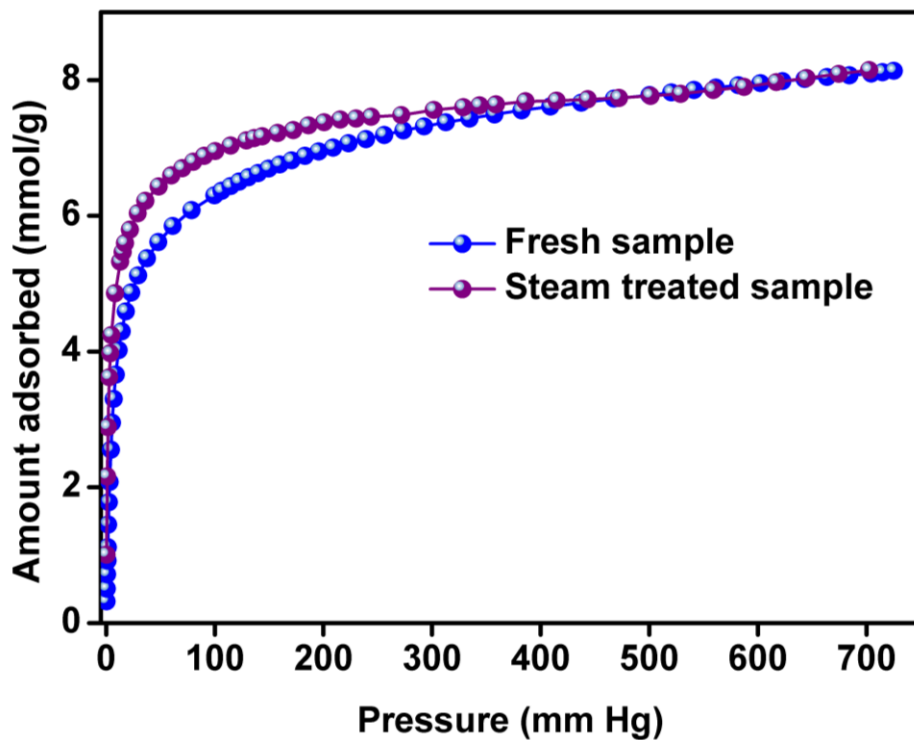


Figure S81. A comparison of 195K CO₂ isotherms obtained from fresh sample vs steam treated sample of IISERP-MOF7.

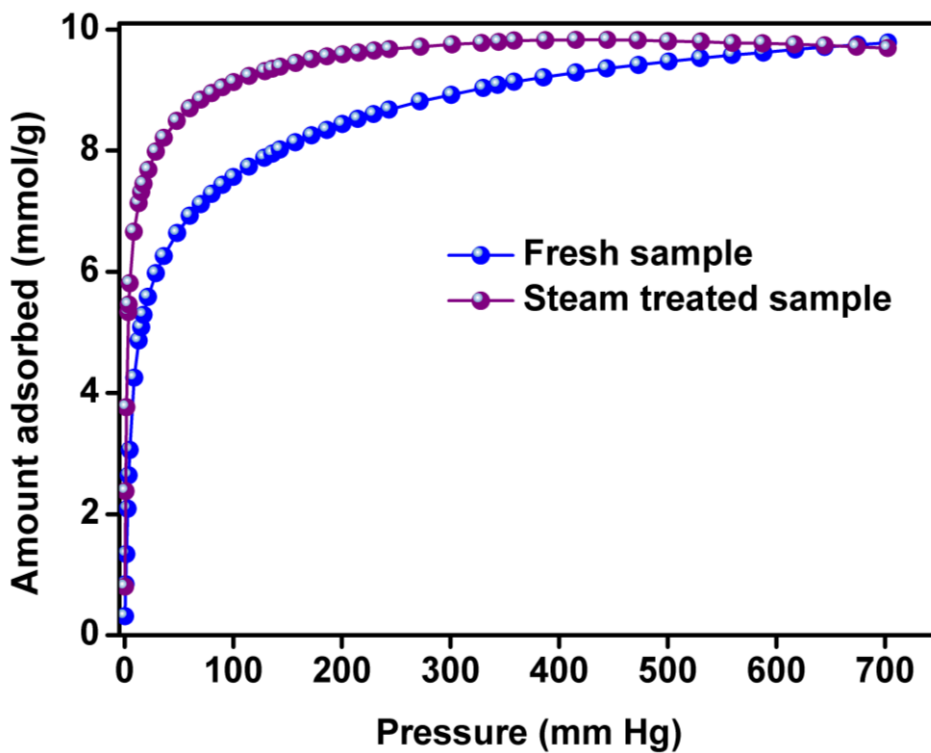


Figure S82. A comparison of 195K CO₂ isotherms obtained from fresh sample vs steam treated sample of IISERP-MOF8.

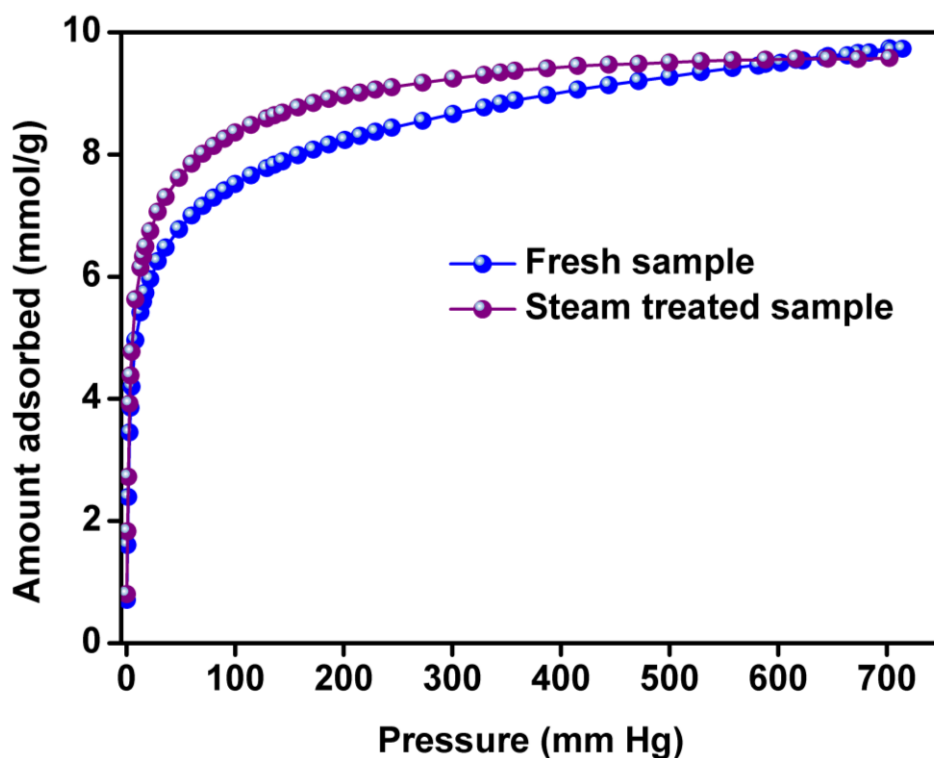


Figure S83. A comparison of 195K CO₂ isotherms obtained from fresh sample vs steam treated sample of IISERP-MOF9.

Steam Conditioning Experiments:

In this experiment the materials were activated according to the proper activation condition. These activated samples were then exposed to a flow of humid N₂ (100ml/min over a 75%RH, saturated NaCl solution maintained at 60°C) for a period of 24hrs. This steam conditioned materials were loaded on to the adsorption cell and without any further activation (no heating or evacuation), a CO₂ adsorption was carried out on the wet materials.

5. Computational details:

The CIF files from the single crystal structure were utilized as inputs. The most probable locations for CO₂ were obtained from a GCMC routine carried out using Materials Studio V. 6.0. For this routine the rotational and translational degrees of freedom were eased for the adsorbate molecules and a Metropolis Algorithm was employed. The resulting simulated model revealed a total of 29 CO₂ molecules per unit cell of Mg-triazolyl MOF. Following this, the direct positions of CO₂ were located by carrying out a geometry optimization using the Simulated Annealing routine of the Materials Studio. During this, the framework atoms were constrained and the CO₂ molecules were optimized with both rotational and translational freedom. The default force fields were employed..

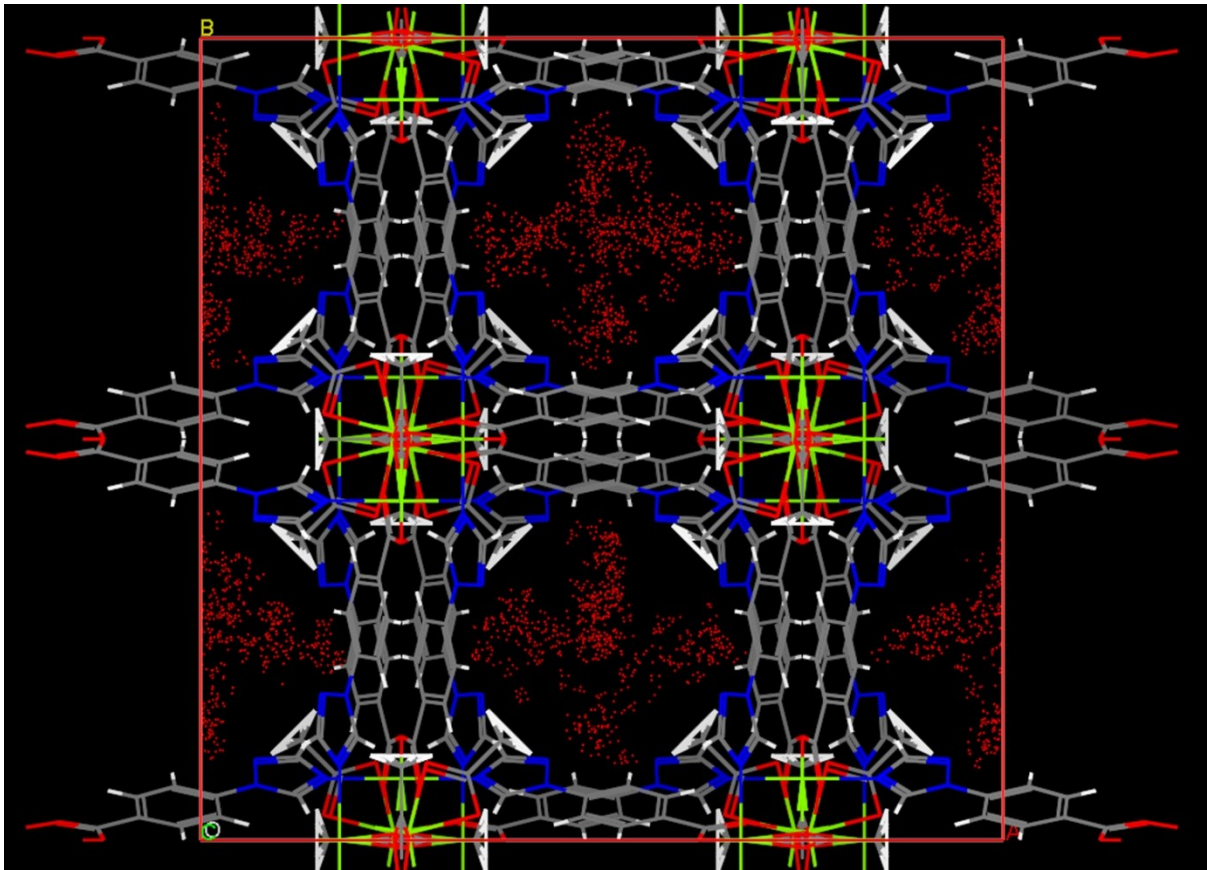


Figure S84. Shows the most probable positions for CO₂ molecules within the unit cell of **IISERP-MOF4** obtained from the Simulated Annealing method.